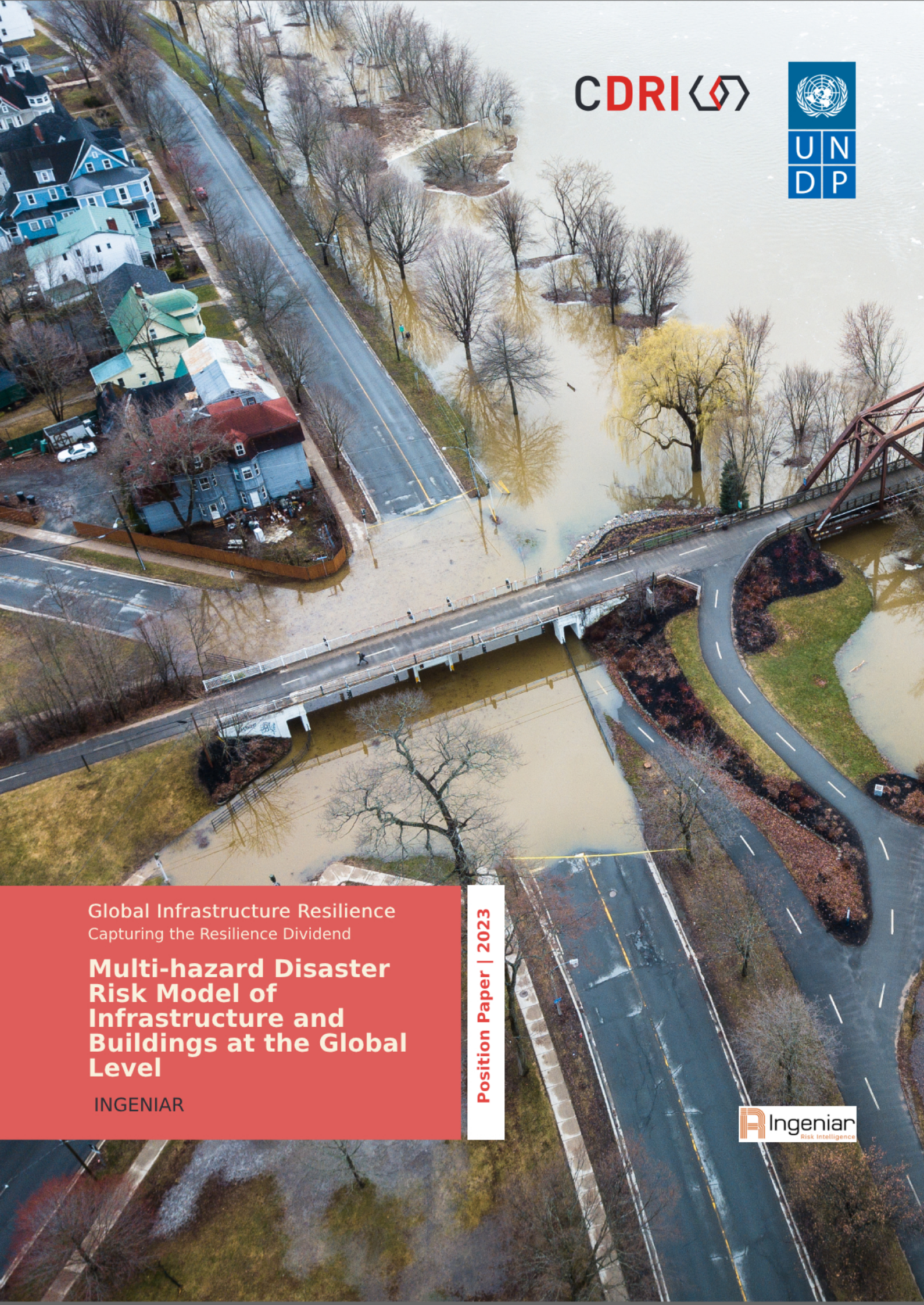

Global Infrastructure Resilience

Capturing the Resilience Dividend

Multi-hazard Disaster Risk Model of Infrastructure and Buildings at the Global Level

INGENIAR

Position Paper | 2023

Ingeniar
Risk Intelligence

GIRI: Global Infrastructure Risk Model and Resilience Index

Background report

Multi-hazard Disaster Risk Model of Infrastructure and Buildings at the Global Level

CDRI
Coalition for Disaster Resilient Infrastructure

UNDP

August, 2023

Risk Model and Resilience Index Developer

INGENIAR CAD/CAE Ltda.
Carrera 19A # 84-14 OF 504, Bogotá
www.ingeniar-risk.com

This background paper has been made in the framework of the project "Development of a Global Infrastructure Risk Model and Resilience Index (GIRI) for the Coalition for Disaster Resilient Infrastructure (CDRI) Flagship Report on Disaster and Climate Resilient Infrastructure", supported by the United Nations Development Program (UNDP), and developed by the consortium INGENIAR CAD/CAE LTDA., UNIGE, NGI, and CIMA.

Please cite this document as:
Cardona, O.D., Bernal, G.A., Villegas, C.P., Molina, J.F., Herrera, S.A., Marulanda, M.C., Rincón, D.F., Grajales, S., Marulanda, P.M., Gonzalez, D., Maskrey, A. (2023). *Multi-hazard Disaster Risk Model of Infrastructure and Buildings at the Global Level*. Background Report, INGENIAR: Risk Intelligence for the CDRI Flagship Report.

CONTENTS

1 Introduction

Effective risk management involves making informed decisions based on forecasts of uncertain consequences. Unfortunately, stakeholders often lack access to risk models, prospective forecasts, and measures of the uncertainty inherent to risk, leading to uninformed decisions and uncertain outcomes. It's widely acknowledged that relying solely on historical data is inadequate for making sound decisions, not only because of the limited information regarding catastrophic events that occurred in the past, but also because the worst events are still yet to occur. Therefore, forecasting the potential consequences of extreme events based solely on historical information is often impossible.

When looking ahead to assess the potential consequences of upcoming events, various uncertainties can cloud stakeholders' judgment, hindering their decision-making abilities. To address this challenge, it is essential to use analytical probabilistic models that rationally incorporate the related uncertainties and provide metrics sensitive to uncertainty. This empowers stakeholders to anticipate the occurrence of catastrophic events and their feasible consequences while considering the uncertainties associated with their estimated severity and frequency.

Examining a country's fiscal responsibility portfolio, losses caused by disasters represent implicit contingent liabilities that increase a country's fiscal vulnerability, including damage to public infrastructure. Essentially, future disasters can be seen as hidden public debt that becomes certain when the event occurs. This "contingent debt" must be added to the existing explicit debt. If the total value exceeds the present discounted value of future primary surpluses, it creates an imbalance in the country's fiscal sustainability equation. Governments must acknowledge that future disasters should be factored into the country's financial health, as they can lead to significant macroeconomic imbalances.

Therefore, future disasters should be considered a "sovereign risk" for a country, requiring collective responsibility akin to compliance with the constitution and legislation. To assess this responsibility adequately, it's crucial to use loss assessment models that account for the inherent uncertainties of the phenomenon and enable decision-making considering the aleatory nature of such losses. Quantifying these potential losses is necessary because "what is not quantified cannot be managed." Probabilistic models like GIRI provide an effective means to measure disaster risk within the context of fiscal sustainability. This allows governments to identify optimal financial protection strategies, whether through transferring or retaining sovereign risk, thereby reducing losses and minimizing the risk of insolvency as well as the effects on the development and the quality of life of the population.

1.1 What is GIRI?

GIRI is the Global Infrastructure Risk and Resilience Model developed by CDRI, and the comprehensive system of indicators derived from it encompassing all countries and territories worldwide. Currently, GIRI addresses six natural hazards: earthquakes, tsunami, landslides, floods, tropical cyclones, and droughts[1].

[1] As droughts do not have a direct physical impact on infrastructure elements, the drought assessment methodology is not included in this document. Instead, drought losses are estimated based on their impact on the performance of the energy sector,

These last three include climate change-induced modifications, providing hydrometeorological risk metrics related to various greenhouse gas emissions scenarios in the future, alongside stationary risk metrics for geological hazards. GIRI also extends its coverage to nine infrastructure sectors: power, highways, railways, transportation, water and wastewater, communications, oil and gas, education, health, and housing.

In summary, GIRI boasts the following key features:

- Flexibility and Scalability: It serves as both a metric and a modeling framework for assessing disaster risk in infrastructure systems supporting socio-economic activities. This versatility allows for potential expansion to include other hazards and sectors (e.g., windstorms, wildfires, agriculture, ecosystems, etc.), while maintaining compatibility and comparability of results at various resolution levels, from global to local scales, allowing countries to carry out risk assessments with higher resolution with the same methodology.
- Probabilistic Approach: GIRI employs a fully probabilistic methodology, delivering probabilistic metrics and incorporating climate change through imprecise probability estimates. The incorporation of climate change modifies the underlying mathematical hypothesis of the risk model, making it necessary to transcend from probability theory to random sets theory. Notably, GIRI is the first global catastrophe risk assessment grounded in random sets.
- Incorporation of Socio-Economic Context: Recognizing the complexity of disaster risk, GIRI incorporates socio-economic context variables that exacerbate risk, offering insights into a country's resilience performance. This comprehensive view provides an operational picture of risk, thus enhancing risk awareness and resilience, allowing for meaningful comparisons and rankings among countries.
- Consideration of Non-Stationarity: GIRI goes beyond historical events by incorporating events that have not yet occurred. Specifically, for hydrometeorological hazards, the inclusion of modifications by climate change prevents the application of a stationarity hypothesis, challenging the assumption of constant hazard patterns. GIRI is the pioneering global catastrophe risk assessment to include non-stationarity in its model and results.

GIRI's model comprises three primary components: hazard, this component defines sets of mutually exclusive and collectively exhaustive events, covering all potential manifestations of hazards in each territory. As abovementioned, for hydrometeorological hazards, climate change modifications are considered; exposure: the collection of elements and components of infrastructure systems, including their replacement values; and vulnerability: This component relates hazard intensity to the cost of damage for individual elements within the infrastructure. Their appropriate combination using a catastrophe risk modeling process rooted in random sets theory, provides essential metrics like the Loss Exceedance Curve (LEC), the Probable Maximum Loss (PML) curve, and the Average Annual Loss (AAL). The AAL represents the sum of the product, for all the stochastic events considered in the loss model, of the expected losses

water supply sector, and the fluvial navigation sector. Consequently, this hazard is approached differently and was addressed in a separate stage of the project.

in a specific event and the annual occurrence probability of that event (Ordaz, 2000; Grossi & Kunreuther, 2005).

In brief, GIRI is a pioneering global risk assessment tool that integrates various hazards, sectors, and climate change effects, offering valuable insights into disaster risk and resilience for countries and territories worldwide.

Figure 1 shows the risk and resilience assessment framework (Cardona, 1986; Ordaz, 2000; Marulanda, 2013, Bernal et al., 2019). It becomes the basis for the definition of a system of indicators that emulates a *performance curve*, commonly used to express the infrastructure and operational view of resilience.

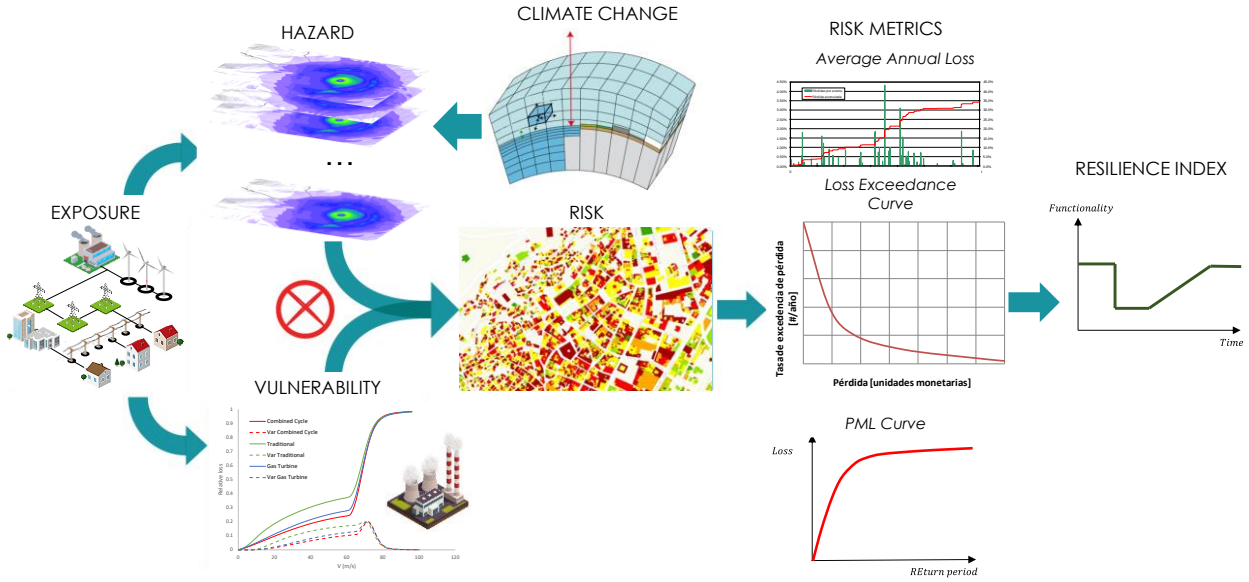

Figure 1. Illustration of GIRI's model components

1.2 Scope of the Model

As previously mentioned, GIRI is a multi-hazard risk model that assesses multiple infrastructure sectors, including power, roads and railways, transportation, communications, water and wastewater, oil and gas, education, health, and residential buildings (See Table 1).

GIRI's primary objective is to evaluate the performance of a system in the face of natural hazards, quantifying how each event affects the elements within the system. It's worth noting that the specific nature of the event (e.g., earthquake, flood, landslide) is irrelevant in the sense that it results in a measurable (modellable) perturbation on the system, ultimately leading to economic losses. This underscores the inherently multi-hazard nature of disaster risk, where multiple hazards contribute to a single overall disaster risk.

The calculation process is repeated for the entire set of hazard events across all considered hazards. Each event induces unique perturbations in exposure elements, defining a theoretical range of possible consequences. Using the appropriate arithmetic, individual losses are summed for each event, providing a comprehensive assessment of the hazard scenario's impact on the exposure portfolio. Additionally,

through the use of indicators, GIRI calculates how socioeconomic conditions exacerbate the system's vulnerability, offering an overall snapshot of the system's resilience.

Hence, GIRI's primary objective is to provide risk measures that systematically integrate relevant uncertainties. This enables decision-makers to make well-informed choices aimed at mitigating the potential consequences of hazard events. This, in turn, supports the formulation and execution of policies and strategies geared towards creating a safer environment and adeptly managing unforeseen circumstances.

Table 1. Hazards and sectors covered by the GIRI model[2]

Sector / Hazard		Energy			Highways			Railways			Transp.		Water and Wastewater			Comms.			Oil & Gas			Buildings				
		Generation	*Transm.*	*Distribution*	*Roads*	*Bridges*	*Tunnels*	*Tracks*	*Bridges*	*Tunnels*	*Airports*	*Seaports*	*Water delivery*	*Wastewater collection*	*Wastewater treatment*	*Wireline services*	*Wireless services*	*Submarine cables*	*Exploitation*	*Production*	*Distribution*	*Residential*	*Government*	*Industry*	*Health*	*Education*
EQ		■	■	■	■	■	■	■	■	■	■	■	■	■	■	■	■	■	■	■	■	■	■	■	■	■
TS		■	■	■	■	■	■	■	■	■	■	■	■	■	■	■	■	■	■	■	■	■	■	■	■	■
TC	C	■	■	■	■	■	■	■	■	■	■	■	■	■	■	■	■	■	■	■	■	■	■	■	■	■
	B	■	■	■	■	■	■	■	■	■	■	■	■	■	■	■	■	■	■	■	■	■	■	■	■	■
FL	C	■	■	■	■	■	■	■	■	■	■	■	■	■	■	■	■	■	■	■	■	■	■	■	■	■
	A	■	■	■	■	■	■	■	■	■	■	■	■	■	■	■	■	■	■	■	■	■	■	■	■	■
	B	■	■	■	■	■	■	■	■	■	■	■	■	■	■	■	■	■	■	■	■	■	■	■	■	■
EQ-LS					■			■																		
RN-LS	*C*				■			■																		
	A				■			■																		
	B				■			■																		

[2] As for the hazard/sector combinations, for earthquakes and tsunami, as well as for tropical cyclones and floods, including the effect of climate change, all the combinations are covered, as shown by the squares in each cell in Table 1. Whereas for landslides, both earthquake and rain triggered, the assessment is only performed on the roads and railway tracks of the world, where it makes more sense. Finally, the match between landslides and other infrastructure sectors is not as well represented in this model due to scale constraints.

2 Probabilistic Approach to Climate-Influenced Catastrophe Risk

A fully probabilistic approach to the risk problem, from an actuarial point of view, was first proposed by Filip Lundberg in his famous doctoral thesis of 1903 (Lundberg, 1903). Around 1930, Harald Cramér formalized Lundberg's theory into what today is known as *Ruin Theory* (Cramér, 1930). Lundberg defined an income-outcome model in which an insurance company starts its operation with a certain capital amount, which increases over time as premiums are collected. Moreover, losses (that the company must cover) occur randomly in time. If due to the payment of claims, the capital falls below zero, then the company faces bankruptcy.

Certainly, ruin theory considers (as it is natural) that the occurrence of claims is not deterministic. Lundberg proved that the occurrence of losses in time can be modelled as a *Poisson process*. In fact, any renewal process[3] is valid within ruin theory (Sparre Andersen, 1957). A Poisson process is a stochastic point process, widely used in multiple applications in science and engineering, that sets the occurrence of events in a totally random way. The events, within this context, do not refer to hazardous events but to the occurrence of losses, independent from their origin. This is the reason why ruin theory is suitable for any phenomenon, natural or not.

The Poisson process is defined in terms of a unique parameter, its intensity, or rate. In risk assessment, this parameter is the *loss exceedance rate*. It is the inverse value of the average time between the occurrence of events that exceed a loss amount p. Therefore, when calculating risk on a portfolio of exposed elements (i.e. the probability that a certain loss p is exceeded within a time window), its exceedance rate $v(p)$ must be calculated as a function of the probability of occurrence of any of the possible hazardous events that will cause the exceedance of p. This configures a Poisson process which enables the estimation of the probability of exceedance of loss p in any time frame.

As expected, the assessment of the exceedance rates $v(p)$ is not limited to a unique value of p. Therefore, the *Loss Exceedance Curve* (LEC) is calculated (i.e. $v(p)$ is calculated for any p). The LEC provides an exhaustive quantification of the risk problem, in terms of probability. It will never be possible to know the exact magnitude of a future disaster (in terms of the loss and consequences that will cause), but it is possible with the LEC to know the probability that any loss amount will be exceeded within any time frame and use this information to support the decision-making process for risk reduction. The LEC is recognized to be the most robust tool for representing catastrophe risk (Cardona 1986, Ordaz 2000).

2.1 Prospective Assessment of the Loss Exceedance Curve

When undertaking a probabilistic catastrophe risk analysis, the relevant components of risk, which include the exposed assets, their physical vulnerability, and the hazard intensities, must be represented in such a way that they can be consistently estimated through a rigorous and robust procedure, in both analytical and conceptual terms. The probabilistic risk model is comprised of three components, as follows:

[3] A renewal process is a type of time-continuous, increasing, point process in which the inter-event times are mutually independent and identically distributed random variables, with an expected value equal to the inverse of the mean occurrence rate.

- *Hazard assessment*: For each of the natural phenomena considered, a set of events is defined along with their respective frequencies of occurrence, forming an exhaustive representation of hazard. Each scenario contains the spatial distribution of the probability parameters to model the intensities as random variables.
- *Exposure assessment*: An inventory of the exposed assets must be constructed, specifying the geographical location of the asset, its replacement value or fiscal liability cost, and its building class.
- *Vulnerability assessment*: For each building class a vulnerability function is defined, for each type of hazard. This function characterizes the structural behavior of the asset during the occurrence of the hazard event. Vulnerability functions provide the probability distribution of the loss as a function of increasing hazard intensity.

Because the occurrence of hazardous events cannot be predicted, it is common practice to use sets of scenarios, obtained as an output of the hazard model. The set of scenarios contains all the possible ways in which the hazard phenomenon may manifest in terms of both frequency and severity. Event-based probabilistic risk assessments have been extensively applied in the past for different hazards at different scales (see, for example, Bernal et al. 2019, Bernal et.al. 2017a, Bernal et.al. 2017b, Salgado-Gálvez et al. 2017, Salgado-Gálvez et al. 2015, Cardona et al. 2014, Salgado-Gálvez et al. 2014, Wong, 2014, Niño et al. 2014, Quijano et al. 2014, Torres et al. 2013, Jenkins et.al. 2012). The calculation of the LEC follows the next sequence of steps:

2.1.1 Step 1: Loss in a single exposed element

The intensity occurring at the location of an exposed element, and the loss caused, are both random variables. The relationship between hazard (intensity *a*) and vulnerability (loss *p* given intensity *a*), for a single exposed element, is modeled by applying the total probability theorem, integrating for the complete dominium of the intensity:

$$f_P(p) = \int_0^\infty f_A(a) \cdot f_P(p|a) \cdot da \qquad \text{Eq. 1}$$

Where $f_P(p)$ is the probability density function (pdf) of the loss, $f_A(a)$ is the pdf of the intensity at the location of the exposed element, and $f_P(p|a)$ is the intensity-dependent pdf of the loss at the exposed element. Note that the integral covers the full dominium of the intensity, so there is no need to perform simulations of the intensity field for each scenario.

2.1.2 Step 2: Scenario loss

Step 1 is repeated for all the elements in the portfolio. If the individual losses of the exposed elements were independent, then the pdf of the total loss would simply be the successive convolution of the individual loss pdfs (rendering a Normal distribution according to the central limit theorem). However, it is recognized that there is a certain amount of correlation between the losses for the same scenario. Under this condition, the total loss is modeled by adding the probability moments of the individual losses.

$$m_P = \sum_{j=1}^{NE} m_{Pj} \qquad \text{Eq. 2}$$

and,

$$\sigma_P^2 = \sum_{j=1}^{NE} \sigma_{Pj}^2 + 2 \sum_{\substack{k=1 \\ k<j}}^{NE-1} \sum_{j=2}^{NE} \rho_{k,j} \sigma_{Pk} \sigma_{Pj} \qquad \text{Eq. 3}$$

Where m_{Pj} and σ_{Pj}^2 are the mean and variance of the j^{th} exposed element, $\rho_{k,j}$ is the correlation coefficient of the loss in elements *k* and *j*, *NE* is the total number of exposed elements and m_P and σ_P^2 are the mean and variance of the total scenario loss. There is no general methodology to determine the value of ρ. In practice, each modeler chooses its value by observing the coherence of the results. A commonly used, blanket value is 0.3. From the probability moments of the total scenario loss, a *Beta* distribution is parametrized (see, for example, ATC-13, 1985). The choice to use a Beta distribution to describe the loss, however arbitrary, is based on three properties that make it very convenient for this purpose:

- Its dominium is the interval [0,1], i.e., it directly fits into the description of a relative loss.
- It accommodates multiple shapes, showing different mode locations (left-sided, symmetrical, right-sided), and even adopting an exponential-like form (both increasing and decreasing).
- It is characterized by only two parameters.

2.1.3 Step 3: Totalize the loss

Step 2 is repeated for all hazard scenarios so that a set of loss pdfs is obtained, each corresponding to the total loss for a single scenario. To totalize the effect of all scenarios, the total probability theorem is used in the same way as Equation 4.

$$v(p) = \sum_{j=1}^{N} P(P > p | Event_i) \cdot F_A(Event_i) \qquad \text{Eq. 4}$$

where $v(p)$ is the rate of exceedance of loss p, N is the total number of hazard scenarios, $F_A(Event_i)$ is the annual frequency of occurrence of the i^{th} hazard event, and $P(P > p | Event_i)$ is the probability of exceeding p, given that event i occurred. The sum of the equation is made for all hazard scenarios. Figure 2 summarizes the calculation process.

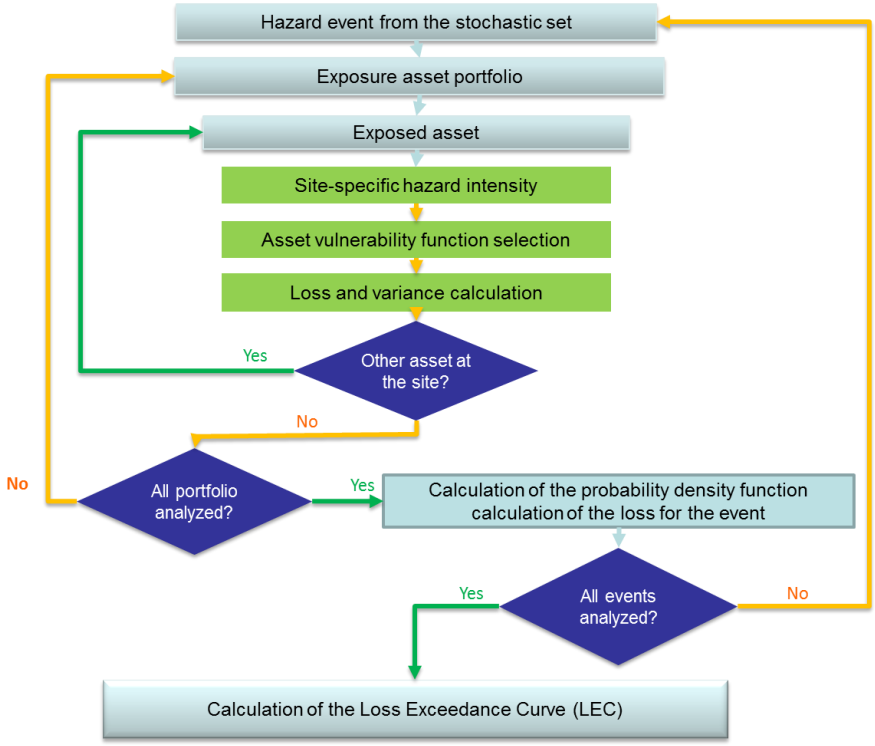

Figure 2. Flowchart of probabilistic risk assessment process.

2.2 Risk Metrics

As indicated above, the LEC contains all the information required to characterize the process of occurrence of losses. However, it is sometimes impractical to use the complete curve. Instead, it is convenient to use specific metrics that allow the risk to be expressed by a single number. The most used metrics are described next.

2.2.1 Probable Maximum Loss (PML)

This is a loss that does not occur frequently, that is, a loss usually associated with long return periods (or, alternatively, a low exceedance rate). The *return period* is the inverse of the exceedance rate (i.e. is the expected value of the inter-event times):

$$Tr(p) = \frac{1}{v(p)} \qquad \text{Eq. 5}$$

There is not a single PML value, but a complete curve which is analogous to the LEC. However, it is common practice to define a PML value by fixing a return period. There are no universally accepted standards to define what is meant by "not very frequently". In the insurance industry, for example, the return periods used to define the PML ranges from 200 up to 2,500 years.

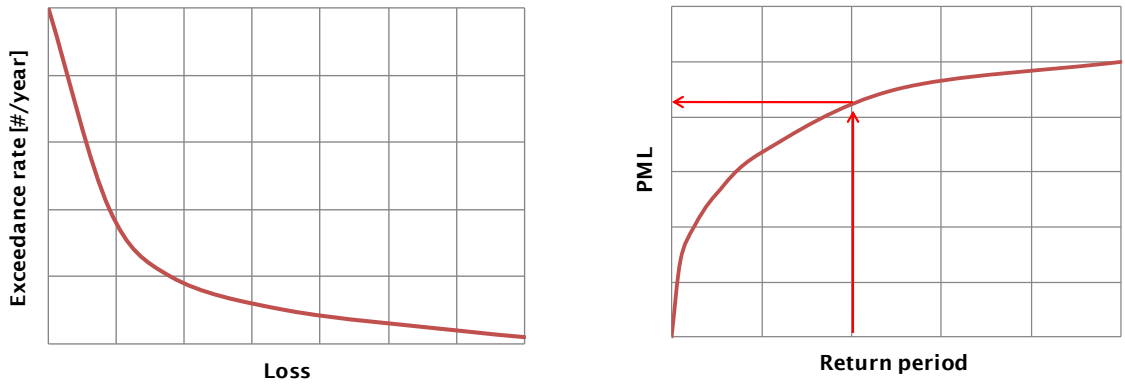

Figure 3. Risk curves. Left: in terms of the exceedance rate (Loss Exceedance Curve). Right: in terms of the return period (PML curve). Note that the value of the PML requires an arbitrary selection of the return period.

2.2.2 Average Annual Loss (AAL)

The Average Annual Loss (AAL) is an important indicator because it integrates into a single value the effect, in terms of loss, of the occurrence of hazard scenarios over vulnerable exposed elements. It is considered as the most robust risk indicator, not only for its ability to resume the loss-time process in a single number but for having low sensitivity to the uncertainty.

The AAL corresponds to the expected value of the annual loss. Indicates the annual value to be paid to compensate in the long term all future losses. In a simple insurance scheme, the AAL would be the annual pure premium. It is calculated as the integral of the loss exceedance curve,

$$AAL = \int_0^\infty v(p)dp \qquad \text{Eq. 6}$$

From the set of loss events, AAL can be calculated as,

$$AAL = \sum_{i=1}^{N} E(p|Event_i)\, F_A(Event_i) \qquad \text{Eq. 7}$$

where $E(p|Event_i)$ is the expected value of the loss given the occurrence of the event i. Furthermore, in those cases in which the hazard is not expressed as a set of scenarios, but as a collection of uniform hazard maps, despite the impossibility to fully assess risk, it is possible to calculate the AAL as:

$$AAL = \sum_{i=1}^{NE} \int_0^\infty -\frac{1}{v(0)} \frac{dv(a)}{da} E(p|a)da \qquad \text{Eq. 8}$$

Where the quantity $E(p|a)$ is obtained from the vulnerability functions of the exposed elements. The AAL is the only mappable risk metric. Risk maps are a remarkably effective communication tool. High-resolution AAL maps, both absolute and relative (to the exposed value of each asset), are highly desirable outcomes to orient risk management. Figure 4 presents an example of AAL maps for Bogotá, Colombia.

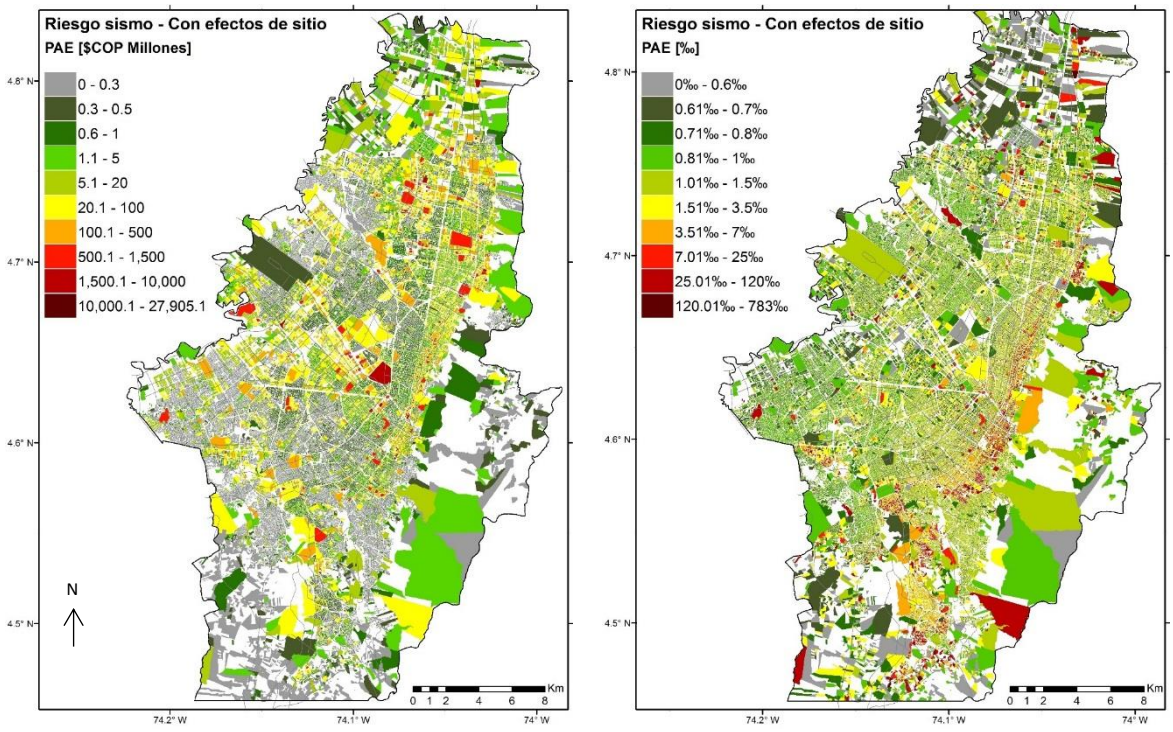

Figure 4. Maps of multi-hazard (earthquake and landslide) AAL for Bogotá, Colombia. Left: absolute; Right: relative. The exposure database has more than 1 million buildings. (From Cardona et.al. 2016)

2.2.3 Other Metrics

In addition to the abovementioned metrics, many results may be obtained from the LEC by the direct application of the Poisson point process that describes the loss occurrence in time.

2.2.3.1 Probability of Ruin

A commonly used metric in insurance is the probability of ruin. It is defined as the probability of exceeding a reference PML in an operational period. In general, the probability of exceeding a loss amount *p* at least once in *T* years, is:

$$P(P > p) = 1 - e^{-\nu(p)\cdot T} \qquad \text{Eq. 9}$$

Equation 13 has the advantage of being a standard formula. Only by knowing the return period of the loss and the operational time window (or exposure time) is it possible to calculate its exceedance probability.

2.2.3.2 Inter-Event Times

In many risk applications, it is necessary to make inferences on the time between loss events. The pdf of the inter-event times is:

$$f_T(t) = \nu(p)e^{-\nu(p)t} \qquad \text{Eq. 10}$$

This is particularly useful when testing the effectiveness of land use or risk management plans which are usually executed gradually in the short and medium-term.

2.2.3.3 *Number of Events*

In many risk applications, it is necessary to make inferences on the number of loss events expected to occur in a fixed time window. The probability mass function of the number of events in time window *T* is:

$$p_N = \frac{(\nu(p) \cdot T)^N e^{-\nu(p) \cdot T}}{N!} \qquad \text{Eq. 11}$$

This is particularly useful when designing risk management instruments that require reinstallations. For example, some financial protection instruments, as well as some structural protection devices are commonly designed considering reinstallations.

2.2.3.4 *Next Event*

It is possible to estimate the probability of exceeding loss *p* in the next event (or any randomly selected event):

$$Pr(P > p) = \frac{\nu(p)}{\nu(0)} \qquad \text{Eq. 12}$$

This result is quite useful for emergency preparedness activities, as well as for quantifying the cost of financial instruments and mitigation strategies.

2.3 Incorporating Background Trends

Stationarity in the occurrence of hazard events is an important assumption for risk assessment, one inherited directly from Lundberg's theory. Although this is hardly the case, it is widely accepted as the best approximation due to the difficulty to incorporate time-dependent hazard, exposure and vulnerability models, and the large uncertainty arising from incorporating them. Nevertheless, in cases in which, to the extent of knowledge, the stationarity condition is far too unrealistic, and the future dynamics of the risk components are known or can be approximated reasonably, it is possible to extend the model to a non-stationary process.

Consider a LEC resulting from a probabilistic risk assessment. This result is expressing the possibility of loss given the incidence of hazard, exposure and vulnerability, as modeled for a specific moment in time. If there is a reasonable way to model the changes of these risk components in time, it is possible to calculate new LECs for different, future dates. Therefore, the LEC now exhibits a time dependency, transforming into a Loss Exceedance Surface (LES, see Figure 5). The LES, constructed from the LECs of future conditions, contains all the $\nu(p,t)$ functions required to define the occurrence in time of losses greater than *p* as a *non-homogeneous Poisson process*.

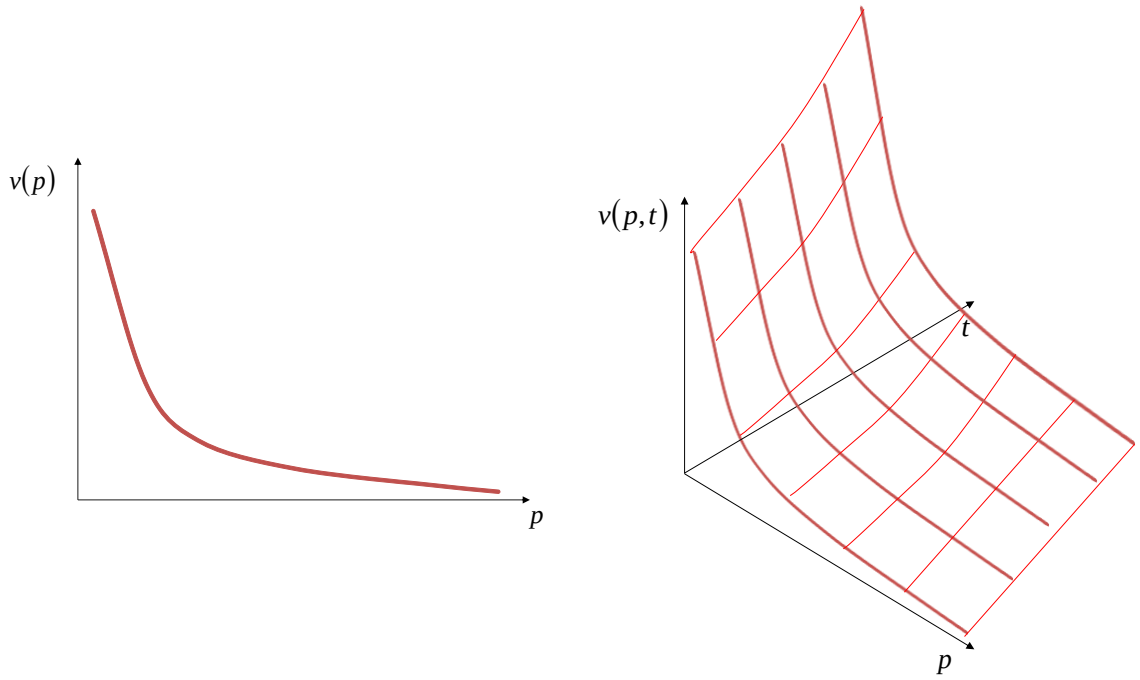

Figure 5. Time dependency added to the loss exceedance rates. Left: loss exceedance curve; Right: loss exceedance surface

A non-homogeneous Poisson process satisfies the same basic properties of a homogeneous one, i.e. independent and Poisson distributed increments. The main difference is that the rate of the process is a function of time, $v(t)$. For an overview of the non-homogeneous Poisson process, the reader is referred to Kirgman (1992). Note that when assessing disaster risk as an LES, the following properties hold:

- The loss occurrence process is still stochastic.
- The mean rate of the process changes in time.
- All risk metrics (AAL, PML, etc.) are functions of time.

The latter means that single-valued metrics, as the AAL, are no longer single-valued. This implies losing some of the desirable characteristics of condensed, comprehensive metrics. To obtain single-valued metrics, a simple time average is required, with an arbitrary choice of its limits.

2.4 Incorporating Climate Change

This approach works very well when incorporating climate change into risk calculations. For example, Figure 6 and Figure 7 show time-dependent risk metrics, calculated from probabilistic risk assessment to Puerto Barrios, Guatemala (due to tropical cyclones) and to the wheat stock of Kazakhstan (due to droughts), and including the effect of climate change (up to 2050)[4]. In both cases the time-dependent loss exceedance rates $v(p,t)$ were calculated for different moments in time, allowing for an estimation of the time-dependency of v, and therefore increasing the applicability of the risk assessment methodology.

[4] In both cases for RCP 8.5 and selecting the climate model that best fits the historical observations.

Furthermore, the inclusion of climate change as a background trend of the risk process provides a unique mathematical framework for both risk management and climate change adaptation.

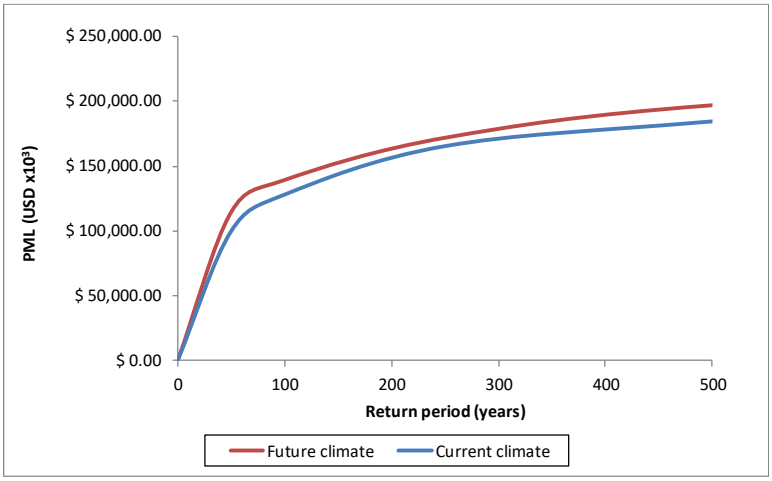

Figure 6. Time dependent PML curves for Puerto Barrios, Guatemala, due to tropical cyclones and the effect of climate change. (From Cardona et.al. 2013)

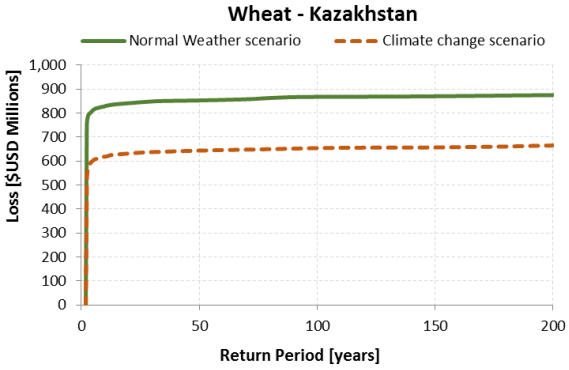

Results		Normal Weather	Climate Change
Exposed value	USD Millions	$1,621	
Annual Average Loss	USD Millions	$361	$260
	%	22.3%	16.0%

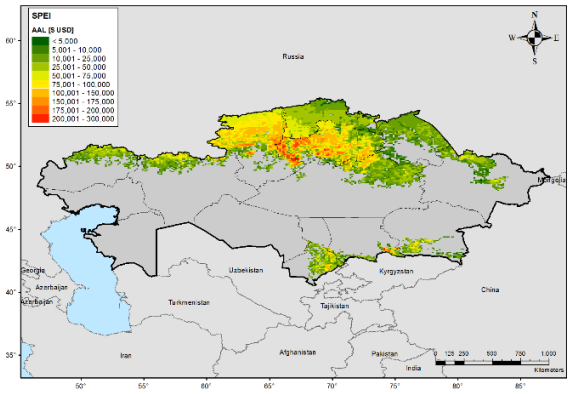

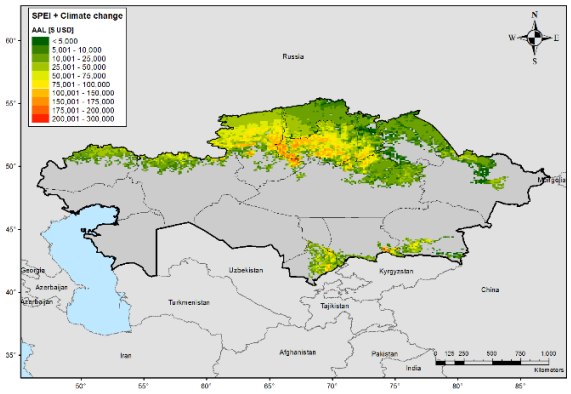

Figure 7. Time dependent risk metrics for wheat in Kazakhstan due to droughts and the effect of climate change. (From Maskrey et.al. 2019)

Introducing background trends into probabilistic risk assessment requires complex models of the future dynamics of hazard, exposure, and vulnerability. Even though these models may exist, they should be introduced with care, keeping in mind the additional uncertainty brought into. Such uncertainty is extremely difficult to model from the probabilistic point of view, being commonly referred to as *deep uncertainty*. An overview of the treatment of deep uncertainty is presented in the next section.

2.5 Dealing With Deep Uncertainty

The future characteristics of the built environment, the dynamics of the socio-technical systems, or the exact conditions of the future climate are desirable inputs for risk modelling, useful for designing the actions and policies to anticipate the materialization of risk. However, knowing with arbitrary precision how non-stationary natural phenomena, exposed elements, and their vulnerability will change in the far, or even near future, is practically impossible. Furthermore, assigning any kind of probability model to such dynamic and complex behavior is extremely difficult without arbitrariness.

Most of the variables involved in probabilistic risk assessment fit well into probability models. It is even possible to insert background trends into the calculation, keeping the problem within the reach of probability theory. Nevertheless, it must be recognized that in the process of building a risk model, many assumptions are made, based on expert criteria and common sense, but inevitably rendering a model that is not truly "fully probabilistic". However, within good modelling practice, all the assumptions made are sufficiently trustworthy so, again, the problem fits into a fully probabilistic approach.

But what happens when incorporating a new variable from which there cannot be made any reasonable point assumptions, there is no observed data (or not enough), it is not possible to truly predict its behavior from physical models, and there is no bounded consensus on how it will perform? This configures a problem with *deep uncertainty*.

In a broad sense, uncertainty is inherent in any approach to model complex dynamical systems. It can be understood as the gap between the outcome of the model and the real behavior of the system. This gap is composed by the uncertainty on the available observations, the estimation of model parameters, the functional form of the model itself (typically simplifying the phenomena), the value of model inputs, the transformations of scale (commensurability) and the natural randomness. The latter is usually referred to as *aleatory* uncertainty. All the other mentioned sources compose the *epistemic* uncertainty. It is widely recognized that epistemic uncertainty is reducible as more data or knowledge is added to the problem. However, deep uncertainty, which holds both aleatory and epistemic uncertainty, is exceedingly difficult to reduce. In practice it would require, for example, waiting until the future conditions of the assets at risk are known, which invalidates the purpose of risk assessment and overthrows any planning attempt.

Dealing with deep uncertainty in risk assessment requires an expansion of the methodological approach. Recently, several authors have proposed innovative approaches to deal with problems with deep uncertainty and orient decision making, grouping them under the name *Decision Making under Deep Uncertainty* (DMDU). For further details, the reader is referred to Marchau et.al. 2019. All DMDU approaches share key methodological steps: 1) framing the analysis, 2) simulation, 3) exploration of results, 4) analysis of compensations (tradeoffs) of strategies and 5) iteration and reexamination. In short, DMDU methods recognize that it is not possible to achieve robust decision making without considering

the multiple ramifications that define the domain of the future possibilities. But how to reasonably define those ramifications or paths of the risk problem?

Step 2 of DMDU approaches (simulation) is strongly related to risk assessment. Its purpose is to explore possible unforeseen or uncertain futures. In other words, robust decision making must be based on the universe of all possible outcomes that a problem with deep uncertainty can evolve into, to consider them all when deciding. Probabilistic risk theory follows a similar approach, seeking to quantify the consequences of all possible future catastrophic events (without the need to know which will be next) to consider those consequences in the decision-making process. Therefore, as far as disaster risk management respects, probabilistic risk assessment is the most appropriate way to approach step 2, although some expansion of its analytical potential is required.

The main limitation of probabilistic risk assessment is precisely that of being probabilistic. Nonetheless, regardless of that limitation, it is a robust approach, good enough in most risk assessment applications. As models evolve and gain complexity, more variables are added that not necessarily fit into a probabilistic representation. In the past decades, many mathematical theories have arisen as an attempt to formally conceptualize the treatment of *non-probabilistic* uncertainty problems. In the 1960s, Zadeh proposed the *fuzzy set theory* as an approach to deal with epistemic uncertainty, allowing the representation of concepts expressed by linguistic terms. A few years later, Dempster (1967) develops what today is known as *Dempster-Shafer evidence theory* (formalized by Shafer, 1976), seeking the representation of epistemic knowledge on probability distributions and, in the process, relaxing some of the strong rules of probability theory. In parallel, and within the context of stochastic geometry, Kendall (1974) and Matheron (1975) developed the foundations of what is nowadays known as the *random sets theory*. In short, random sets theory deals with the properties of set-valued random variables (in contrast to point-valued random variables in probability theory). In 1991, Peter Walley introduces the *theory of imprecise probabilities*, in which sets of probability measures are explored as a more general case of the classical probabilistic approach to random variables. Other theories to give formal treatment to non-probabilistic uncertainty have appeared recently. It is worth mentioning the *theory of hints* (Kohlas et.al. 1995), the *info-gap theory* (Ben-Haim, 2001), and the *theory of fuzzy randomness* (Möller and Beer, 2004).

From the above-mentioned approaches, random sets theory excels as the most general approach to uncertainty to date, allowing many different types of uncertainty structures (e.g. Dempster-Shaffer bodies of evidence, info-gap structures, probability boxes, raw intervals, fuzzy sets, probability distribution functions, among others) to be represented as random sets. Alvarez (2008) proved that *infinite random sets of the indexable type* can accommodate all these uncertainty structures. Furthermore, he developed a general method to sample values from all these types of uncertainty structures indistinctively. Therefore, the theory of random sets, and particularly the methods developed by Alvarez (2008) for infinite random sets, provide a mathematically sound framework for the simulation of the ramifications or unforeseen futures in problems with deep uncertainty.

2.5.1 Random Sets

Consider the probability space $(\Omega, \sigma_\Omega, P_\Omega)$ and a universal non-empty set X with a power set $\wp(X)$. Let $(\mathcal{F}, \sigma_\mathcal{F})$ be a measurable space such that $\mathcal{F} \subseteq \wp(X)$. A random set Γ is a $(\sigma_\Omega - \sigma_\mathcal{F})$ – measurable mapping such that $\Omega \to \mathcal{F}, \alpha \to \Gamma(\alpha)$. Every $\Gamma(\alpha)$ is a *focal element* in the *focal set* $\mathcal{F}$.

If all elements in $\mathcal{F}$ are singletons (points), then Γ is a random variable, and therefore the probability of any event *F* in $\mathcal{F}$ is calculable via classic probability theory. Such focal set $\mathcal{F}$ is called *specific*. However, when $\mathcal{F}$ is *nonspecific*, the probability of event *F* cannot be precisely calculated, but only its upper and lower bounds, giving as result an *imprecise probability* measure. Upper (UP) and lower (LP) probabilities for event *F* are given by:

$$LP(F) = P_{\Omega}\{\alpha: \Gamma(\alpha) \subseteq F, \Gamma(\alpha) \neq \emptyset\} \quad \text{Eq. 13}$$

$$UP(F) = P_{\Omega}\{\alpha: \Gamma(\alpha) \cap F \neq \emptyset\} \quad \text{Eq. 14}$$

which means that the lower probability LP is the totalization of the probability or mass assignments of all the elements in $\Gamma(\alpha)$ contained in *F*, i.e., those that imply the occurrence of *F*. Upper probability UP is the total probability of the elements in $\Gamma(\alpha)$ that share at least one element with *F*, i.e., those that may or may not imply the occurrence of *F*. A complete overview of random sets can be found in Molchanov (2005).

2.5.2 Simulation

The process of simulation is performed by means of a Monte Carlo approach. Every variable is represented as a random set in the real line. Each may have a different treatment of the uncertainty, enabling the combination of random variables, fuzzy sets, bodies of evidence, intervals, etc. This may be the more general simulation approach to date.

Sampling from a random set is to randomly obtain focal elements from it, regardless of the type of uncertainty. To enable this process, an indexing procedure must be applied previously, so that the diversity of mathematical structures can be treated equally (α-*indexation*, see Alvarez 2008). Once indexed, it is possible to sample focal elements. Figure 8 shows an illustration of this process.

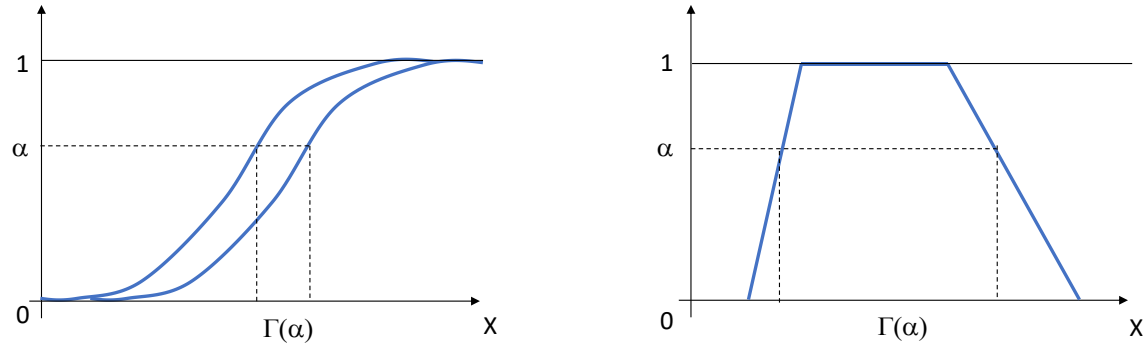

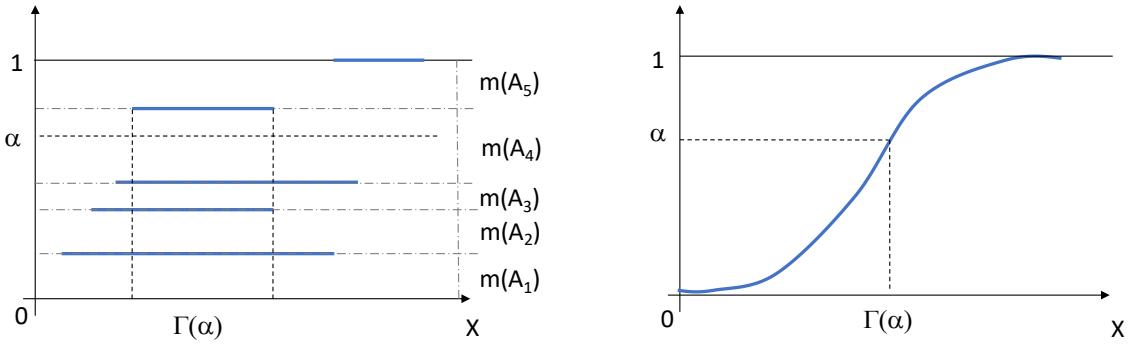

Figure 8. Sampling from α-indexed random sets. Upper left: probability box. Upper right: possibility distribution. Lower left: Dempster-Shafer body of evidence made of raw intervals. Lower right: Cumulative distribution function. (Reproduced from Alvarez 2008).

Note that $\Gamma(\alpha)$ is an interval in the dominium of *X.* If there are many variables involved in the problem, the same process can be applied to a coupled combination of the variables. Let *X* be the vector of all variables, then α becomes a space (the α-space). In such space, the dependence between variables is modeled by a couple, and the quasi-inverse sampling methods for couples can be used to sample the multi-dimensional focal elements (see Nelsen, 1999 for a comprehensive guide of coupled simulation techniques). Figure 9 shows an illustration of sampled focal elements in both the *X*-space and the α -space for the two-dimensional case (two variables). Note that in the *X*-space, the focal elements are multi-dimensional boxes, while in the α-space they are always points, regardless of the number of variables (dimensions).

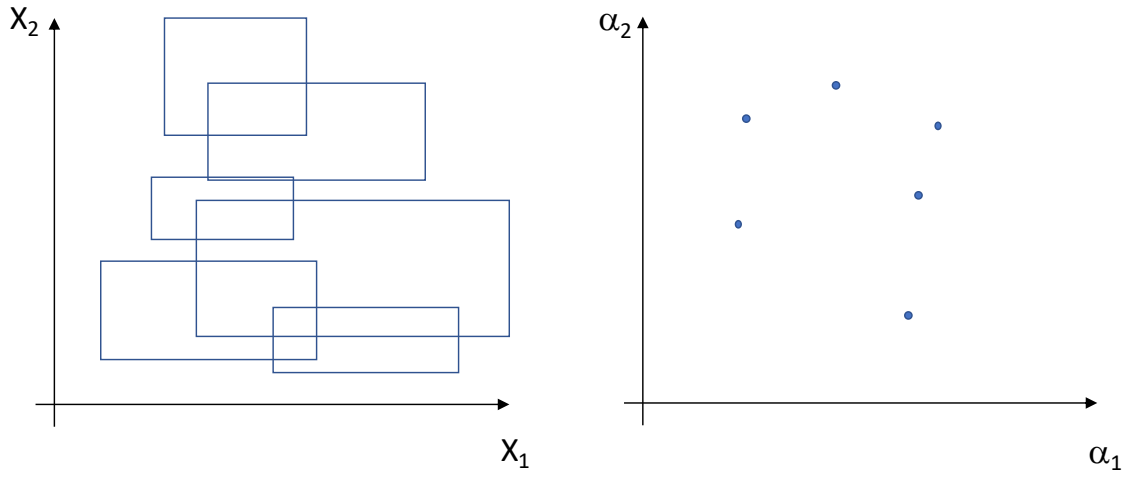

Figure 9. Focal elements for the two-dimensional case in the X-space and in the α -space. (Reproduced from Alvarez 2008).

2.5.3 Functional Propagation

Once the full set of focal elements is sampled, the response of the system must be evaluated. This is to calculate the image of the focal elements by applying on them a function describing the system response,

i.e., to propagate the random focal set. This is achieved by applying the *extension principle*[5] which states that given a function $g: X \to Y$ (the system response) and a random set $(\mathcal{F}, m)$, the image of $(\mathcal{F}, m)$ through g, denoted here as $(\mathfrak{R}, \rho)$ is:

$$\mathfrak{R} = \{R_j = g(A_i) : A_i \in \mathcal{F}\} \qquad \text{Eq. 15}$$

$$\rho(R_j) = \sum_{i=1}^{n} I[R_j = g(A_i)] m(A_i) \qquad \text{Eq. 16}$$

where $I[\cdot]$ is the *indicator function*[6]. A_i is a *d*-dimensional box in $\mathbb{R}^d$ with 2^d vertices obtained as the cartesian product of the finite intervals sampled from each variable in the *X*-space. For those systems in which there is not an explicit functional form for g (e.g. risk assessment), the extension principle can be sequentially applied as the process of calculation moves forward.

2.6 Calculation of the Loss

Each focal element contains a sampling of the input variables in a stage of the calculation. Getting to assess the loss requires a series of steps that are presented here. Note that these steps are the most general sequence for risk assessment. None of the particularities of, for example, hazard modelling, are included here because they are different for each hazard for obvious reasons. Nonetheless, each hazard model (and in general each component of the risk problem) would require similar approaches for the whole process to be consistent.

1. Sample the occurrence of the event.
2. Sample the intensity field. In some cases (e.g. earthquake hazard) this would require the definition of correlation parameters.
    2.1. At the location of the exposed elements, sample the focal elements of the local intensity.
    2.2. From the vulnerability function of each element, sample the loss caused by each focal element of the intensity.
        - *This requires coupled sampling of the intensity and loss (steps 2.1 and 2.2). An independence couple should suffice in most cases.*
    2.3. Repeat for all exposed elements and add their individual losses using the extension principle.
3. Repeat for all the intensity field simulations.
4. Repeat for all events.

[5] See Alvarez (2008) for a summary of techniques to practically apply the extension principle.

[6] $I[\cdot] = 1$ if $\cdot$ is true and $I[\cdot] = 0$ if $\cdot$ is false.

Note that this approach requires many simulations, making it costly in terms of computational resources. It is recommended to apply any of the many sampling optimization techniques usually implemented when performing Monte Carlo simulations.

Let $(\mathcal{L}, \ell)$ be the random set containing all the images of the loss calculations. Then $\mathcal{L}$ is the collection of loss focal elements (intervals) and $\ell(L_i)$ for $L_i \in \mathcal{L}$ is the mass assignment, i.e., the probability of occurrence of the event that generated the loss focal element. This representation requires a relaxation of the rules applied to mass assignments (rules established in evidence theory and usually transferred to random sets). Given that $\ell(L_i)$ is representing the annual occurrence frequency of the event that generated the focal element L_i, then the sum of mass assignments is not necessarily 1. In practice, this condition can be forced into $\ell(L_i)$ if required and for the sake of coherence; however, it seems unnecessary and may have no practical effect on the final outcomes. In any case, this is an issue that requires further analysis.

Let *F* be the event where the loss *P* exceeds the amount *p* (i.e. $F = \{P: P \geq p\}$) then by rewriting equation 8, upper and lower loss exceedance rates are obtained, i.e., the LEC is transformed into two complementary curves LEC_L (eq. 17) and LEC_U (eq. 18) that may be interpreted as an *imprecise loss exceedance curve*:

$$\nu(p)_L = \sum_{j=1}^{n} I\left[L_j \subseteq F\right] \cdot \ell\left(L_j\right) \qquad \text{Eq. 17}$$

$$\nu(p)_U = \sum_{j=1}^{n} I\left[L_j \cap F \neq \emptyset\right] \cdot \ell\left(L_j\right) \qquad \text{Eq. 18}$$

where *n* is the total number of focal elements in $\mathcal{L}$. Figure 10 shows an illustration of an imprecise loss exceedance curve. Note that all risk metrics now become imprecise. Background trends can still be incorporated by obtaining for every moment in time both LEC_U and LEC_L curves, i.e., rendering an *imprecise loss exceedance surface*.

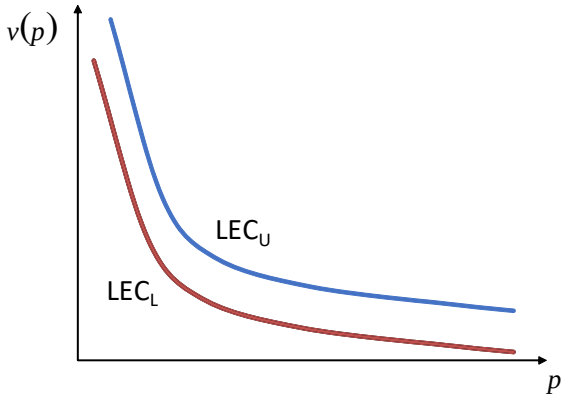

Figure 10. Illustration of an imprecise loss exceedance curve composed by curves LEC_L and LEC_U

3 Climate Model

The influence of climate change on the frequency and intensity of hydrometeorological hazards cannot be neglected. This means that hazard models for tropical cyclones, floods, landslides, and droughts only, must include the available and most up-to-date projections of how climate change will modify the weather patterns at the local level. To tackle this, projections of change in meteorological variables, taken from atmospheric global circulation models fed with the trajectories of emissions of greenhouses gases defined by IPCC in the Assessment Report 6, modify the meteorological forcing on the hazard models. These estimates are properly downscaled and bias-corrected against local observations.

However, the influence of climate change is an imprecise amount, as is illustrated in Figure 11 for an arbitrary location in South America. The further we look into the future, the less precise the range of projections becomes, adding further uncertainty to the risk assessment problem. For this project, the influence of climate change will be modeled as intervals, with lower and upper bounds, capturing the deep uncertainty associated with unknowing how the future climate will develop.

Several hazards are climate driven and often share common or correlated triggers. Several multi hazard studies assess the different hazard components in silos neglecting the fact that consistency is needed throughout the modelling framework to account for mutual dependencies. This is particularly true for floods, droughts, tropical cyclones and landslides that depend on the same climate engine. To overcome this limitation, this study uses the same meteorological and hydrological inputs to model all the afore mentioned hazards so that the statistical properties across hazards will be maintained consistent.

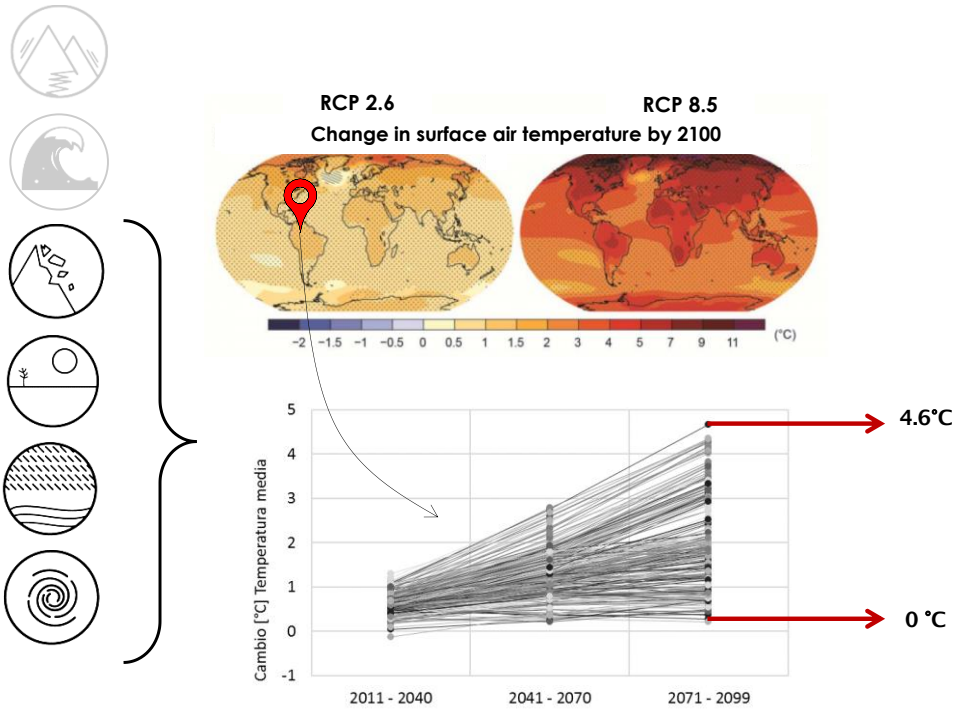

Figure 11. Illustration of the deep uncertainty associated with climate change projections.

4 Hazard Models

For this assessment, six hazards are considered: earthquake, tsunami, tropical cyclones, floods, landslides, and droughts. The latest is not expected to cause any physical damage to the infrastructure elements, so it will follow a somewhat different methodological approach. All the other five hazards will cause physical damage to some extent and were quantified in the model.

These natural hazards are represented as a collection of events. Each event is a single manifestation of the hazard (i.e., one tropical cyclone), that produces some intensity at the location of the infrastructure elements and has some probability of occurrence. The full set of events (i.e., all the simulated tropical cyclones) fully represents the way each hazard may occur.

In the following sections we will describe the different hazard models included in the GIRI.

4.1 Seismic Hazard Model

The seismic hazard at bedrock level is calculated based on historical information recorded in seismic catalogues. Using said information which is related to the magnitude and the location of the hypocenter of each earthquake, the intensity of the events is calculated by a set of stochastic scenarios, mutually exclusive and collectively exhaustive, each with a geographical distribution of probability. This is carried out considering the attenuation of the seismic energy with the distance, in the surroundings from where each event strikes. This evaluation thus gives us a curve of the probability of exceeding the acceleration in a point where certain exposed assets may be subjected. Given that said curve is obtained for each one of the points within the calculation grid, it is possible to calculate the seismic hazard maps for various spectral ordinates and return periods, in other words, according to the characteristics of the dynamic structural response from the exposed structures. This input is fundamental for the probabilistic risk assessment on the inventory of exposed elements conducted in countries with seismic hazard.

A more in-depth description about the global seismic hazard model used in this risk assessment can be found in CIMNE et al. (2012) and Cardona et. al. (2014). The main steps of the methodology followed to calculate the seismic hazard in a fully probabilistic way at global level with a probabilistic approach can be summarized as follows:

1) *Definition and characterization of tectonic regions:* based on geological and neo-tectonic information collected the Globe is divided into tectonic provinces. Each of these are then classified in one of 6 categories (explained below), and they are assigned a depth range and an earthquake maximum magnitude.
2) *Calculation of the seismicity parameters:* three different depth ranges are defined which represent shallow, intermediate, and deep seismicity, and the Globe is divided into a grid in which seismicity is calculated at each node. Based on the seismic catalogue and using a smoothed seismicity methodology, seismicity parameters are calculated (based on statistical methods) for each node of the different grids that have been assigned at different depths in the analysis.
3) *Generation of a set of stochastic set of scenarios:* based on the above-mentioned information, a set of feasible seismic events is generated through sampling of the seismicity parameters in each node. For each node, a set of scenarios is generated with different magnitudes, and whose probabilities of occurrence are obtained from specific magnitude recurrence curves for that point.

4) *Assignation of ground motion prediction equations:* tectonic environment compatible GMPEs are selected and assigned to each tectonic province based on the information collected, which includes previous studies on tectonic environment and the state of current knowledge of the relationships.
5) *Generation of hazard maps for representative events:* maps are generated with the spatial distribution of seismic intensities; since spectral ground motion prediction equations have been considered, hazard curves can be obtained for different spectral ordinates.

4.1.1 Seismic Hazard Maps

Seismic hazard maps were obtained after integrating hazard from the set of stochastic scenarios, for the following spectral ordinates: spectral acceleration at 0.0 sec, 0.2 sec, 0.5 sec, 1.0 sec and 2.0 sec, and for different return periods – 225, 475, 1,000 and 2,500 years. It is important to note that the results are given for intensities at bedrock level (Vs30=1,100 m/s); that is, the effect of local site effects or topographical factors, which in certain cities may be important, are not considered. Figure 12 shows an example of a seismic hazard map calculated for a 475-year return period and a spectral ordinate of peak ground acceleration (0.0 sec).

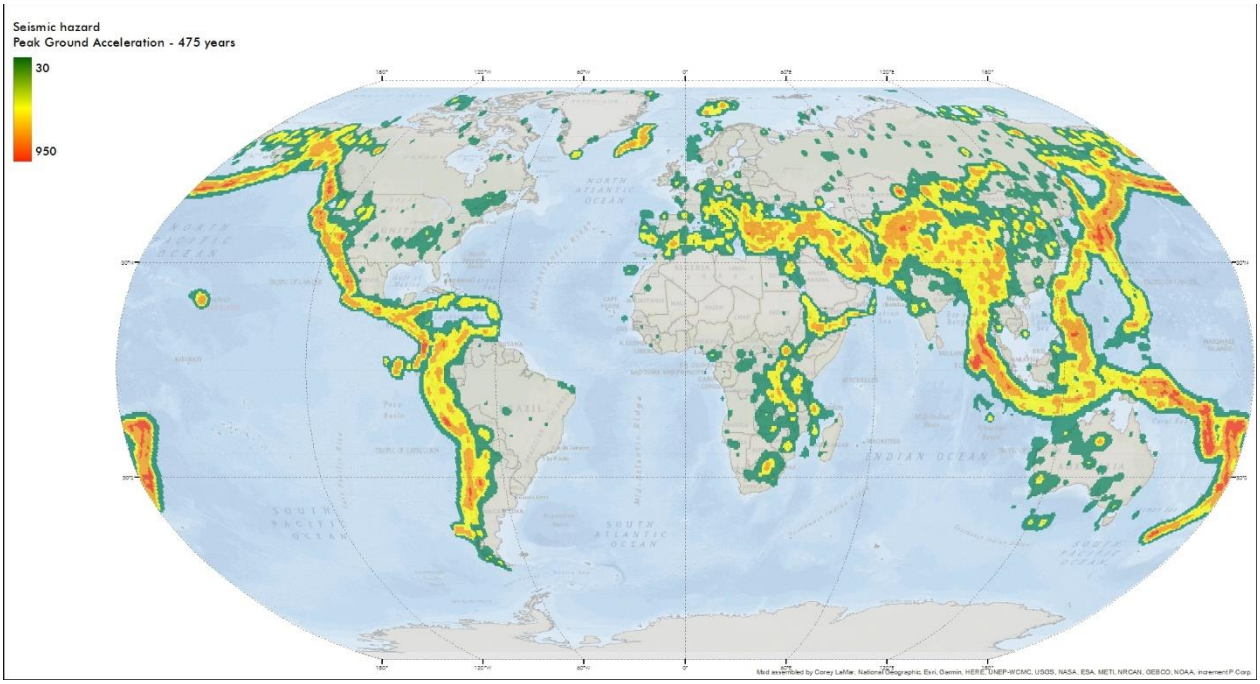

Figure 12. Seismic Hazard map for peak ground acceleration and 475-year return period

4.2 Tropical Cyclones Hazard Model

This hazard model was developed in the framework of the Global Assessment Report on Disaster Risk Reduction of 2015 (GAR15) for catastrophe risk analysis of all countries in the world and detailed information can be found in Cardona et al. (2014).

Hazard for both strong winds and storm surge was assessed for this project using as input an updated catalogue including 5,270 historical tropical cyclones from five different oceanic basins: Northeast Pacific, Northwest Pacific, South Pacific, North Indian, South Indian and North Atlantic. Completeness periods were calculated for each basin to determine the occurrence frequency of historical cyclones. For each historical track, a family of associated "children" tracks was obtained using a bi-dimensional Wiener process. Strong winds speed and storm surge flooding were calculated for each cyclone child track and the results were used to compute probability moments of wind speed and coastal flood for each historical track. The results are expressed, for the strong winds, in terms of the geographical distribution of the peak wind speed of 3-seconds gusts, and for the storm surge, as the distribution along the shorelines of the maximum surge run-up and its associated flooding. In both cases, intensities are modeled as random variables with a Gamma distribution. This analysis was repeated for all historical cyclones. The hazard assessment result is the set of probabilistic wind fields and storm surge floods.

4.2.1 Update of the Catalogue of Historical Tropical Cyclones

The tracks of historical tropical cyclones were obtained from the IBTrACS database (Knapp et al., 2010). This database represents the repository of information associated with tropical cyclones that is the most up to date.

The hazard analysis is divided in oceanic basins. The IBTrACS database contains cyclone records from 1842. Given the scarce number of records from 1842 to the middle of the 20th century, an analysis of the completeness of the number of cyclones recorded per year was carried out, with the aim of determining the cut-off year from which the database can be considered adequate and exhaustive. Following the analysis of the completeness, it is possible to determine the cut off year that is most appropriate for each one of the basins under analysis, value that is presented in Table 2. Figure 13 shows the tracks from the cut off year until 2022. A total of 5,270 historical cyclone tracks were included in the update of the hazard model for the existing climate.

Table 2. Cut-off year for each basin.

Basin	Cut-off year
Northeast Pacific Ocean	1951
South Pacific Ocean	1972
Northwest Pacific Ocean	1951
North Indian Ocean	1990
South Indian Ocean	1964
North Atlantic Ocean	1851

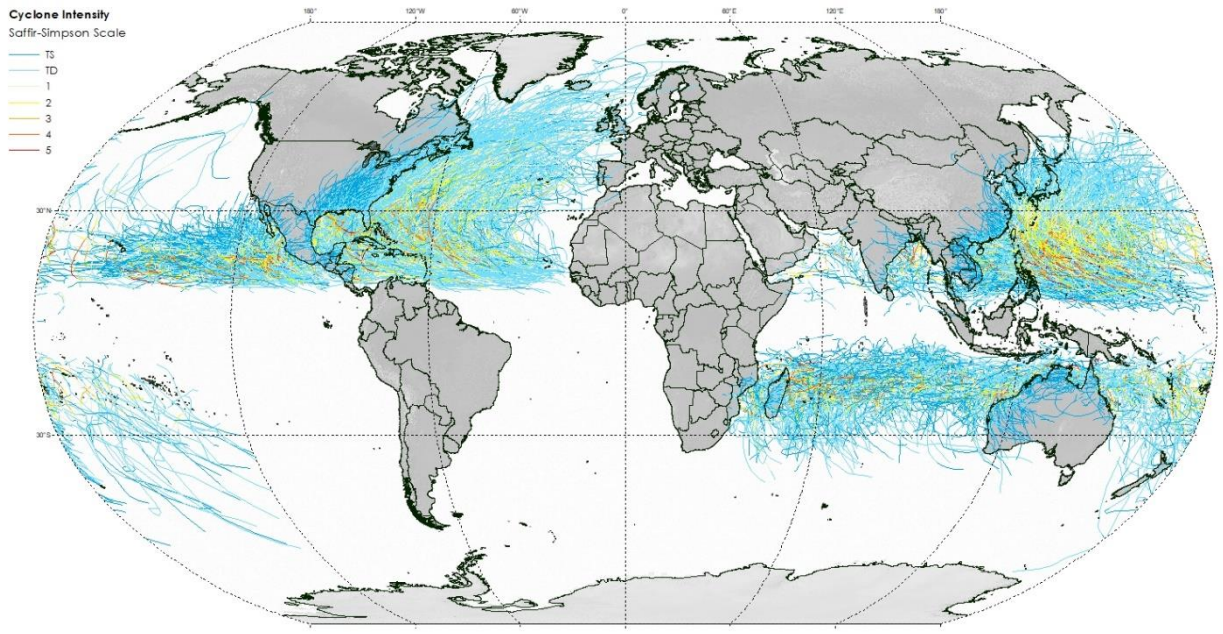

Figure 13. Cyclone tracks used in hazard modelling from IBTrACS

4.2.2 Tropical Cyclone Hazard Maps for Existing Climate

Figure 14 to Figure 19 present the hazard maps for 25, 50, 100, 250, 500 and 1000 years return periods for all basins under analysis for the existing climate case.

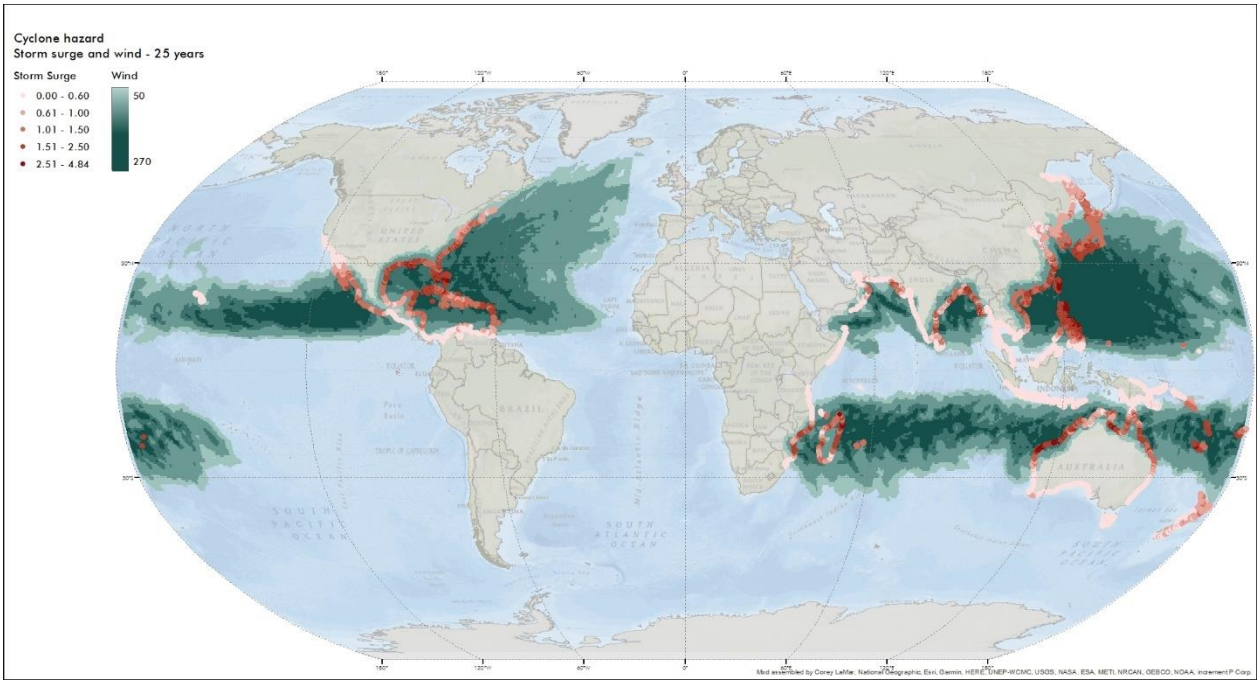

Figure 14. Tropical cyclone's strong winds and storm surge hazard map for 25 years return period.

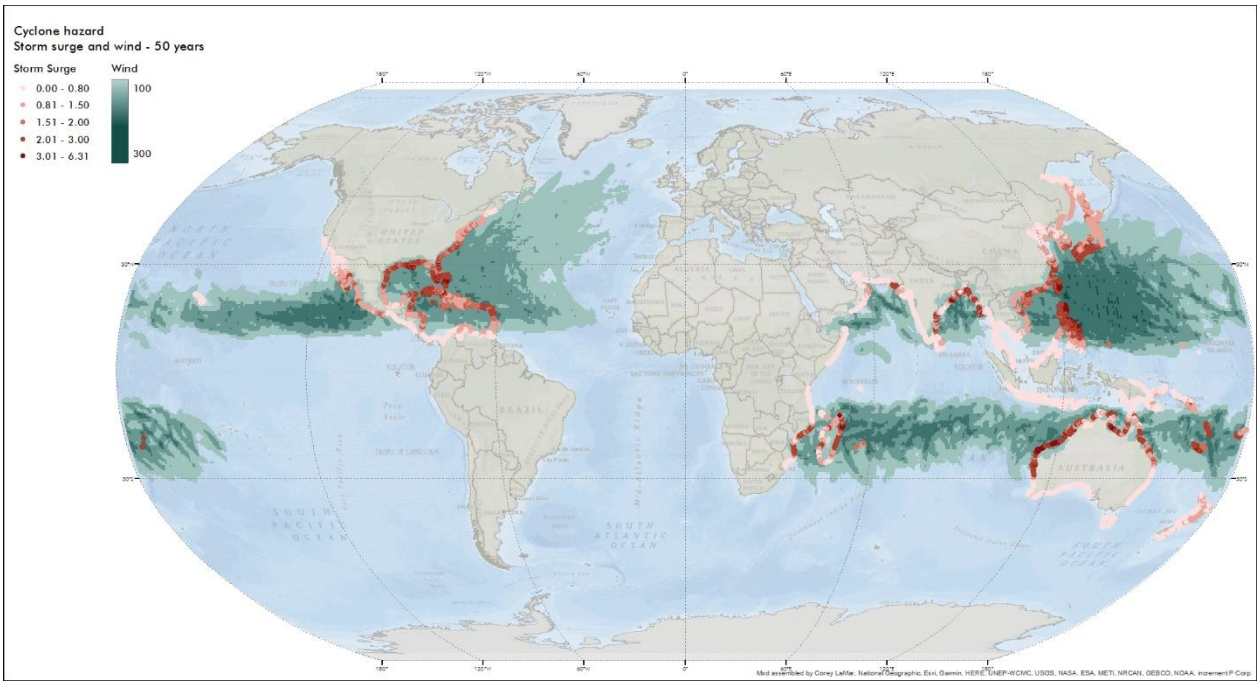

Figure 15. Tropical cyclone's strong winds and storm surge hazard map for 50 years return period.

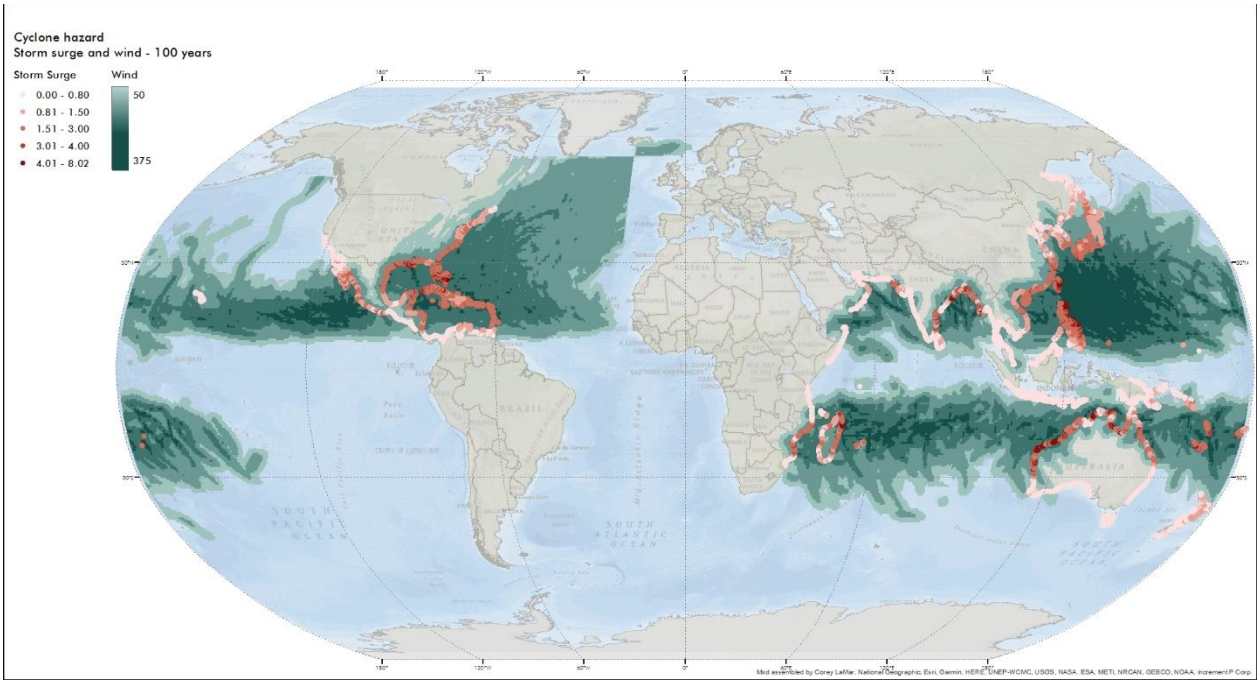

Figure 16. Tropical cyclone's strong winds and storm surge hazard map for 100 years return period.

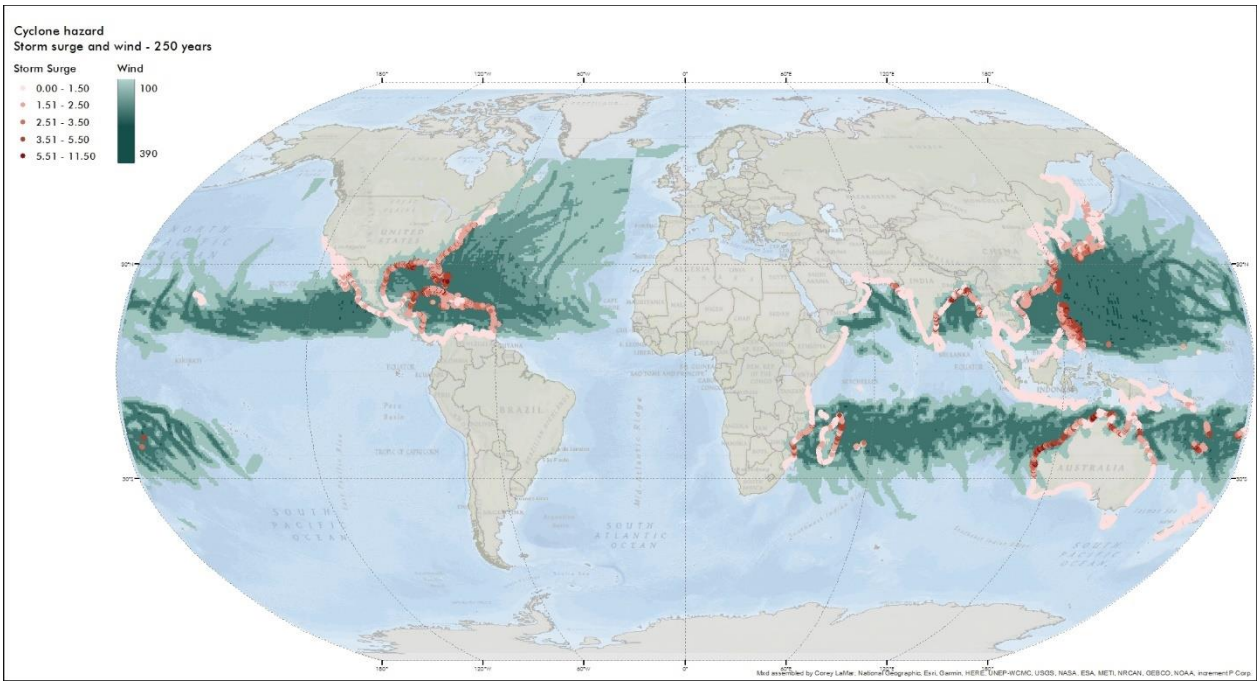

Figure 17. Tropical cyclone's strong winds and storm surge hazard map for 250 years return period.

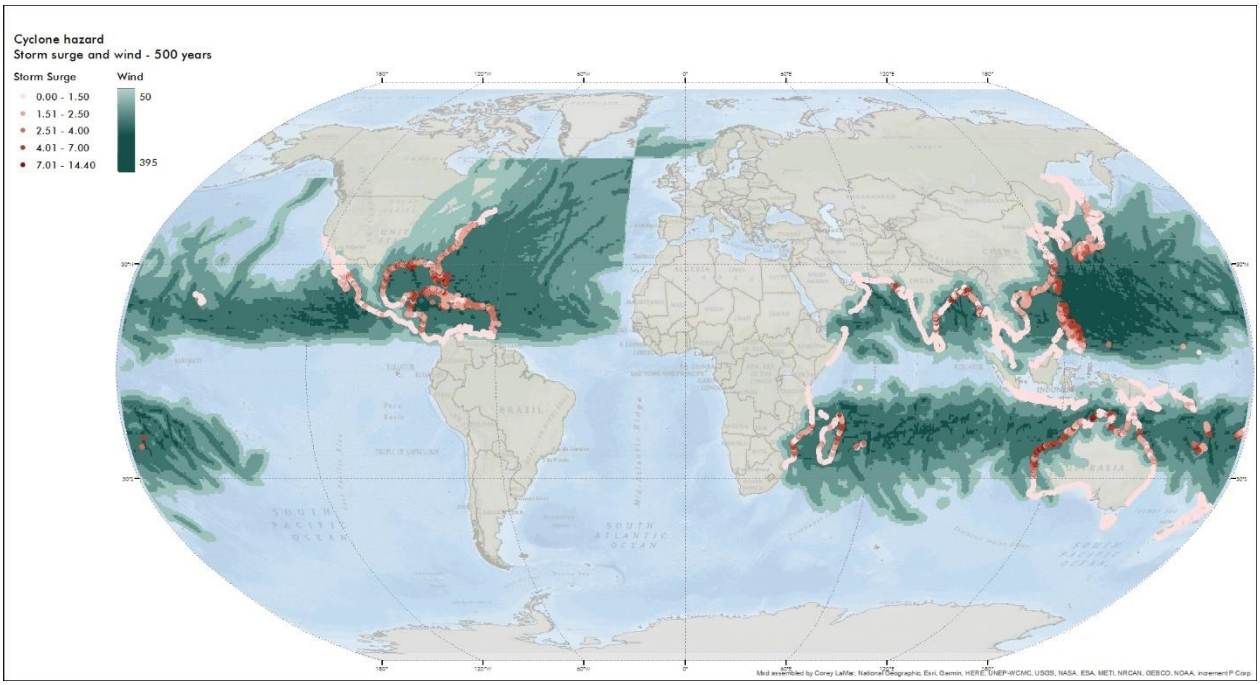

Figure 18. Tropical cyclone's strong winds and storm surge hazard map for 500 years return period.

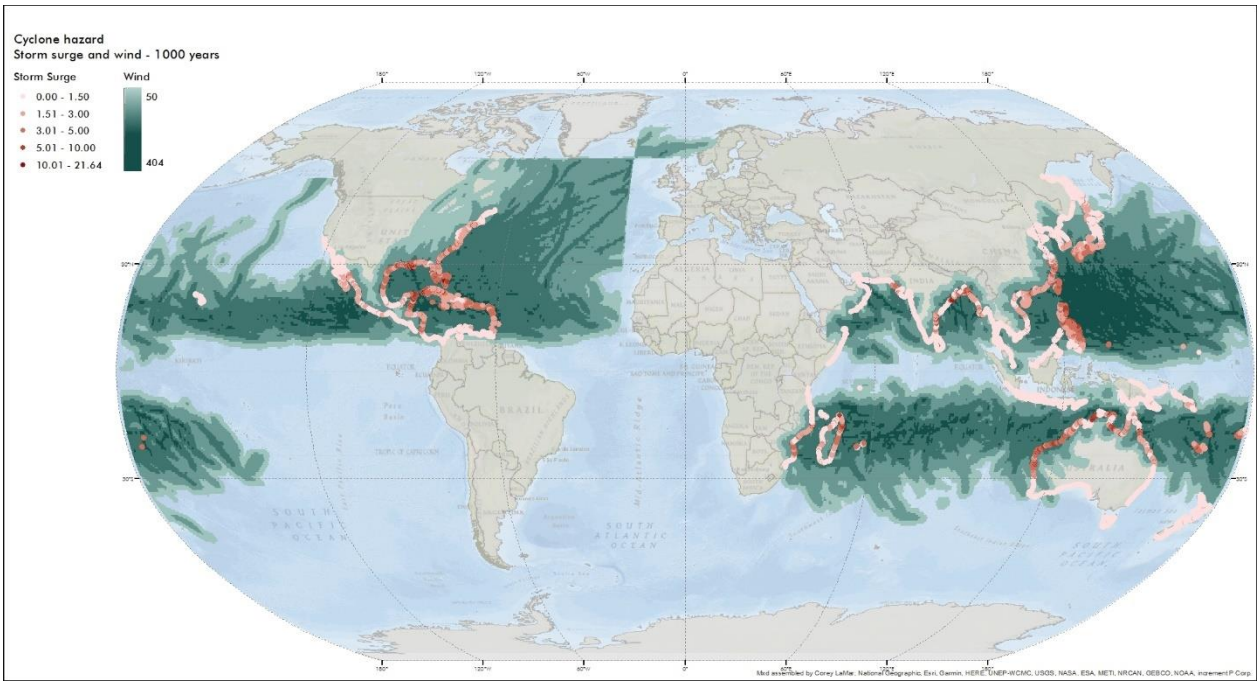

Figure 19. Tropical cyclone's strong winds and storm surge hazard map for 1000 years return period.

4.2.3 Considerations for Future Climate

The tropical cyclone catalog included in the hazard assessment for a future climate is composed of historical records retrieved from IBTrACS and supplemented with a representative sample from the STORM dataset developed by Bloemendaal et al. (2020). This dataset provides 10,000 years of simulated tracks, developed from a stochastic model of the main features that determine the trajectory of tropical cyclones, such us central pressure, forward speed and direction, genesis location, sea surface temperature, mean sea level pressure, among others. Stochastic simulation of new trajectories was performed on this set of tracks to include all possible events covering all ranges of frequencies and intensities.

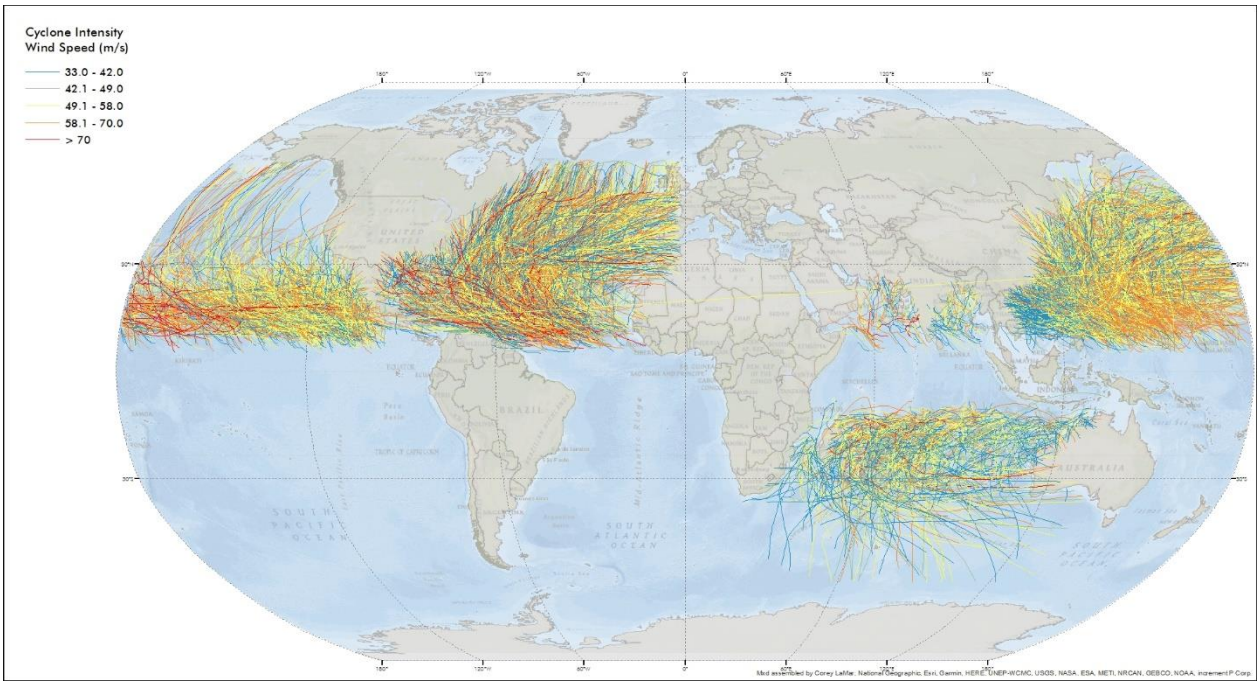

Figure 20. Cyclone tracks used in hazard modelling for future climate

4.2.4 Tropical Cyclone Hazard Maps for Future Climate

Figure 21 to Figure 26 present the hazard maps for 25, 50, 100, 250, 500 and 1000 years return periods for all basins under analysis for future climate conditions.

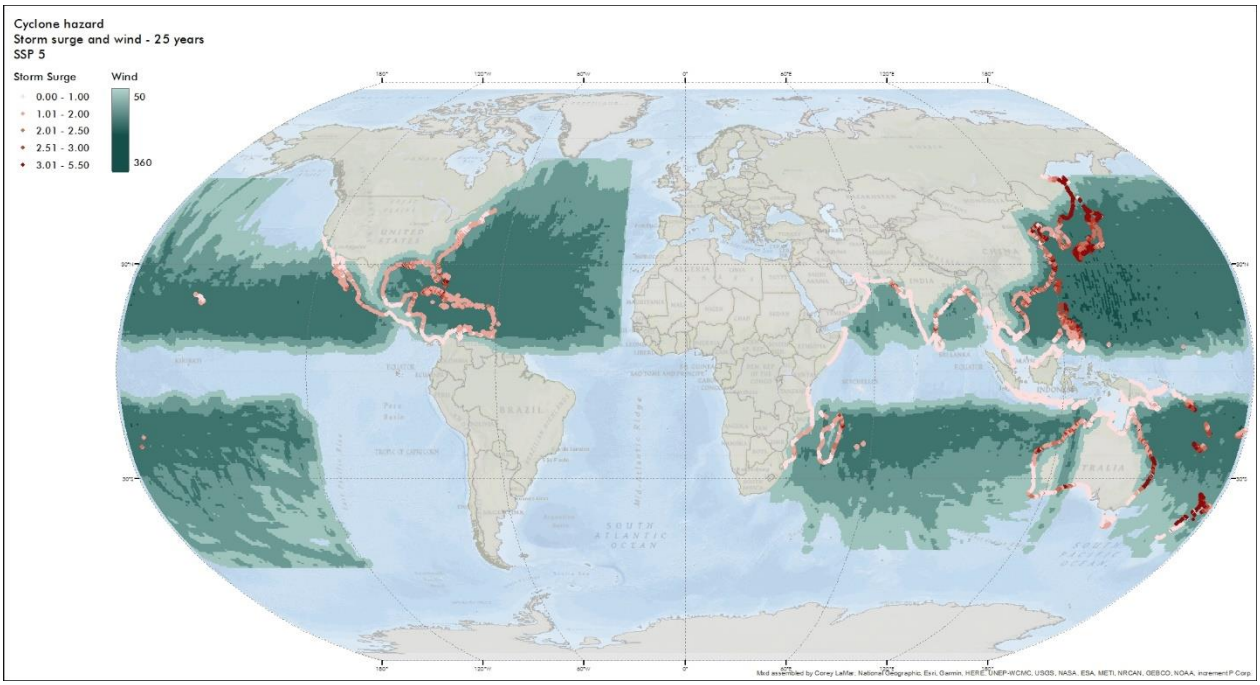

Figure 21. Tropical cyclone's strong winds and storm surge hazard map for 25 years return period for future climate.

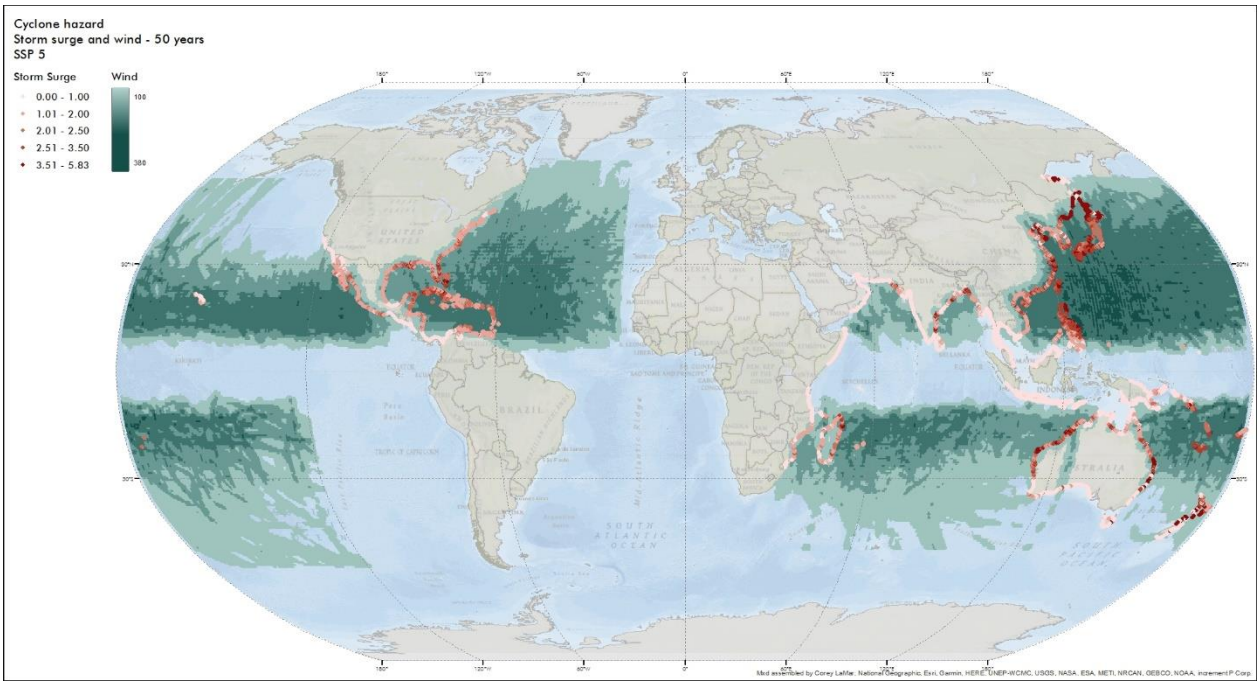

Figure 22. Tropical cyclone's strong winds and storm surge hazard map for 50 years return period for future climate.

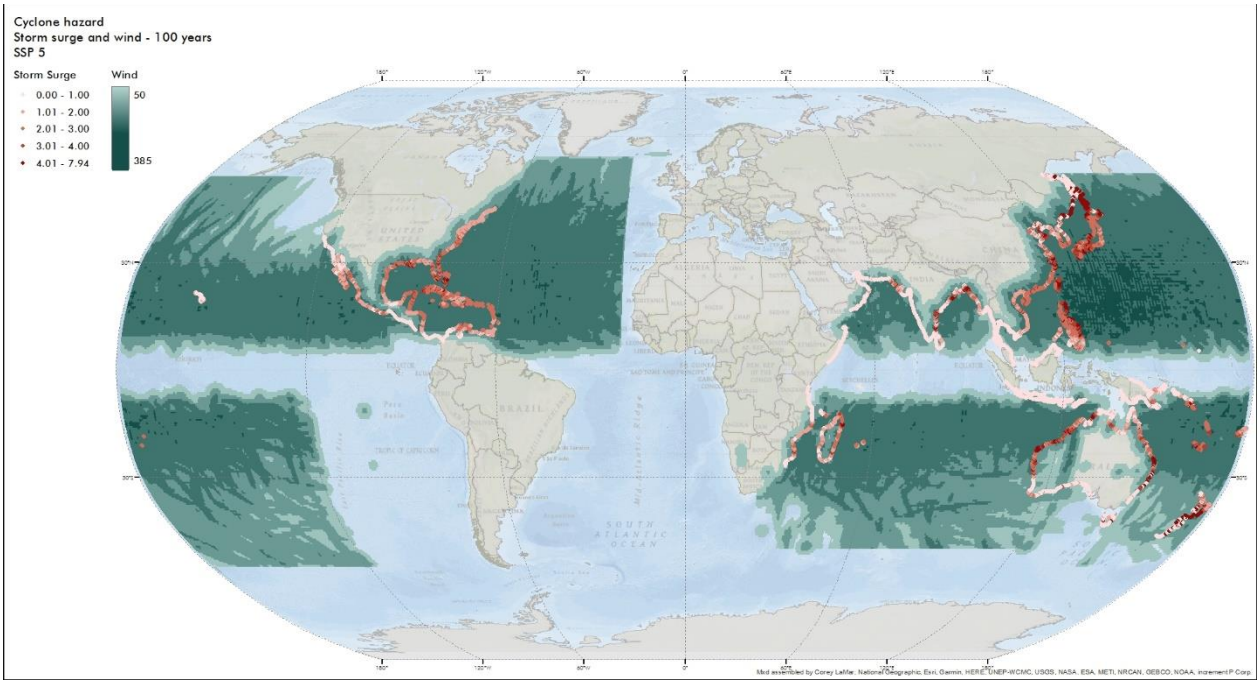

Figure 23. Tropical cyclone's strong winds and storm surge hazard map for 100 years return period for future climate.

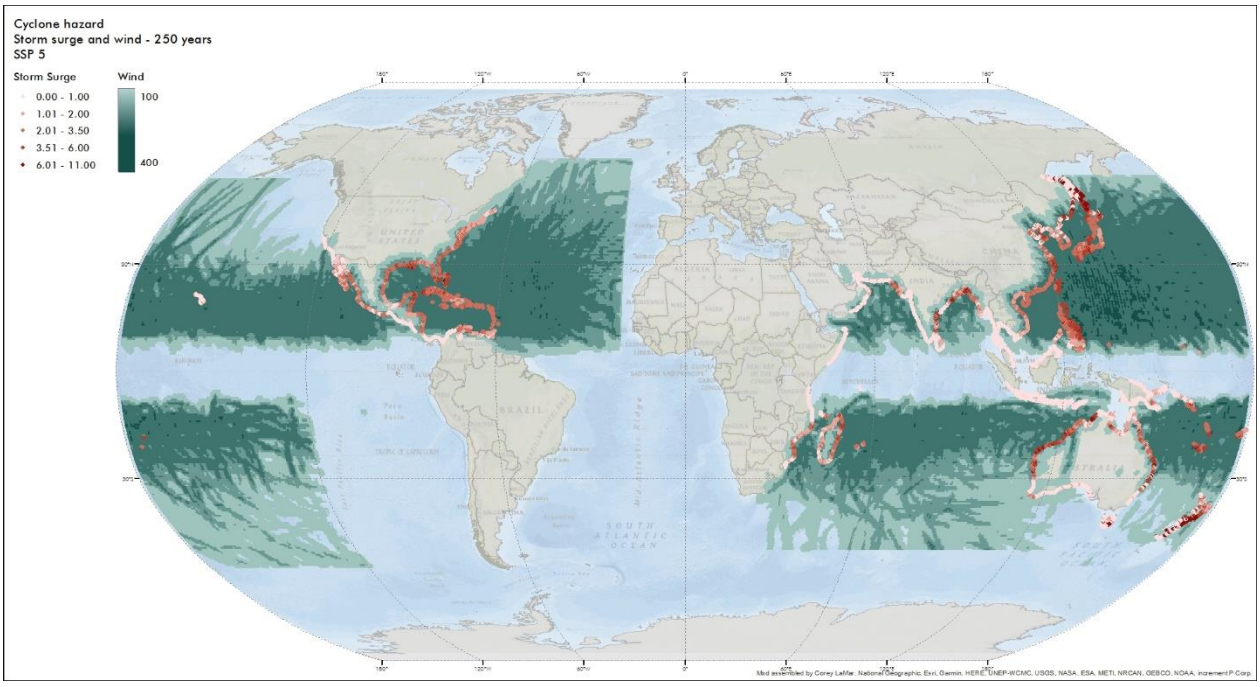

Figure 24. Tropical cyclone's strong winds and storm surge hazard map for 250 years return period for future climate.

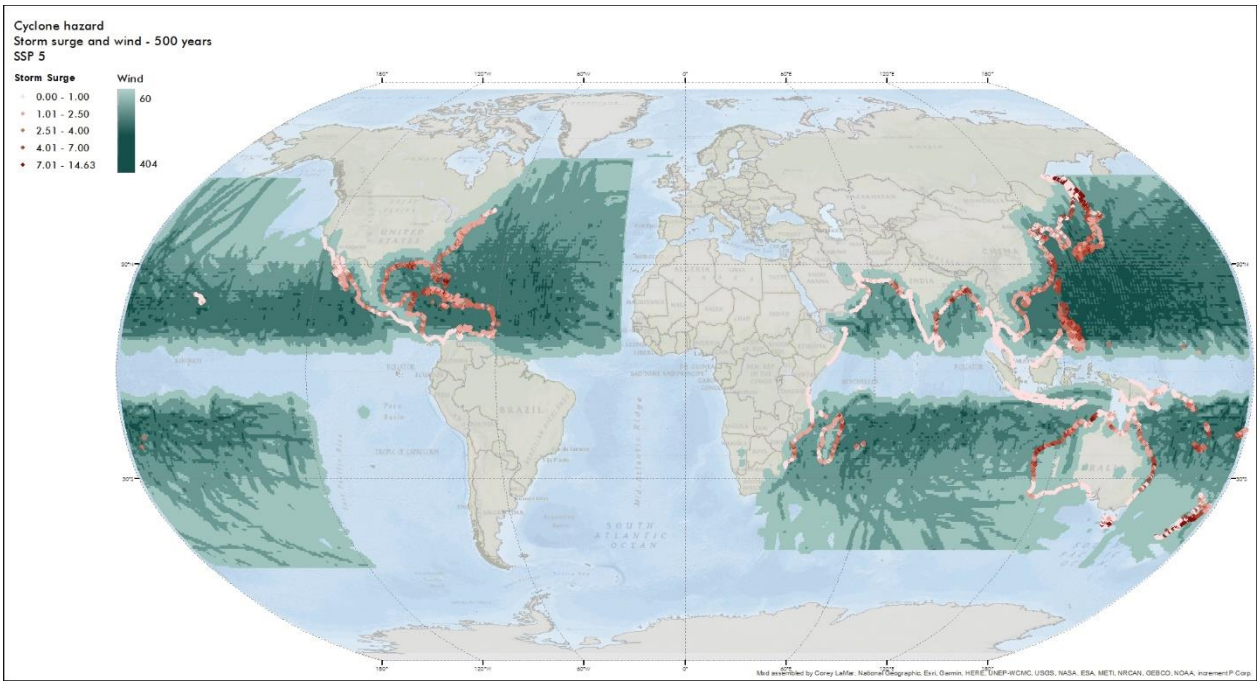

Figure 25. Tropical cyclone's strong winds and storm surge hazard map for 500 years return period for future climate.

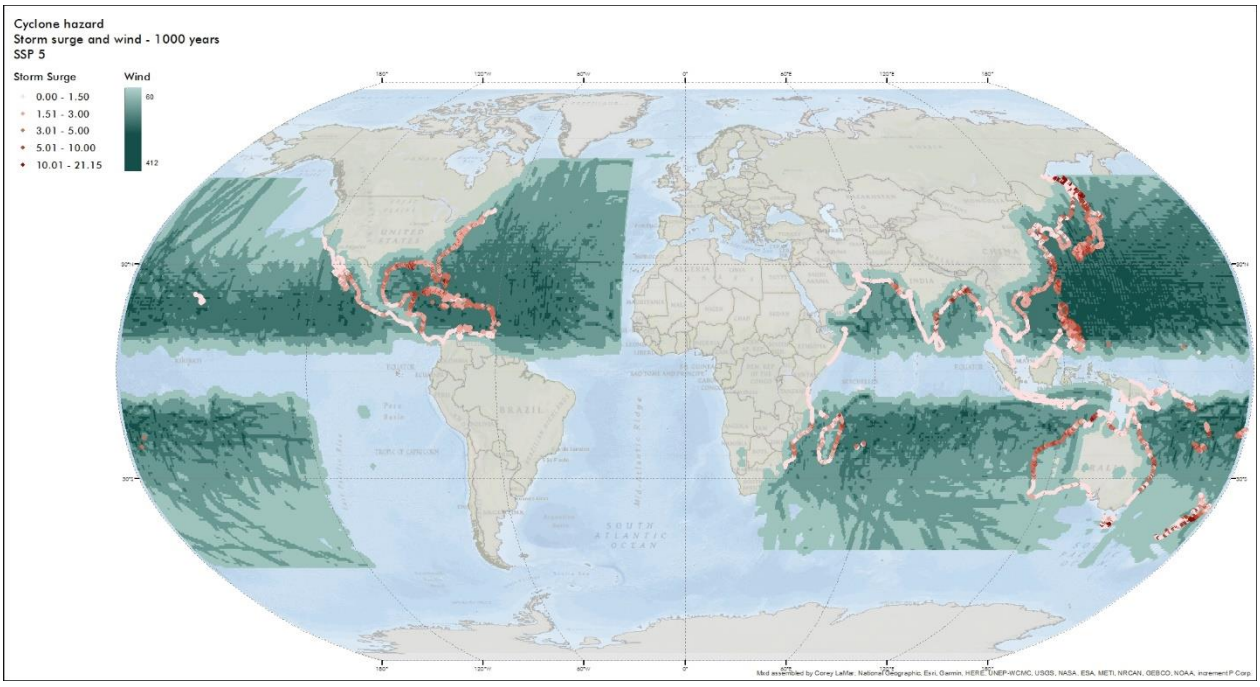

Figure 26. Tropical cyclone's strong winds and storm surge hazard map for 1000 years return period for future climate.

4.3 Flood Hazard Model

CIMA Foundation developed flood hazard maps using the W5E5 Meteo dataset as input for the present climate and the ISIMIP3b Model data as the input for the future climate. The variables used were rainfall, near surface air temperature, near surface air humidity, near surface wind velocity, and surface solar radiation. More in-depth information about the model can be found in Alfieri et al. (2023a) and Alfieri et al. (2023b).

Figure 27 presents the hazard maps for 5, 20, 100 and 500 years return periods for an area in Madagascar.

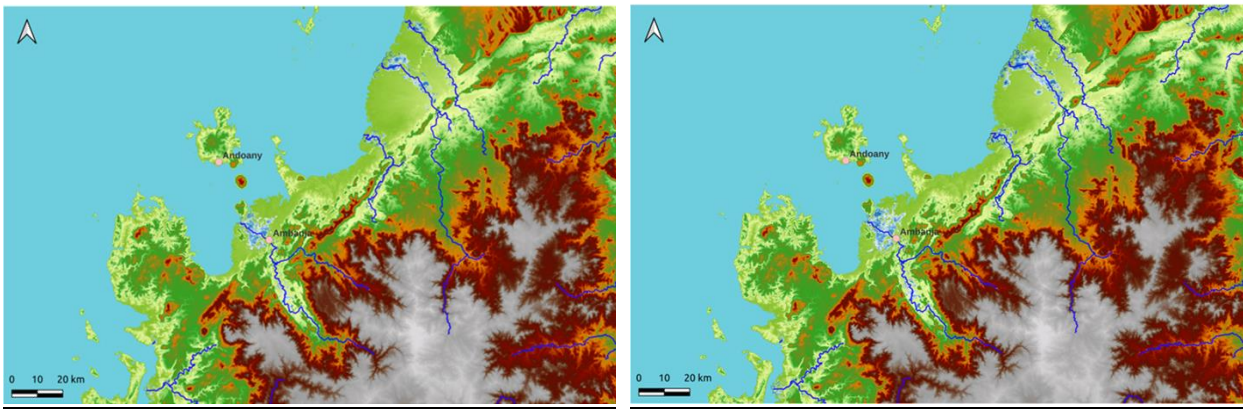

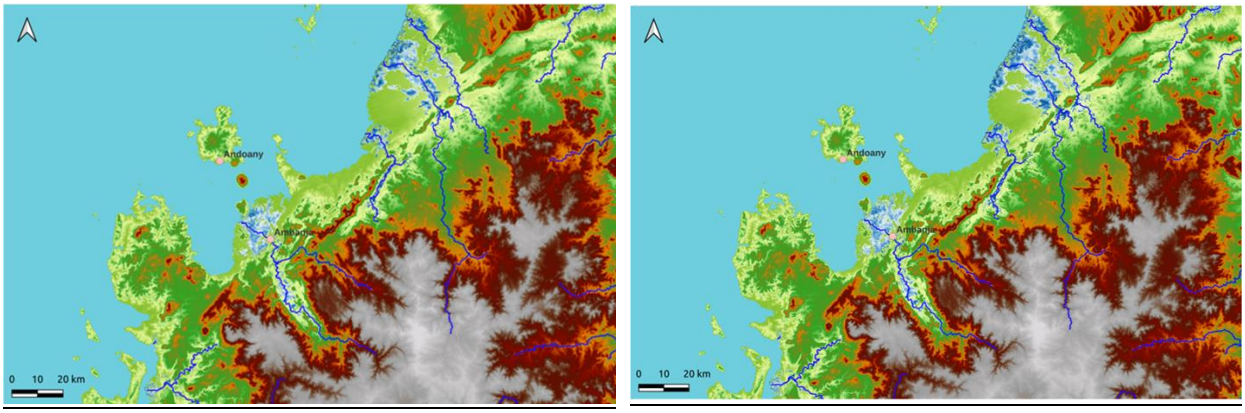

Figure 27. Hazard maps for different return periods (5, 20, 100, 500 years) present climate conditions, Madagascar.

4.4 Landslides Hazard Model

To identify global landslide hazard and risk 'hotspots,' NGI employed a simplified first-pass analysis method based on the procedure proposed by Mora and Vahrson (1994). Their analysis used a grid with approximately 1km x 1km pixels. They estimated landslide hazard, defined as the annual probability of a potentially destructive landslide event, by combining triggering factors (mainly extreme precipitation and seismicity) with susceptibility factors (slope, lithology, and soil moisture). Hazard is primarily calculated as the product of susceptibility and triggering factors. The hazard maps are divided into precipitation-induced landslide hazard and earthquake-induced landslide hazard. More information about the model can be found in Nadim et al. (2023).

Figure 28 illustrates the components of the landslide model in case of rainfall triggered landslides: susceptibility, triggering factors and thresholds, to account for landslide probability. Climate change is incorporated as changes in precipitation patterns following the same approach explained for floods.

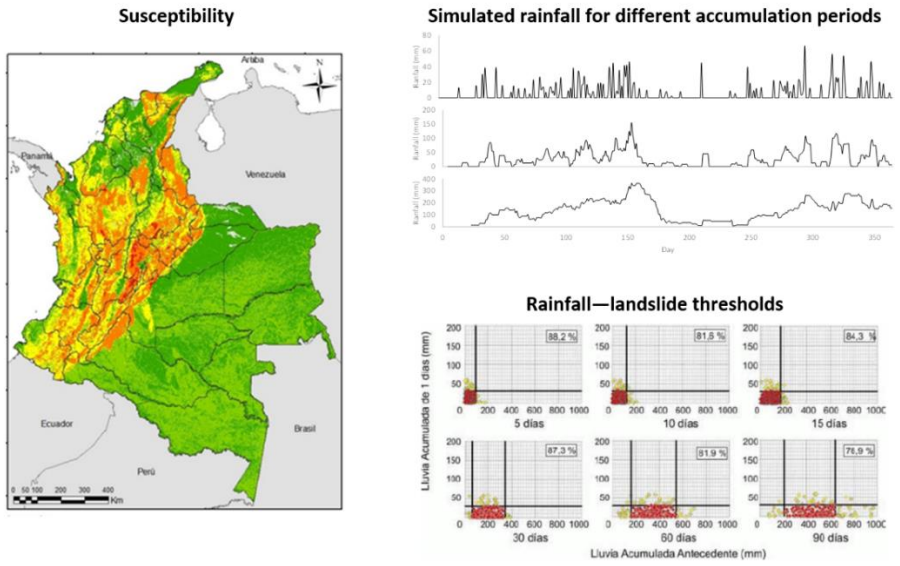

Figure 28. Illustration of components of the rainfall-landslide model for Colombia (INGENIAR, 2021)

4.5 Tsunami Hazard Model

Tsunami was modeled by NGI based in a global model which considers the occurrence rate of earthquakes in major submarine seismic sources. Complete detail on the Probabilistic Tsunami Hazard Assessment (PTHA) method can be found on Løvholt et.al. (2014). NGI defined hazard scenarios for all tsunami-prone regions in the world, and constructed a collection of raster grids with georeferenced information which allows for a probabilistic representation of the recorded tsunami intensity values. The hazard is thus presented in terms of a set of scenarios, where each one of these is characterized by an annual frequency of occurrence and the intensities are defined in terms of two parameters: the expected value and the standard deviation. The coastal areas of the continents were divided into a total of 383 regions as shown in Figure 29.

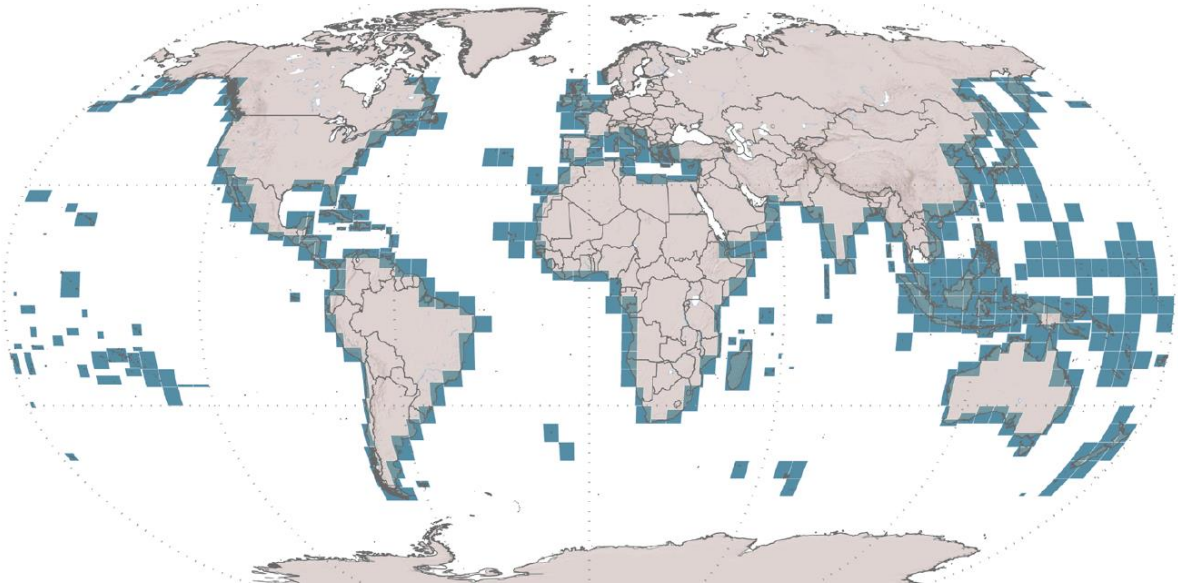

Figure 29. Regions with tsunami calculation

Figure 30 presents the wave height due to tsunami hazard for a 475 year return period.

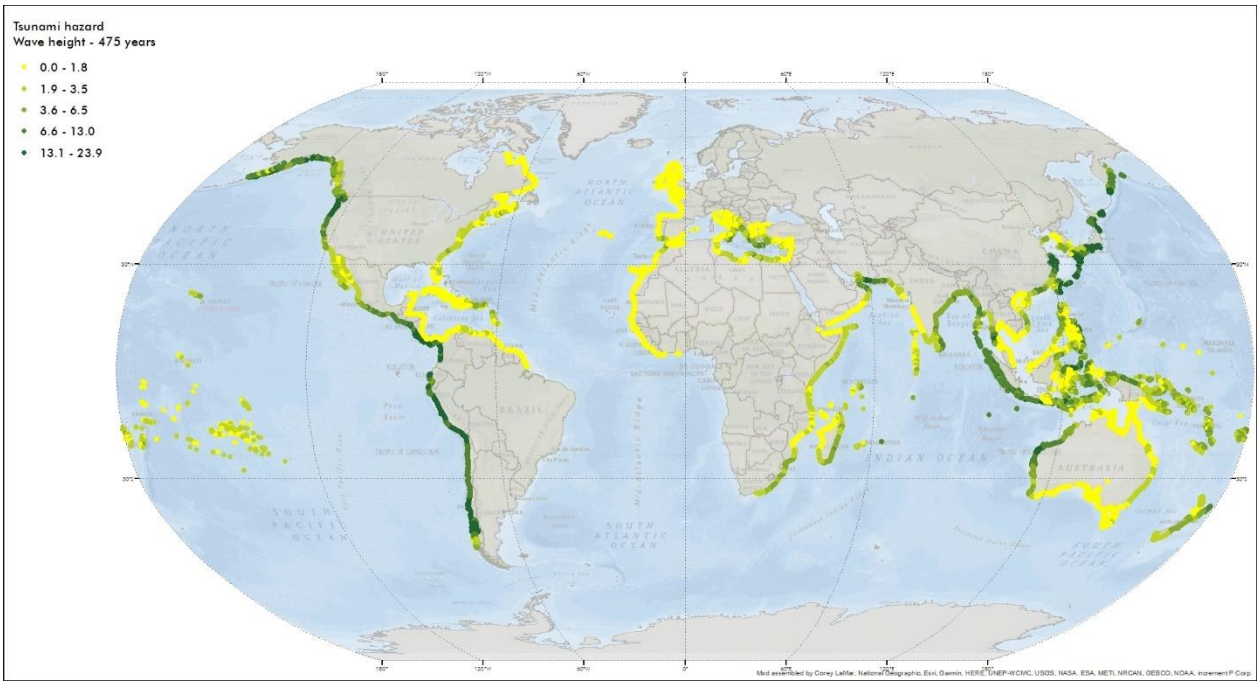

Figure 30. Global tsunami hazard map displaying the run-up height for a return period of 475 years.

5 World Infrastructure Proxy

We present in this chapter the rationale for constructing the World Infrastructure Proxy. In essence, this approach combines a top-down valuation of the infrastructure for each country with a bottom-up distribution of costs within the individual elements of each sector.

The top-down component of the valuation is developed by assuming that the infrastructure represents a certain fraction of the country's capital stock. This fraction is approximated here as a function of the distribution of the country's wealth from produced, natural, and intangible capital stocks.

The bottom-up aspect of the approach assesses the value of individual elements within the territory of each country. This is done using consumption, access, and capacity indicators for each sector, as well as indicative prices of these elements. In the end, the total value obtained from the bottom-up approach is adjusted to align with the top-down valuation. This means that the top-down value remains the true total infrastructure cost for the country, while the bottom-up values serve as a tool for distributing costs to individual elements.

This rationale is applied to all the sectors included in this assignment: power, highways and railways, transportation, water and wastewater, communications, and oil & gas. The first section outlines the top-down approach for assessing the entire infrastructure stock, while the following sections detail the specific procedures for applying the bottom-up approach to each sector.

5.1 Infrastructure Values at Country Level

This section outlines the procedure for estimating total infrastructure values at the country level using the top-down approach. The following indicators are necessary to apply this methodology: total capital stock, total wealth, GNI per capita, and population[7]. All the steps for calculating the value of the infrastructure are provided here.

5.1.1 Total wealth

As defined in "Where is the Wealth of Nations" (2021), a country's total wealth comprises the sum of its produced capital, natural capital, human capital, and net foreign assets. A similar definition is found in the 2006 version of the same report, where total wealth is defined as the sum of produced capital, natural capital, and intangible capital. Considering the descriptions in both reports, it is reasonable to assume that both definitions are valid, thereby offering an approximation for intangible capital.

5.1.1.1 Produced capital

Produced capital encompasses the combined value of machinery, equipment, and structures, which includes infrastructure. This implies that the value of infrastructure is included in this category, and it is presented in the report for each included country.

[7] GNI per capita and Population may be found in the World Bank indicators database. Total Wealth is defined and calculated in the report *Where is the wealth of nations?* by the World Bank.

5.1.1.2 *Intangible capital*

Intangible capital, as defined in the 2006 version of the report, comprises elements such as raw labor, human capital, social capital, and other critical factors, including institutional quality. Intangible capital is quantified as the disparity between total wealth and the sum of produced and natural capital, as follows:

$$Intangible\ capital = Total\ wealth - (Produced\ capital + Natural\ capital)$$

5.1.2 Infrastructure participation in capital stock (produced capital)

This methodology proposes to calculate infrastructure's share in the capital stock by multiplying the percentages of produced capital and intangible capital. In this context, produced capital includes the value of infrastructure assets, while intangible capital encompasses factors like institutional capacity, governance, and the overall human and technological capabilities of the country. It can be considered a measure of the country's technical capacity to develop and maintain infrastructure systems.

$$Infrastructure\ participation = Produced\ capital\ [\%] * Intangible\ capital\ [\%]$$

This value can be computed for the list of 146 countries provided in the "Where is the Wealth of Nations" report. If these values are not available for a specific country (i.e., a country not included in the report), the average for its income group can be used. The income group classification is determined by the GNI per capita of the country. The following table displays the income classification along with the corresponding average percentages of produced and intangible capitals (as a percentage of the total wealth).

Table 3. Average produced and intangible capital by income group.

Income group	GNI per capita (2018)	Produced capital [%]	Intangible capital [%]
Low income	<= 1,025	28	47
Lower middle income	1,026-3,995	27	59
Upper middle income	3,996-12,375	26	66
High income: non-OECD	> 12,375	23	46
High income: OECD	> 12,375	35	63

The proposed method performs effectively for high-income countries but tends to overestimate infrastructure participation in low-income countries. To address this issue, an income group classification is utilized to determine a corrective factor, as detailed in the table below. This factor considers the impact of a country's economic and developmental status as a modifier for investment in infrastructure assets.

Table 4. Corrective factor by income group.

Income group	Factor
Low income	3
Lower middle income	3
Upper middle income	2
High income: non-OECD	1
High income: OECD	1

This factor will affect the infrastructure participation percentage as follows:

$$Infrastructure\ participation = \frac{Produced\ capital\ [\%] * Intangible\ capital\ [\%]}{Factor}$$

5.1.3 Infrastructure value by country

The value of the infrastructure at country level is computed as follows.

$$Value = Infrastructure\ participation\ * Produced\ capital\ (per\ capita) * Population$$

5.2 Economic Valuation of Electricity Infrastructure

The power sector is divided into three subsectors: generation, transmission, and distribution. This section outlines the process for assessing the components of each subsector using the bottom-up approach.

5.2.1 Generation

Evaluating the economic value of generation infrastructure requires access to the following datasets:

1. Global power plant database (WRI).
2. Power plant database (OSM).

The procedure for estimating the cost of generation infrastructure is described below in a series of steps:

i. Cleanse the databases by removing elements that lack information about energy source or generation capacity.
ii. Reclassify the attribute "energy source" in all databases into one of the following categories:

Table 5. Energy sources determined for the studio.

Energy source
Bioenergy (biomass, waste, etc)
Battery (storage)
Coal
Gas
Geothermal
Hydro
Nuclear
Oil (petroleum derivates)
Solar (photovoltaic)
Wave and tidal
Wind
Other

Assign the class "Other" to elements that don't have energy source information.
iii. For the WRI database, a 30-inch buffer (approximately 900 meters) must be generated. Then, apply the following algorithm in conjunction with the *power plant database (OSM):*

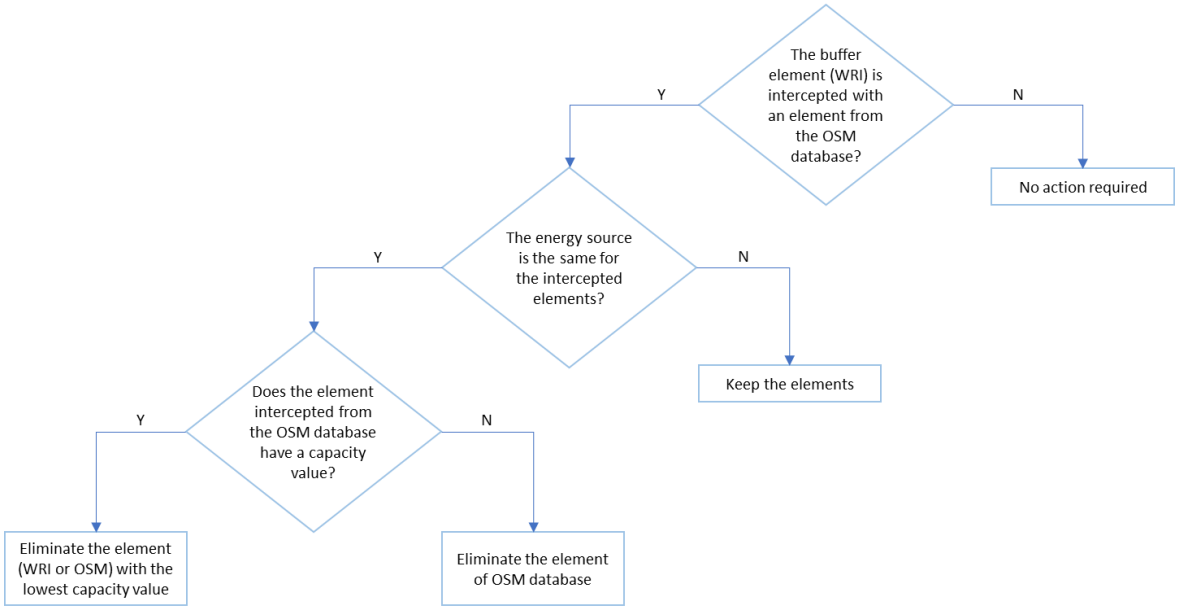

iv. Utilizing the elements from the *WRI database and the OSM power plant database* that contain information on energy production capacity, create a statistical distribution for each type of energy source. Using this statistical distribution, allocate a random value of production capacity to the elements in the OSM power plant database that lack capacity information.

v. Taking into account the assigned values of energy capacity and the energy source, estimate the economic valuation as follows:

$$Economic\ Value_i\ [USD] = Capacity\ [MW] * Value\ indicator_i\ \left[\frac{USD}{MW}\right]$$

Subscript *i* indicates to the type of energy source.

The following table presents recommended costs for each type of energy source.

Table 6. Recommended costs for type of energy source

Energy source	Cost indicator (USD/kW)
Bioenergy (biomass, waste, etc)	2 353
Battery (storage)	758
Coal	875
Gas	1 116
Geothermal	3 991
Hydro	2 135
Nuclear	3 782
Oil (petroleum derivates)	795
Solar (photovoltaic)	857
Wave and tidal	7 038
Wind	1 325
Other	1 134

5.2.2 Transmission

The economic evaluation of the transmission infrastructure requires the use of the following datasets:

1. Power line database (OSM): This database encompasses global electrical transmission networks.
2. Power substations database (OSM).

The procedure for assessing the cost of the transmission lines is outlined below in a series of steps:

i. Calculate the length of each element.
ii. For elements with voltage values, calculate a discrete statistical distribution (based on the total length for each voltage) to assign voltage values to elements lacking this information. It is advisable to perform this by region (e.g., North America, Central America, South America, Europe, Central Asia, East Asia, South Asia, Southeast Asia, Western Asia, etc.).
iii. Considering the values of voltage and length, estimate the economic valuation for each element as follows:

$$Economic\ Value\ [MMUSD] = Length\ [km] * Cost\ indicator\ [MMUSD/km]$$

$$Cost\ indicator\ [MMUSD/km] = f(Voltage\ [kV])$$

The figure below presents a pricing function where prices depend on the transmission line voltage (refer to the equation in the plot). The development of this function stems from identifying economic valuations per kilometer of networks at various voltages.

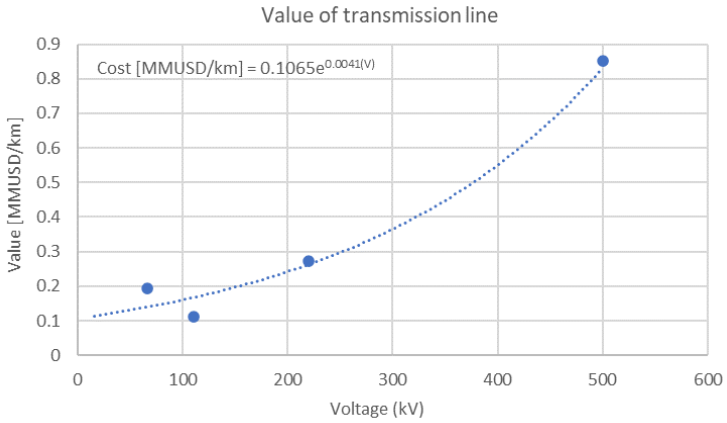

Figure 31. Pricing function (based on transmission line voltage)

For substations, the following steps were taken:

i. Include only the elements classified in the substation field as "distribution" or "transmission." Remove any other items that do not fall into these two classifications.
ii. For elements containing multiple voltage values, retain the maximum transformation voltage value within the substation and remove the others.

iii. To randomize voltage values for elements lacking this information, calculate a discrete statistical distribution using the elements that already have a voltage value. It is recommended to do this by region (e.g., North America, Central America, South America, Europe, Central Asia, East Asia, South Asia, Southeast Asia, Western Asia, etc.).

iv. Considering the voltage value, estimate the economic valuation for each element as follows:

$$Economic\ value\ [MMUSD] = Cost\ indicator\ [MMUSD] = f(Voltage\ [kV])$$

The figure below presents a pricing function where prices depend on voltage at the substation (refer to the equation in the plot). The development of this function stems from identifying economic valuations of substations with different transformation voltages.

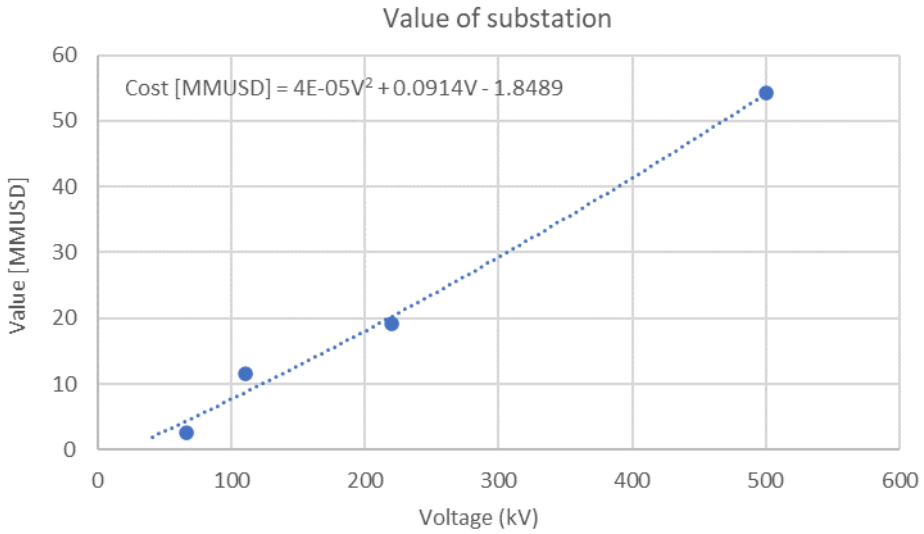

Figure 32. Pricing function (based on voltage at substation)

5.2.3 Distribution

The total cost of energy distribution is indexed to both the population and the economic valuation of transmission:

$$Distribution = f(population, transmission\ economic\ valuation)$$

To evaluate the economic valuation of generation, you the following datasets are required:

1. Population raster.
2. Access to electricity (% of the population) (World Bank).

The steps for valuating the distribution subsector are as follows:

i. Complete the information on access to electricity for countries lacking this indicator. We recommend using average values from neighboring countries with similar economic conditions.

ii. Determine the total population value for each country and the total value of the economic valuation of energy distribution. For the economic valuation, we suggest using this equation:

$$Economic\ valuation\ of\ distribution_i = 2.62^{8} * Economic\ valuation\ of\ transmission_i$$

Subscript *i* indicates each country

iii. The population with access to electricity is used to distribute the total values into population pixels as follows:

$$\%P_{Access} = \frac{\sum(\%P_{Access_c} * P_c)}{P_{Total}}$$

Where:

$\%P_{Access}$ = % of population with access to electricity in the country
P_{Total} = total population in the country
$\%P_{Access\_c}$ = % of population with access to electricity in the cell
P_c = total population in the cell

To estimate the % of the population with access to electricity in the cell ($\%P_{Access\_c}$), it is recommended using a linear function (as illustrated in the next figure) and iteratively adjusting the parameter P_{100} until the equation above is satisfied.

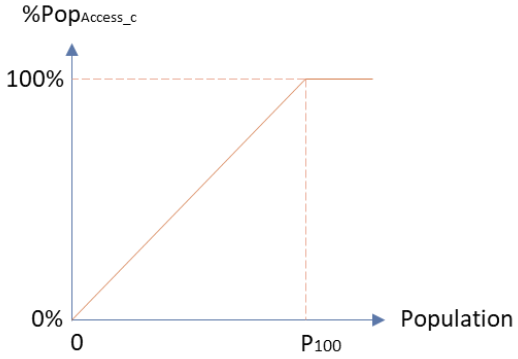

Figure 33. Recommended linear function for the estimation of population with access to electricity.

iv. Then, the economic value of each cell is computed as follows:

$$Value_c = Total\ value * \left(\frac{\%P_{Access_c} * P_c}{P_{Total}}\right)$$

Total value = economic value of the distribution for the country

[8] The factor 2.62 was derived from historical records of global energy investments, sourced from the International Energy Agency (IEA).

This process concentrates the exposed elements for the distribution subsector in cells that ultimately possess some level of economic value.

5.3 Economic Valuation of Roads and Highways

The roads and highways sector is divided into three subsectors: Roadways, Bridges, and Tunnels. For the procedure outlined here, the following data sources are utilized:

1. Global roads network (OSM): This database serves as the primary source of information. It includes various attributes, such as road types like motorway, trunk, primary, secondary, tertiary, and residential. It also contains data on bridges. Other types of roads, such as pedestrian, cycleway, track, and unclassified, are not considered here due to the overall scope of this assignment.

   This source also contains information on other types of roads such as pedestrian, cycleway, track, unclassified, among others, which are neglected here in accordance with the overall scope of this assignment. The road types considered here are (as included in the OSM database): motorway, trunk, primary, secondary, tertiary, and residential. Data on bridges is also obtained from the OSM database.

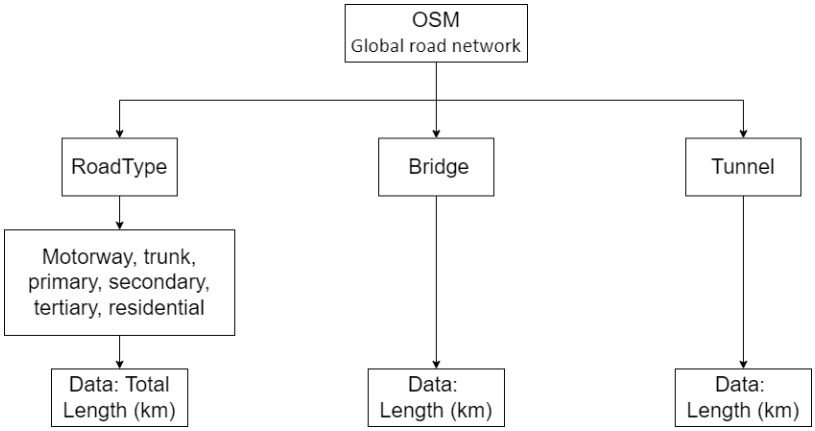

2. GRIP4 global roads dataset (GLOBIO): This dataset is considered a secondary source of information and includes the following attributes:

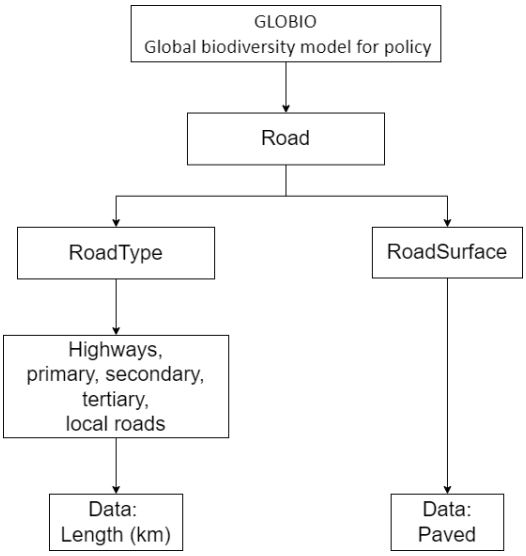

The procedure for creating a roadways dataset involves the following steps:

i. Selection of the database that best represents the sector for each country. It is recommended to compare the total road length by country from both databases, while considering only the following road types:

Table 7. Comparison of total length of roads

Global road network OSM	**GRIP4 global roads dataset GLOBIO**
RoadType*	**RoadType**
Motorway	Highways
Motorway_link	Primary roads
Trunk	Secondary roads

Although OSM is the preferred main data source, this comparison may reveal significant differences or data gaps in OSM compared to GLOBIO for certain countries. In such cases, both datasets can be merged for a country, or GLOBIO may be chosen over OSM. The final source dataset is determined at the discretion of the user. It is also recommended not to use OSM as a source if the "unclassified" road type exceeds 60% of the total data for any country.

ii. Assign a terrain classification to each road segment based on the average topographic slope of the segment:

Table 8. Terrain classification

Terrain Classification	**Slope (º)**
Plain	0 – 10
Rolling	10 – 25
Steep	>25

We suggest using the Global Polygons for Terrain Classification, divided into uniform slopes and basins.[9]

iii. Assign a cost to each road segment according to the unitary costs presented here:

Table 9. Road segment costs

Road Type	Terrain	US$/Km
Highway, motorway	Plain	1,090,000
	Rolling	1,715,000
	Steep	2,120,000
Primary, trunk	Plain	800,000
	Rolling	1,150,000
	Steep	1,460,000
Secondary, tertiary, residential	Plain	690,000
	Rolling	1,130,000
	Steep	1,420,000

iv. Assign a cost to the bridge and tunnel segments in OSM. In this case, a general value is used for simplicity, considering the broad variety of elements in this category that cannot be accurately captured with the attributes included in OSM.

Table 10. Cost for the bridges and tunnels segments

Component	US$/Km
Bridge	9,840,000
Tunnel	19,800,000

5.4 Economic Valuation of Communications Infrastructure

The communications sector is divided into three subsectors: wireline services, cable services, and wireless services. This section outlines the process for valuating the components of each subsector using the bottom-up approach. For this procedure, the following indicators and data sources are utilized:

1. GDP per capita (current US) - Source: World Bank.
2. Fixed broadband subscriptions (per 100 people) - Source: World Bank.
3. Cable subscriptions (per 100 people) - Multiple sources.
4. Mobile cellular subscriptions (per 100 people) - Source: World Bank.
5. Population raster.
6. Cell towers database (Provider: Open Cell ID) - This database contains the location of cell towers.

To execute the procedure, establish the reference cost per subscriber for the three services based on each country's GDP. It is recommended to use the following values:

Table 11. Reference cost per subscriber

GDP/per capita (USD)		Services infrastructure cost (USD/subscriber)		
		Wireline	Wireless	Cable
	<10 000	1 552	399	899
10 000	20 000	2 328	599	1 348

[9] Dataset available in: https://gisstar.gsi.go.jp/terrain2021/

GDP/per capita (USD)		Services infrastructure cost (USD/subscriber)		
		Wireline	Wireless	Cable
20 000	30 000	2 586	665	1 498
30 000	40 000	2 715	699	1 573
40 000	50 000	2 793	719	1 618
>50 000		3 103	799	1 798

5.4.1 Wireline and cable services

The process for evaluating the cost of wireline and cable services infrastructure is detailed below in a series of steps:

i. Calculate the economic value of the service for each country using the following equation:

$$Economic\ Value\ [USD] = \frac{1}{100} * Subs_{service} * P_{total} * Value_{sevice}$$

Where:
$Subs_{service}$ = subscriptions per 100 people for each service (value per country)
P_{total} = total population in the country
$Value_{service}$ = cost of infrastructure per subscriber for the service

ii. Assign the population's access to services (wireline and cable) for each raster cell using the following process:

$$\frac{1}{100} * Subs_{service} = \frac{\sum(\%P_{subscriber\_c} * P_c)}{P_{total}}$$

Where:
$\%P_{subscriber\_c}$ = % of population subscribed to the service in the raster cell
P_c = total population in the raster cell

To estimate the percentage of the population subscribed to the service in the raster cell ($\%P_{subscriber\_c}$), it is suggested to utilize a linear function (as illustrated in the following figure) that adjusts the P_{100} value until the equation above is satisfied.

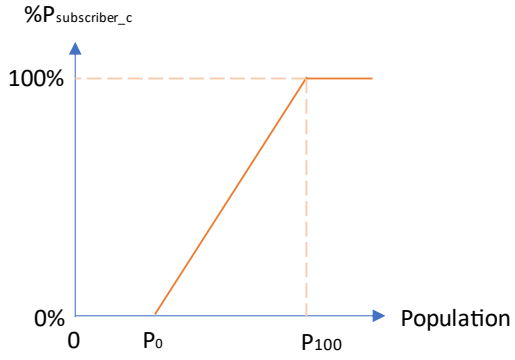

Figure 34. Linear function for the estimation of population subscribed to the service.

The P_0 value is the lower limit of the linear function. It's considered that there are no subscribers or wireline networks in the cell with population density ranging from 0 to P_0. The recommended value for P_0 is 1000 people/km^2.

iii. The economic value of each cell is computed as follows:

$$Value_c = Total\ value * \left(\frac{\%P_{Access_c} * P_c}{P_{Total}}\right)$$

Total value = economic value of the distribution for the country

5.4.2 Wireless services

The procedure for assessing the cost of wireless services infrastructure is outlined here in a series of steps:

i. Calculate the economic valuation of the service for each country using the following equation.

$$Economic\ Value\ [USD] = \frac{1}{100} * Subs_{service} * P_{total} * Value_{sevice}$$

Where:
$Subs_{service}$ = subscriptions per 100 people for each service (value per country)
P_{total} = total population in the country
$Value_{service}$ = cost of infrastructure per subscriber for the service

i. Remove antennas (from the cell tower database) with a value equal to or less than four (<=4) in the "samples" field of the attribute table.
ii. Allocate the country's economic valuation to the antennas.

$$Economic\ Value_{antenna} = \frac{Economic\ Value_{country}\ [USD]}{\#\ total\ antennas}$$

5.4.3 Submarine Telecommunication Cables

The economic valuation of submarine cables (without association to countries) relies on the following dataset:

1. Submarine cables database (TeleGeography).

The procedure for assessing the cost of submarine cables is provided below in a series of steps:

i. Calculate the valuation of each submarine cable using the following equation:

$$Economic\ Value\ [USD] = Length\ [km] * Indicator\ Value\ \left[\frac{USD}{km}\right]$$

Where:
Length = cable length
Indicator Value = Economic valuation per km for submarine telecommunications cables

A value of 27 000 USD/km is recommended.

5.5 Economic Valuation of Railways

The economic valuation of railway infrastructure relies on the following dataset:

1. Railways database (OSM).

The procedure for determining the cost of railway infrastructure is presented as a series of steps:

i. Classify the railways into the following categories:
   a) Economy of the country[10]:

Table 12. Classification of income groups by GNI per capita

Income group	GNI per capita (2021)	Classification
Low-income	<$1,085	EG_1
Lower middle-income	$1,086 - $4,255	
Upper middle-income	$4,256 - $13,205	
High-income	>$13,205	EG_2

   b) Railway type (RT):

Table 13. Classification according to railway type

Type	subway	light_rail tram funicular	miniature_railway monorail narrow_gauge rail other
Category	RT_1	RT_2	RT_3

ii. Calculate the length of each element in kilometers.
iii. Determine the economic valuation of each element (per kilometer) based on the category. The following values are recommended:

Table 14. Suggested values for economic valuation of railways elements

Region	**RT_1**		**RT_2**		**RT_3**	
	EG_1	**EG_2**	**EG_1**	**EG_2**	**EG_1**	**EG_2**
Africa	50.28	N/A	25.54	N/A	6.17	N/A
Asia*	47.54	49.02	34.35	41.79	8.58	11.38

[10] Classified countries can be consulted here:
https://datahelpdesk.worldbank.org/knowledgebase/articles/906519-world-bank-country-and-lending-groups

Oceania	189.83	189.83	46.05	46.05	11.26	11.26
Europe	30.02	66.67	27.40	17.50	20.55	31.44
North America**	52.13	70.46	39.62	57.86	25.05	22.01
South America	123.19	113.40	10.91	12.10	2.28	2.28
China	52.47	N/A	38.46	N/A	10.18	N/A
India	32.97	N/A	27.13	N/A	4.82	N/A

*Excludes China and India
**Includes Central America
***Economic valuations are in millions of dollars per km (MMUSD/km)

iv. Determina the economic valuation of each element based on the length of the element and the valuation per kilometer.

5.6 Economic Valuation of Water Infrastructure

The water sector includes water supply, water treatment, water storage, water delivery, wastewater collection, and wastewater treatment infrastructure. Due to limited georeferenced information on the elements of these subsectors, only water delivery, wastewater collection, and wastewater treatment infrastructure will be considered. The first two will be indexed to the served population due to the absence of a georeferenced global database.

5.6.1 Water delivery

The total cost of water delivery infrastructure is linked to both the population and the cost of infrastructure per capita:

$$Water\ delivery = f(population, water\ sector\ value\ per\ capita)$$

To assess the economic valuation of water infrastructure, the following datasets are necessary:

1. Population raster.
2. People using safely managed drinking water services (% of the population). Source: World Development Indicators. Percentage by country.

The process for evaluating the cost of water delivery infrastructure is presented in a series of steps:

i. Complete the information regarding access to safely managed drinking water services for countries lacking this indicator. It is recommended to use average values from countries with similar economic conditions, as illustrated in the table below. The income group classification is determined by the GNI per capita of the country.
ii. The total cost of water delivery infrastructure is indexed to the population and to the cost of infrastructure per capita.

$$Water\ delivery = f(population, water\ sector\ value\ per\ capita)$$

Table 15. % of population by income group with access to safely managed drinking water

Income level	% pop
High income	97.14

Low income	21.99
Lower middle income	48.68
Upper middle income	76.21

iii. Determine the total population for each country and the total economic valuation of the water delivery infrastructure. For the economic valuation we suggest the following values obtained for the listed countries from the 2017 Global Infrastructure Outlook Report:

$$Economic\ valuation\ of\ water\ delivery_i = 0.5 * Value\ of\ water\ sector\ per\ capita * Population_i$$

Subscript *i* indicates each country

Table 16. Suggested values of water sector per capita

Country	ISO	Value of water sector per capita [USD/hab]	Country	ISO	Value of water sector per capita [USD/hab]
Angola	AGO	$1,659	Malaysia	MYS	$ 527
Argentina	ARG	$ 450	Mexico	MEX	$ 141
Australia	AUS	$4,223	Morocco	MAR	$ 206
Azerbaijan	AZE	$ 766	Myanmar	MMR	$ 136
Bangladesh	BGD	$ 92	New Zealand	NZL	$1,749
Benin	BEN	$ 191	Nigeria	NGA	$ 122
Brazil	BRA	$ 526	Pakistan	PAK	$ 64
Cambodia	KHM	$ 61	Paraguay	PRY	$ 78
Canada	CAN	$2,596	Peru	PER	$ 522
Chile	CHL	$ 163	Philippines	PHL	$ 135
China	CHN	$ 377	Poland	POL	$1,281
Colombia	COL	$ 287	Romania	ROU	$ 567
Cote d'Ivoire	CIV	$ 171	Russia	RUS	$ 173
Croatia	HRV	$ 968	Rwanda	RWA	$ 58
Ecuador	ECU	$ 176	Saudi Arabia	SAU	$ 954
Egypt	EGY	$ 139	Senegal	SEN	$ 130
Ethiopia	ETH	$ 570	Singapore	SGP	$1,787
France	FRA	$1,156	South Africa	ZAF	$ 273
Germany	DEU	$ 354	South Korea	KOR	$1,918
Ghana	GHA	$ 268	Spain	ESP	$1,522
Guinea	GIN	$ 33	Tanzania	TZA	$ 506
India	IND	$ 78	Thailand	THA	$ 331
Indonesia	IDN	$ 187	Tunisia	TUN	$ 181
Italy	ITA	$ 693	Turkey	TUR	$ 266
Japan	JPN	$1,318	United Kingdom	GBR	$1,757
Jordan	JOR	$ 177	United States	USA	$ 242
Kazakhstan	KAZ	$ 514	Uruguay	URY	$ 751
Kenya	KEN	$ 116	Vietnam	VNM	$ 231

For countries not listed in the previous table, the following values are suggested, based on their economic conditions:

Table 17. Suggested values of water sector per capita (countries not listed in Table 16)

Income Group	Value per capita [USD/hab]
Low income	$220
Lower middle income	$246

Upper middle income	$349
High income	$1,333

iv. The population with access to safely managed drinking water services is utilized to allocate the total values among the population pixels in the following manner:

$$\%P_{Access} = \frac{\sum(\%P_{Access_c} * P_c)}{P_{Total}}$$

Where:
$\%P_{Access}$ = % of population with access to safely managed drinking water services in the country
P_{Total} = total population in the country
$\%P_{Access\_c}$ = % of population with access to safely managed drinking water services in the cell
P_c = total population in the cell

To estimate the percentage of the population with access to safely managed drinking water services in the cell ($\%P_{Access\_c}$), we recommend using a linear function (as illustrated in the following figure) and iteratively adjusting the parameter P_{100} until the equation mentioned above is met.

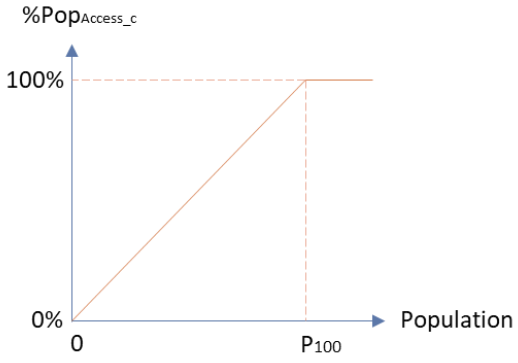

Figure 35. Linear function for the estimation of the % of population with access to safely managed drinking water

v. The economic value of each cell is calculated using the following formula:

$$Value_c = Total\ value * \left(\frac{\%P_{Access_c} * P_c}{P_{Total}}\right)$$

Where:
Total value = economic value of water delivery for the country
This process concentrates the exposed elements for the water delivery subsector in cells that ultimately have some economic value.

5.6.2 Wastewater collection

The total cost of wastewater collection infrastructure is linked to both the population and the cost of infrastructure per capita:

$$Wastewater\ collection = f(population, water\ sector\ value\ per\ capita)$$

To assess the economic valuation of wastewater collection infrastructure, the following datasets are necessary:

1. Population raster.
2. People using safely managed sanitation services (% of the population). (World Development Indicators)

The process for evaluating the cost of wastewater collection infrastructure is presented in a series of steps:

i. Complete the information regarding access to safely managed sanitation services for countries lacking this indicator. It is recommended to use average values from countries with similar economic conditions, as displayed in the following table. Income group classification is determined by the GNI per capita of the country.

Table 18. % of population by income group with access to safely managed sanitation services

Income level	% pop
High income	86.85
Low income	16.32
Lower middle income	47.39
Upper middle income	45.20

vi. Determine the total population value for each country and the overall economic valuation of wastewater collection. For economic valuation, it is suggested to use the values presented in the previous section (water delivery) from the 2017 Global Infrastructure Outlook Report.

$$Economic\ valuation\ of\ water\ delivery_i = 0.25 * Value\ of\ water\ sector\ per\ capita * Population_i$$

Subscript *i* indicates each country

vii. The population with access to safely managed sanitation services is utilized to allocate the total values among the population pixels as follows:

$$\%P_{Access} = \frac{\sum(\%P_{Access_c} * P_c)}{P_{Total}}$$

Where:
$\%P_{Access}$ = % of population with access to safely managed sanitation services in the country
P_{Total} = total population in the country
$\%P_{Access\_c}$ = % of population with access to safely managed sanitation services in the cell
P_c = total population in the cell

To estimate the % of the population with access to safely managed sanitation services in the cell ($\%P_{Access\_c}$), we suggest employing a linear function (as illustrated in the next figure) and iteratively adjusting the parameter P100 until the equation above is satisfied.

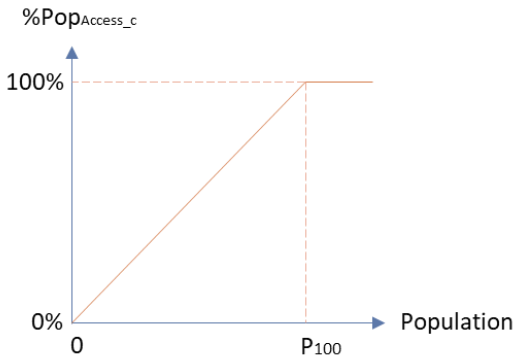

Figure 36. Linear function for the estimation of the % population with access to safely managed sanitation services

viii. The economic value of each cell is calculated as follows:

$$Value_c = Total\ value * \left(\frac{\%P_{Access_c} * P_c}{P_{Total}}\right)$$

Where:
Total value = economic value of wastewater collection for the country.
The exposed elements for the wastewater collection subsector are therefore concentrated in the cells that end up with some amount of economic value.

5.6.3 Wastewater treatment

The economic valuation of wastewater treatment infrastructure relies on the following dataset:

1. HydroWASTE: This database contains the location of 58,502 wastewater treatment plants (WWTPs) and their characteristics[11].

The procedure for evaluating the cost of wastewater treatment infrastructure is presented in a series of steps:

i. Begin by performing a cleanup of the database. Remove elements categorized as 'Non-Operational,' 'Projected,' and 'Proposed' in the attribute field STATUS of the database.
ii. Determine the total population served by each element using the attribute field POP_SERVED in the database.
iii. Establish the economic valuation for each wastewater treatment plant. For economic valuation, we recommend using the values presented in the first section of the 2017 Global Infrastructure Outlook Report:

$$Economic\ valuation\ of\ wastewater\ treatment\ plant_i = 0.25 * Value\ of\ water\ sector\ per\ capita * Population\ served_i$$

Subscript *i* indicates each wastewater treatment plant

[11] https://www.hydrosheds.org/products/hydrowaste.

5.7 Economic Valuation of Oil and Gas Infrastructure

The economic valuation of the sector is divided into three subsectors:

$$Energy\ Sector = Exploitation + Production + Distribution$$

5.7.1 Exploitation

The economic valuation of exploitation subsector requires the following datasets:

1. Wells Vector Grid -in Global Oil & Gas Features Database. (NETL).
2. Wells -in Global Oil & Gas Features Database. (NETL).

The procedure for the exploitation subsector comprises two main steps:

i. Consolidate the databases (Wells Vector Grid and Wells) into a single database.
ii. Assign economic valuation to each element in the unified database.

The process for determining the cost of exploitation is outlined in a series of steps:

i. Generate a vector grid (covering the global extent) with a cell size matching the "Wells Vector Grid" shapefile's cell size. In this document, we'll refer to this unified grid as the "Global Grid of Wells."

ii. Convert the polygons from the "Wells Vector Grid" shapefile into points (centroids), retaining the "Value" field at the centroid.

iii. Save the following attributes in the "Global Grid of Wells" shapefile as follows:
   - Name field: WELL_VECTOR. The field's value corresponds to the value stored by the centroid point (from the "Wells Vector Grid" shapefile) that spatially coincides with the cell.
   - Name field: WELL_POINTS. The field's value corresponds to the total sum of points (from the "Wells" shapefile) within each cell.
   - Name field: MAX_WELLS. The field's value corresponds to the maximum value between the two previous fields (WELL_VECTOR and WELL_POINTS).

iv. Apply the following equation to calculate the economic valuation of each cell in the "Global Grid of Wells" shapefile:

$$Economic\ Value_{Wells} = (MAX\_WELLS)_{cell} * \left(\frac{Value}{well}\right)$$

The recommended economic valuation per well is 7.82 million USD (MMUSD).

5.7.2 Production

The economic valuation of production subsector requires the following datasets:

1. Refined petroleum products – production. (The world factbook - CIA)[12].
2. Refineries -in Global Oil & Gas Features Database. (NETL).

The process for economic valuation in the production subsector comprises three main steps:

i. Link data from The World Factbook - CIA to the respective countries.
ii. Compute the production for each refinery in the "Refineries" shapefile.
iii. Assign the economic valuation to each refinery in the database.

The procedure for determining the cost of production is detailed in a the following steps:

i. Allocate the production values from The World Factbook to a shapefile representing countries.
ii. Implement the following algorithm:

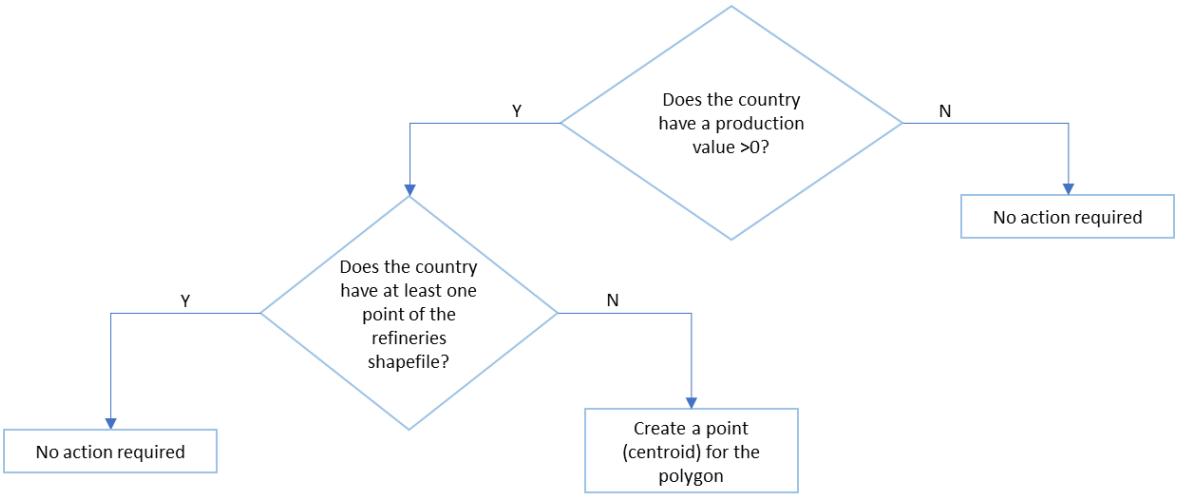

iii. Connect the points generated from the previous step to the refineries shapefile.
iv. Distribute the production from each country (country shapefile) to the points (refinery shapefile) located within that country. It is recommended to divide the production among the number of refineries in the country.
v. Apply the following equation for the economic valuation of each refinery (point):

$$Economic\ Value_{Refinery} = Production_{refinery}\left[\frac{bbl}{day}\right] * Cost\ indicator\left[\frac{USD}{\frac{bbl}{day}}\right]$$

The recommended cost indicator is 27,235 USD per barrel per day (USD/bbl/day).

5.7.3 Distribution

The economic valuation of distribution requires the following datasets:

1. Pipelines -in Global Oil & Gas Features Database (NETL).

[12] https://www.cia.gov/the-world-factbook/field/refined-petroleum-products-production

The procedure for determining the cost of distribution is outlined in a series of steps:

i. Remove atypical data or text-based information from the "Diameter" field. Note that the database contains diameter data in inches.

ii. Compile statistics for diameter by regions, taking into account the length of the pipeline as a weighting factor. The proposed regions based on pipeline length are as follows:

- World
- Africa
- Asia
- Oceania
- Europe
- North America (exclude the United States of America and include Central America)
- South America
- United States of America.

iii. For pipelines with no diameter value, randomly assign a diameter value based on the previous statistics for the pipelines in that region. If a region lacks representative statistics, use the global statistics.

iv. Calculate the value of the pipeline per kilometer as a function of the diameter, as shown in the figure below.

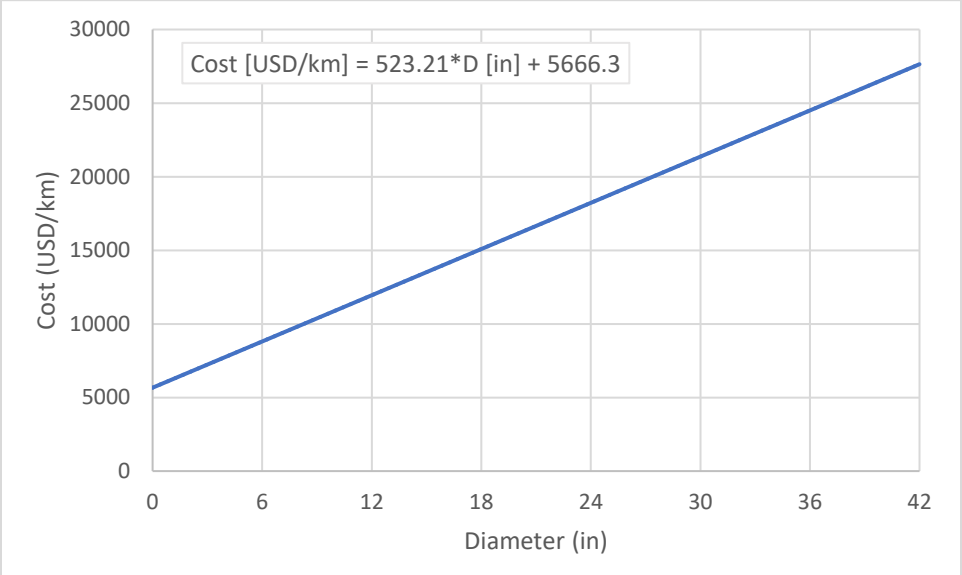

Figure 37. Linear function for the estimation of the value of the pipeline per kilometer

For the economic valuation of each pipeline, apply the following formula:

$$Economic\ Value_{Pipeline} = Length_{pipeline}[km] * Cost_{diameter}\left[\frac{USD}{km}\right]$$

6 Update of the Global Exposure Database

As part of the creation of the global Risk Model for the GAR reports, a methodology for the creation of building portfolios was generated and applied, resulting in a global exposure model of buildings. In this project, the methodology incorporates newer input databases, allowing the recalculation of the full global buildings model into an updated version for 2021.

The global buildings exposure model considers new data and methodologies, that have come available in recent years, for example: population distribution (HRSL High Resolution Settlement Layer) urban patterns and footprints (WSF-2015 - World Settlement Footprint 2015), Replacement costs estimation (METEOR - Modelling Exposure Through Earth Observation Routines) and height of buildings, among others. For more details on the update version of the GED that includes 245 countries/territories with updated exposed values refer to Piller et at. (2023).

Figure 38 illustrates the database construction details. Using raster information on the population density of any region, along with local socioeconomic indicators, such as hospital beds, number of students, distribution of workforce, among others, the number of buildings of each use is estimated and transformed into built area and exposed value, at each pixel in the population distribution raster. The total amount of exposed value is the distributed according to the typical construction practices of the region, into set of exposed elements, each of a specific combination of use, construction type and economic value.

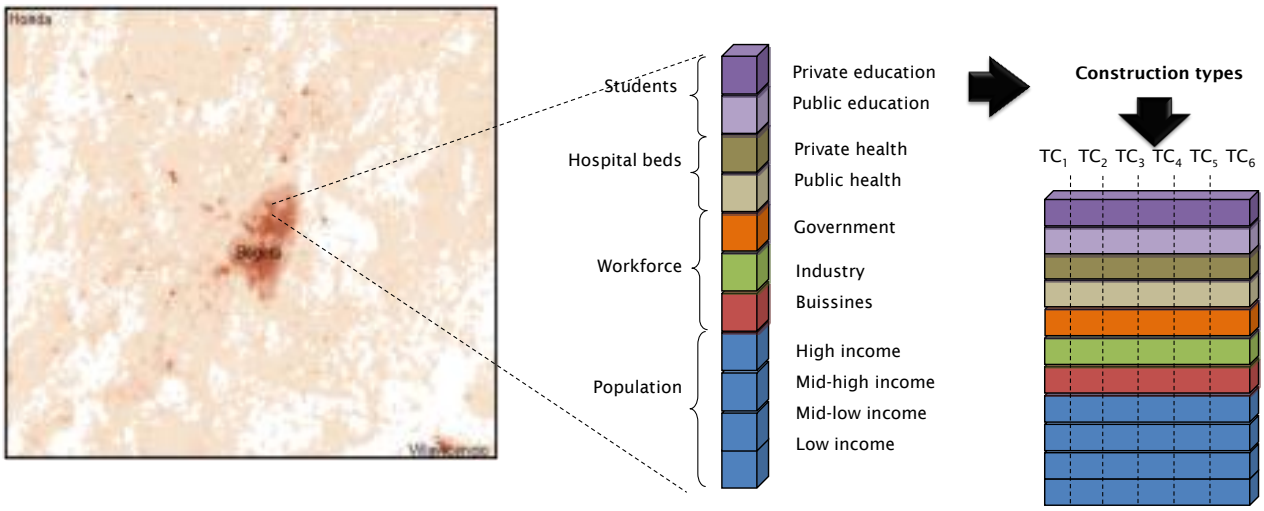

Figure 38. Summary of the process for the update of the global buildings exposure database

7 Archetypes of Vulnerability Functions

The vulnerability of exposed elements is defined using mathematical functions that relate the intensity to the direct physical impact. Such functions are called *vulnerability functions* and they must be estimated and assigned for each one of the asset types identified in the exposure database. Vulnerability functions provide the variation of the probability moments of the *relative loss* with increasing intensity. Figure 48 illustrates a schematic representation of a vulnerability function.

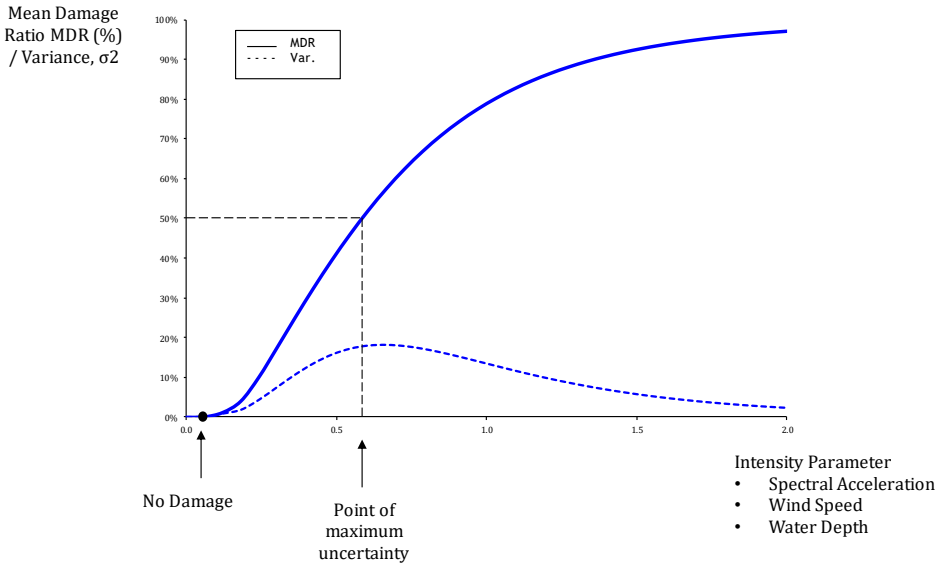

Figure 39. Schematic representation of a vulnerability function

Vulnerability functions facilitate the conversion from the occurrence of a hazard event and the local intensities it generates to a quantification of direct losses incurred by the exposed elements. Each type of element needs to be characterized based on its expected response to the intensities induced by each event. This characterization considers how the element may suffer damage and experience a reduction in its ability to provide service.

Damage can occur in various ways, necessitating that vulnerability functions rely on an understanding of how exposed infrastructure assets behave when subjected to external demands triggered by hazardous events. For instance, let's consider earthquake hazard. The response of a structure to ground shaking (structural dynamics) and its gradual loss of strength and stiffness (non-linear behavior) can be represented as a structural capacity curve, summarizing the overall behavior of the structure.

Defining loss (L) as a random variable, vulnerability curves describe the variation of the loss statistical moments for different values of seismic demand. Loss probability distribution is usually assumed Beta, where statistical moments correspond to mean and standard deviation. Beta distribution $p_{L|S}(L)$ is defined as follows:

$$p_{L|S}(L) = \frac{\Gamma(a+b)}{\Gamma(a)\Gamma(b)} L^{a-1}(1-L)^{b-1} \qquad \text{Eq. 19}$$

where Γ is the Gamma function and parameters a and b are:

$$a = \frac{1 - \left(1 + c^2(L|S)\right)E(L|S)}{c^2(L|S)} \quad \text{Eq. 20}$$

$$b = a\frac{1 - E(L|S)}{E(L|S)} \quad \text{Eq. 21}$$

where E(L|S) is the loss mean or expected value and c(L|S) is the loss variation coefficient, given a hazard intensity S (note that c(L|S)=SD(L|S)/E(L|S) where SD(L|S) is the loss standard deviation given a hazard intensity S).

Vulnerability curves provide all the necessary information to calculate the probability of reaching or exceeding a loss value, given as hazard intensity. Loss is defined using numerical scales instead of qualitative scales as for damage states (for example the ratio of repair cost to the asset replacement value), which allows its direct use in probabilistic risk and loss calculations. The probability of reaching or exceeding a loss value is calculated as follows:

$$\Pr\left(L \geq l|S\right) = \int_{l}^{\infty} p_{L|S}(L)dL \quad \text{Eq. 22}$$

where *l* is a loss value in the random variable *L* dominium.

7.1 Infrastructure Archetypes

We are working with a novel approach to develop vulnerability functions, based on the definition of archetypes of infrastructure components or elements. Such archetypes are simplified representation of the set of subcomponents some infrastructure element typically has. Those subcomponents may be buildings or other structures, machinery, electrical or electronical equipment, among others. They all exhibit a behavior or response to the hazards included in this study, that depend on the condition of emplacement of the subcomponent in the archetype. Therefore, all subcomponents have their own vulnerability functions, which combined, make up the vulnerability function of the archetype.

Table 19 presents an overview of all the desired infrastructure components to be defines as archetypes. The full extent of archetypes created is still unknown as it highly depends on the quality and level of detail of information in the exposure model, making it possible, or otherwise preventing, the representation of some archetype into the exposed elements database. Therefore, not all the elements listed in Table 19 will have corresponding archetypes.

To illustrate this approach, next we include an example of the construction of vulnerability functions for thermal power plants.

Table 19. Overview of infrastructure components under consideration

Power	Highways and Railways	Transportation	Water and wastewater	Communications	Oil & Gas
Power Generation • Coal power plants • Nuclear power plants • Hydroelectric power plants • Natural gas power plants • Fuel oil power plants • Dual-Fired Power Plants • Alternate/Renewable Energy Power Plants • Distributed Power Plants • Back-up Generators • Power Plant Substations **Power Transmission** • Transmission Lines and Towers • Transmission Substations • DC Converter Stations • Regional Control Centers **Power Distribution** • Distribution Lines • Distribution Substations • Step Down Transformers	**Road Transport** • Roads and Highways (including Toll Roads) • Bridges (including Toll Bridges) • Tunnels (including Toll Tunnels) • Operations and Traffic Management Centers • Border Crossing Facilities • Truck Terminals **Rail Transport** • Rail Cars (Freight and Passenger) • Tracks • Bridges • Tunnels • Yards • Passenger Stations • Operation Centers	**Waterway Transport** • Locks and Canals • Dams • Docks • Navigation Facilities **Sea Transport** • Seaports (Shallow and Deep Draft) **Air Transport** • Airports (Certified, Non-Certified, and Military) • Airstrips and Airfields • Heliports • Spaceports • Air Traffic Control and Navigation Facilities **Mass Transport** • Subway Systems • Commuter Rail Systems (Heavy and Light Rail) • Bus Systems • Tramway and Ferry Systems	**Water Supply, Storage and Treatment** • Raw Supply Assets (River, Lake, Spring Inlets, and Wells) • Raw Water Storage Assets (Reservoirs and Tanks) • Desalination Plants • Water Treatment and Filtration Plants • Finished Water Storage Assets (Towers, Clearwells, and Standpipes) **Water Delivery** • Water Tunnels • Aqueducts • Transmission Mains • Pumping Stations • Pipeline Interconnections • Distribution Mains • Service Pipelines • Control and Monitoring Stations **Wastewater Collection** • Sewer Inlets and Mains (Sanitary, Storm and Combined **Treatment, and Discharge** • Influent Storage (Tanks, Pits, Ponds and Basins) • Wastewater Treatment Plant • Pumping and Discharge Facilities • Control and Monitoring Stations	**Wireline Services** • End Office Switching Facilities • Access Tandems • Cables (including Submarine Cables) • Submarine Cable Landings • Telecom Hotels • Interexchange Carrier Points of Presence • Carrier Data Centers • Internet Service Provider Points of Presence • Internet Service Provider Routers **Cable Services** • Cable Broadcast Provider Headquarters • Headend/Distribution Hubs • Cables **Wireless Services** • Cell Towers • Base Transceiver Stations • Base Station Control Stations • Mobil Switching Offices **Broadcast Services** • Television/Radio Network Headquarters • Local Broadcast Centers • Transmitter Sites **Data Processing/Network Management** • Data Centers • Operation Centers	**Exploration and Production** • Offshore Drilling and Production Platforms • Subsea Facilities • Permanent Onshore Drilling Facilities • Wells (Production, Injection, Observation, and Disposal) **Oil and Gas Gathering and Separation** • Crude Oil Gathering Pipelines • Gas Oil Separation Plants • Tank Batteries (Field Separation and Storage) • Crude Oil Lease Automatic Custody Transfer Units • Gas Gathering Pipelines and Compressors • Field Gas Processing Plants (Dehydration, Sweetening, and Nitrogen Rejection) • Gas Sales Meters **Oil Storage, Refining, Transport and Distribution** • Bulk Storage Facilities (Terminal, Refinery, and Pipeline Breakout) • Offshore Mooring Systems • Underground Crude Storage • Refineries • Oil Main Pipelines and Interconnections • Pumping Stations • Control Centers • Truck and Rail Racks **Natural Gas Processing, Transport and Storage** • Gas Processing Plants • NGL Fractionation Plants • Gas Transmission Pipelines and Interconnections • Transmission Compressor Stations • Control Centers • Natural Gas Market Hubs • Natural Gas Storage Facilities • City Gates and Distribution Pipelines • LNG Trains and Regasification Facilities • LPG/Propane Interconnected Assets

7.2 Example Archetype: Thermal Power Plant

A thermal power plant is a type of power generation station in which heat energy is converted to electrical energy. In a steam-generating cycle (also known as traditional), heat is used to boil water in a large pressure vessel to produce high-pressure steam, which drives a steam turbine connected to an electrical generator. The low-pressure exhaust from the turbine enters a steam condenser where it is cooled to produce hot condensate which is recycled to the heating process to generate more high-pressure steam.

We have identified three different types of thermal power plants for which functions are created:

- Tradition thermal plant, that is based on a steam-generating cycle, in which coal, oil or natural gas is burned, heating water, and expanding water vapor.
- Gas turbines plant, that is based on a compressed air heating cycle, in which oil or natural gas is burned, expanding compressed heated air to work the turbine.
- Combined cycle, which uses both the previous cycles to increase efficiency.

In this example, we develop in detail the *traditional thermal plant* archetype. This archetype has a collection of components that interact, allowing the plant to provide the required service. Figure 40 shows a general block diagram of the interaction of some of the power plant components.

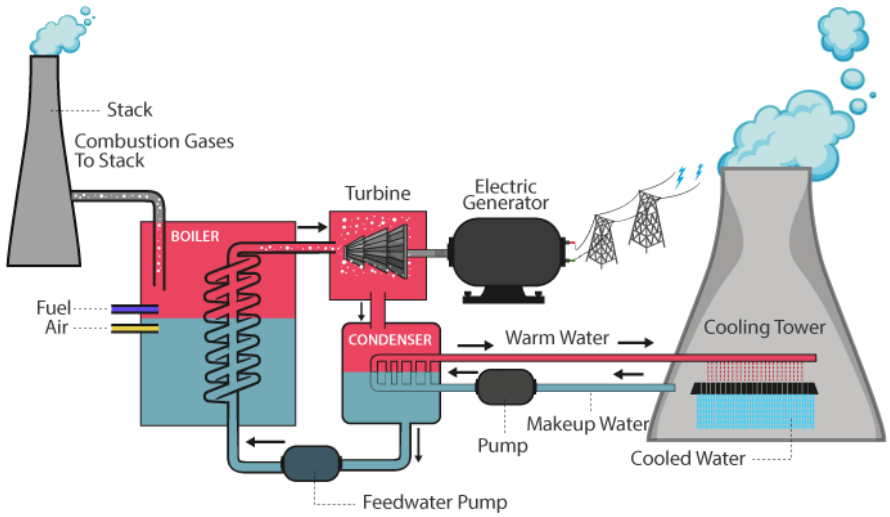

Figure 40. Simplified block diagram of a thermal power plant (taken from https://byjus.com/physics/fossil-fuel/)

In our archetype of a traditional thermal power plant, we are considering the following list of components:

- Main building
- Coal conveyers
- Pulverizer
- Boiler
- Ash collector
- Air preheater
- Precipitator
- Chimney

- Turbine
- Generator
- Condenser
- Cooling tower
- Transformers
- Switchboard and power lines

The full set of components are required for the plant to operate correctly. However, all these components are quite different among them. Such differences are considered here in a simplified way, by setting condition variables to each component. A component's condition is defined as the combination of the following features:

- *Elevation* (over some predefined ground level)
- Type of *foundation*
- Is it *watertight* or not
- Is it *protected*, up to some extent and for some hazards, by any other component in the archetype
- Component *type*:
    - Thermal equipment
    - Mechanical equipment
    - Electromechanical equipment
    - Electrical equipment
    - Construction (any type of civil work different form a building)
    - Building

Although probably not exhaustive, this list of features is assumed to sufficiently qualify the condition of any component inside the archetype. Table 20 summarizes the condition of the components for the traditional thermal power plant.

Table 20. Condition for each component of the traditional thermal power plant

Component	Elevation (m)	Foundation	Watertight	Protection	Buried	Type
Main building	0	Normal	No	No	No	Building
Coal conveyers	3	Normal	No	No	No	Mechanical
Pulverizer	0	Normal	No	No	No	Mechanical
Boiler	0	Stiff	No	Yes	No	Thermal
Ash collector	0	Normal	No	No	No	Mechanical
Air preheater	1	Normal	No	Yes	No	Mechanical
Precipitator	0	Normal	No	Yes	No	Electromechanical
Chimney	0	Normal	No	No	No	Construction
Turbine	0	Isolation	Yes	Yes	No	Electromechanical
Generator	0	Normal	Yes	Yes	No	Electromechanical
Condenser	0	Normal	Yes	Yes	No	Thermal
Cooling tower	0	Normal	No	No	No	Construction
Transformers	2	Normal	No	Yes	No	Electrical
Switchboard	0	Normal	No	Yes	No	Electrical

Each component will have a set of vulnerability functions that capture its behavior against the hazards included in this project. In general, some of the individual functions will come from existing studies

focusing on infrastructure. Nonetheless, it is worth mentioning that such efforts are rare[13], making it very difficult to find previously proposed and tested vulnerability functions for infrastructure components and subcomponents. Therefore, most of the individual functions are proposed by INGENIAR based on our own expertise.

Continuing the example, from Figure 41 to Figure 44 we show the individual vulnerability functions for the main building, boiler, cooling tower and turbine, only to illustrate the differences that depend on the element's condition.

Furthermore, all the elements in the archetype have some relative level of importance in the operation of the plant. Although it is debatable to assign importance based on component's price, we use it as a proxy with high confidence that it captures the relevance of each component for most archetypes. In the case of the traditional thermal power plant, we assume the value distribution presented in Table 21.

Table 21. Value participation for each component of the traditional thermal power plant

Component	Value participation
Main building	8%
Coal conveyers	4%
Pulverizer	2%
Furnace	16%
Ash collector	2%
Air preheater	2%
Precipitator	2%
Chimney	8%
Turbine	16%
Generator	16%
Condenser	2%
Cooling tower	20%
Transformers	1%
Switchboard	1%

[13] The most prolific sources are HAZUS of the US FEMA and the European SYNER-G project. Nonetheless, most functions are defined for earthquakes only.

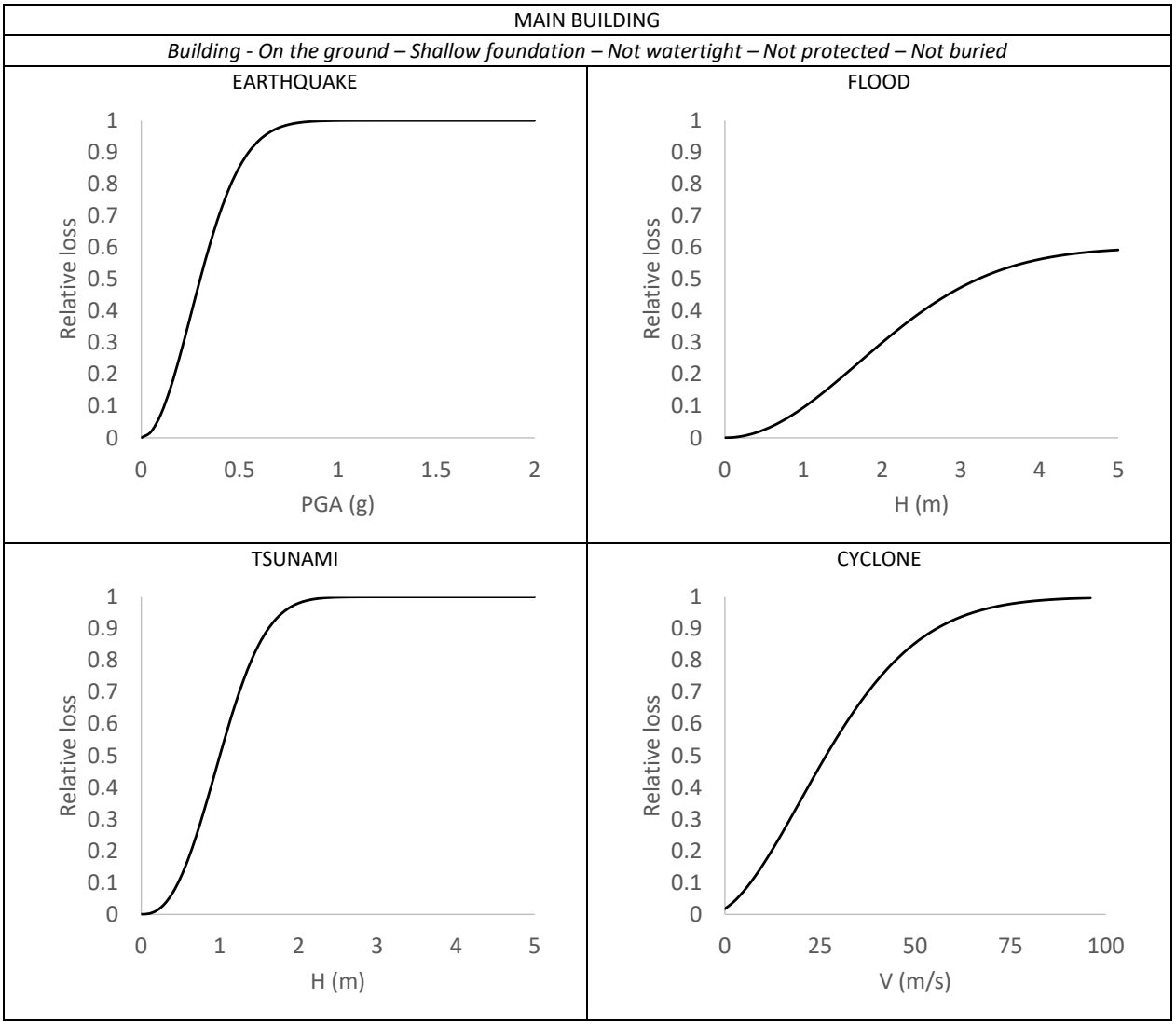

Figure 41. Vulnerability functions for the Main Building

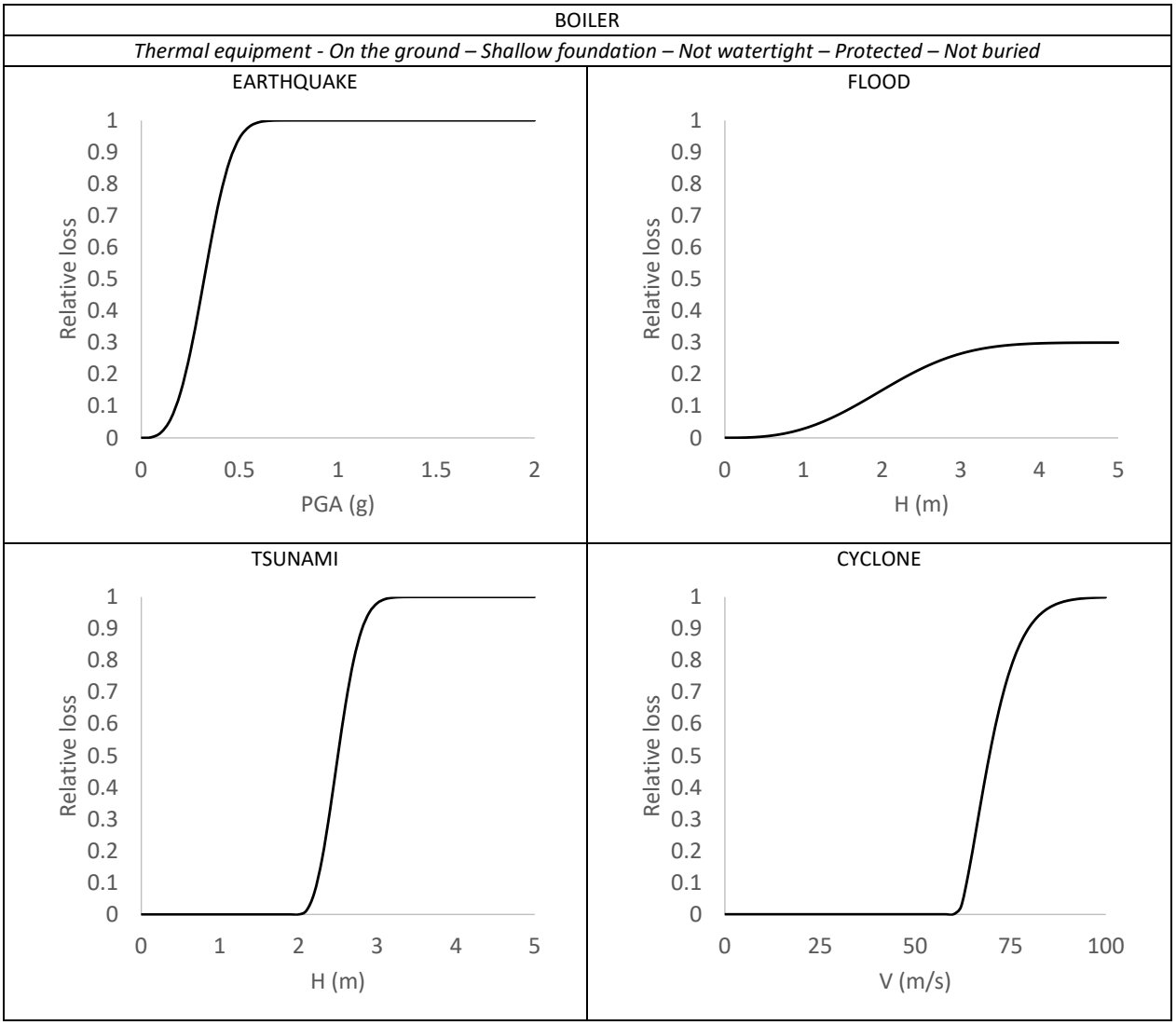

Figure 42. Vulnerability functions for the Boiler

COOLING TOWER

Construction - On the ground – Shallow foundation – Not watertight – Not protected – Not buried

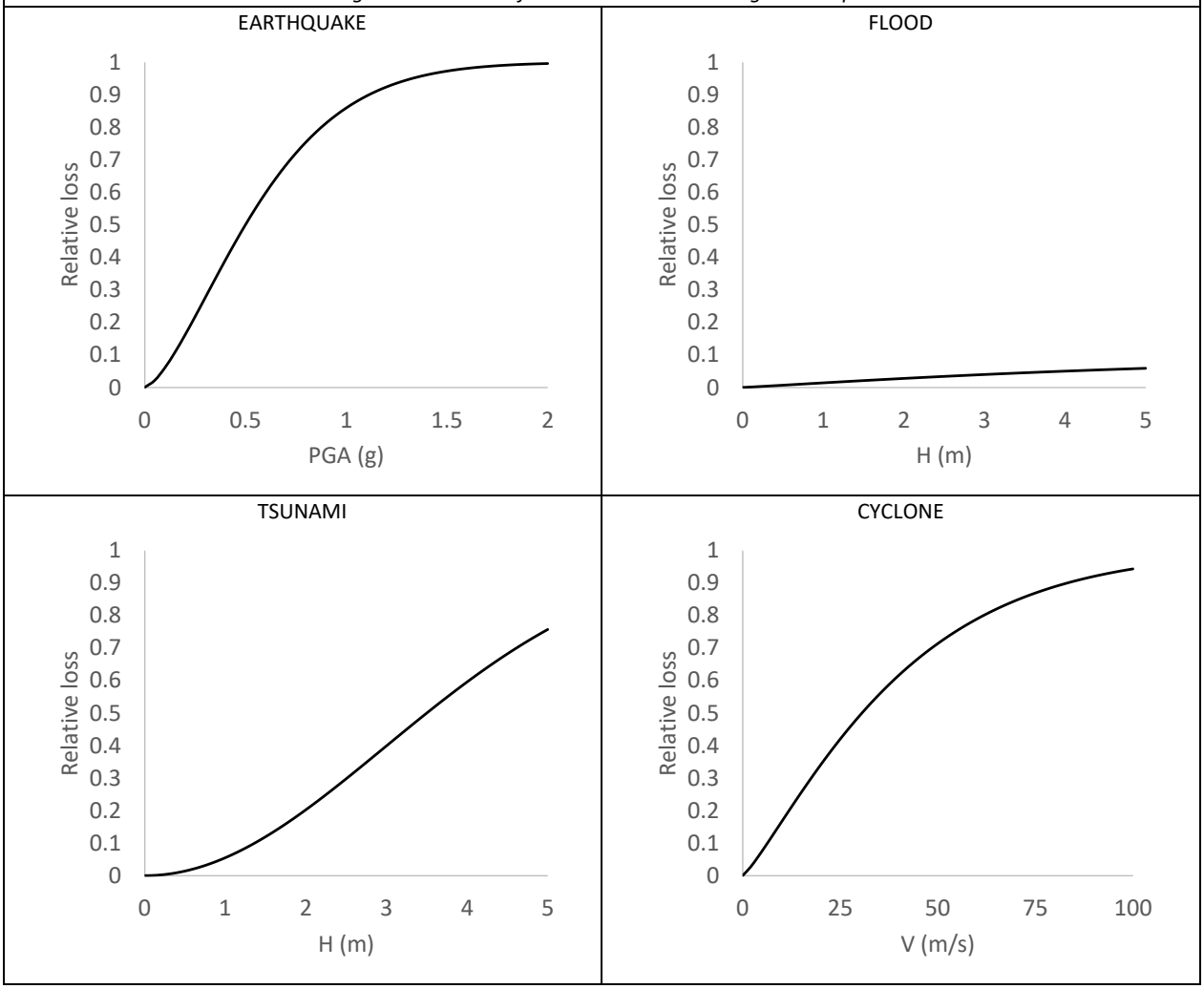

Figure 43. Vulnerability functions for the Cooling Tower

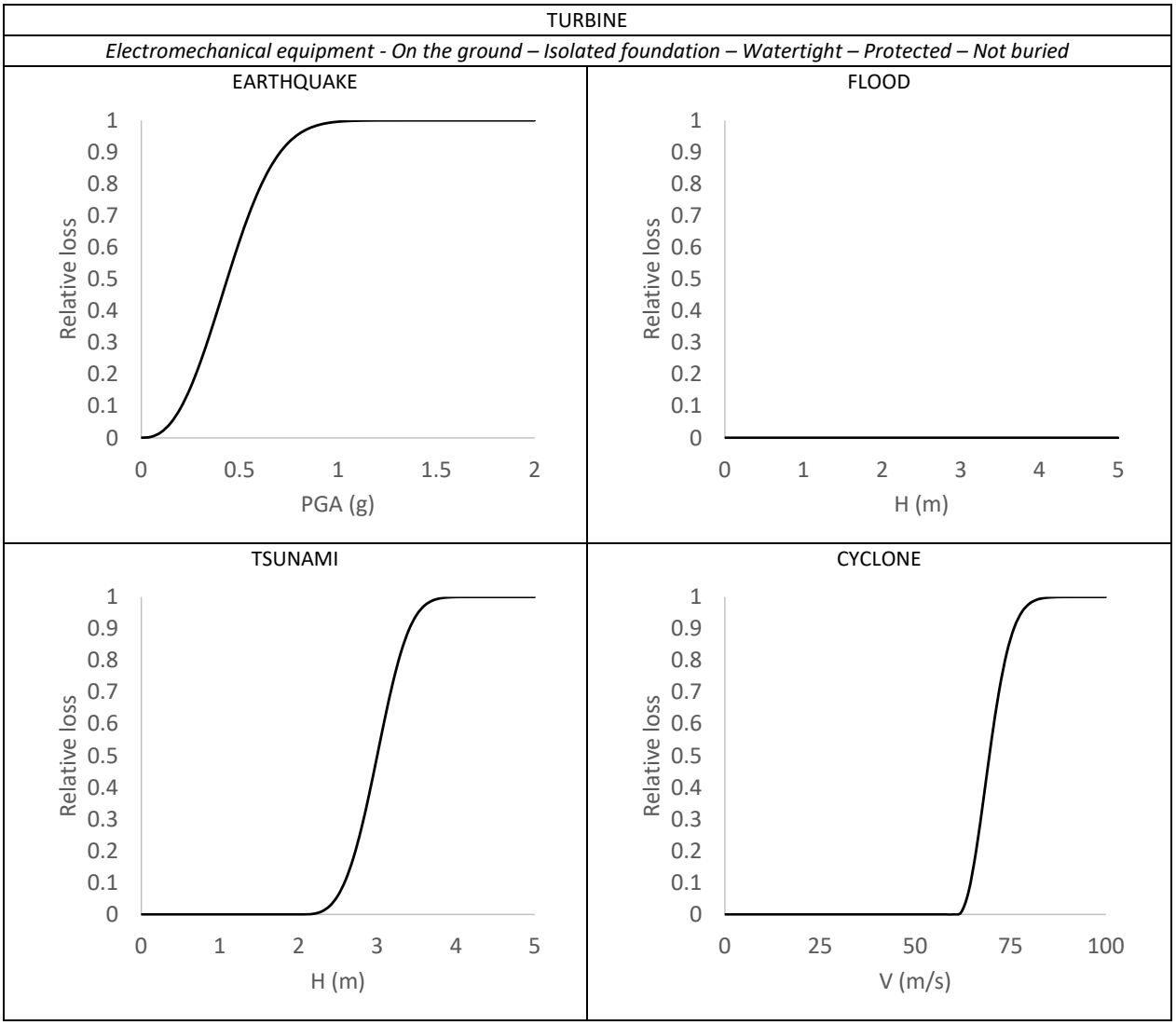

Figure 44. Vulnerability functions for the Turbine

The individual vulnerability functions are combined for the same hazard[14] into the overall function for the archetype, using value participations a weights. Figure 45 to Figure 48 show the individual functions and the combined one for earthquakes, floods, tsunami and tropical cyclones wind for the traditional thermal plant. The same procedure may be applied to the other thermal plant archetypes, producing different curves given the different collection, conditions and price distribution of the corresponding components. From Figure 49, we show the comparison of vulnerability functions for the three thermal plant archetypes included here.

[14] Note that this implies that all individual functions are expressed in the same intensity variable.

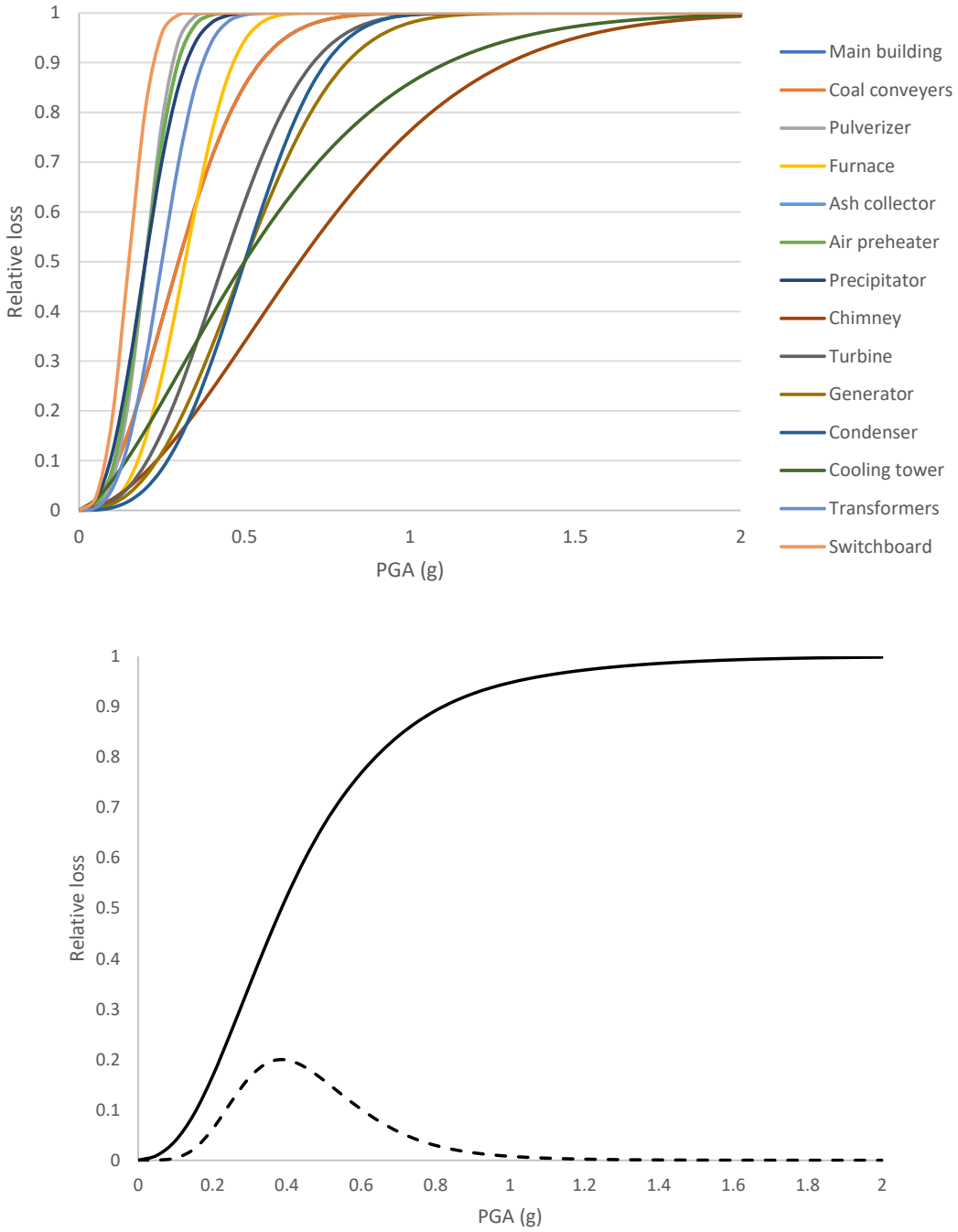

Figure 45. Vulnerability functions for earthquake. Top: by component. Bottom: total.

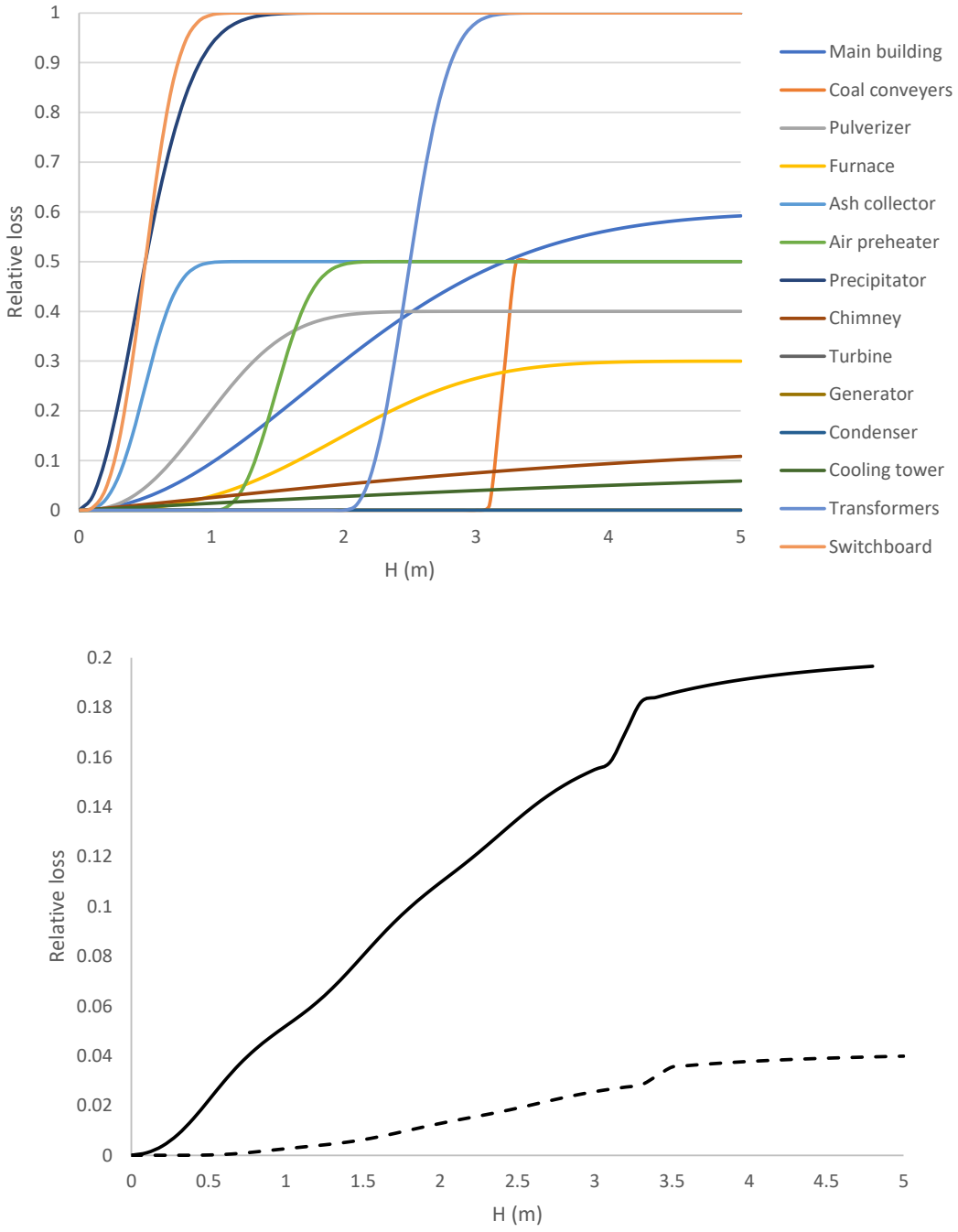

Figure 46. Vulnerability functions for floods. Top: by component. Bottom: total.

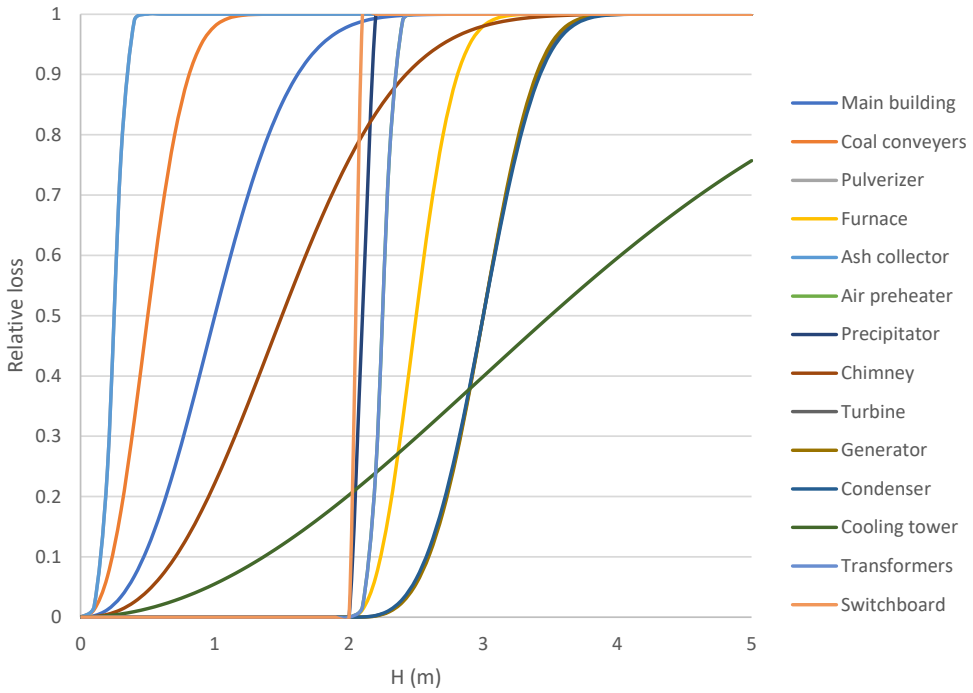

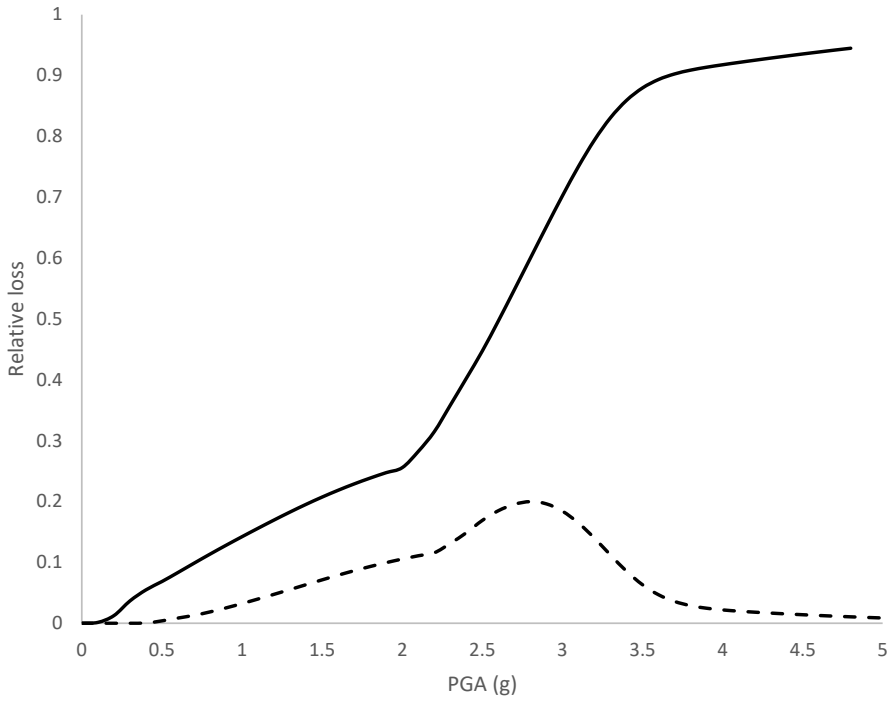

Figure 47. Vulnerability functions for tsunami. Top: by component. Bottom: total.

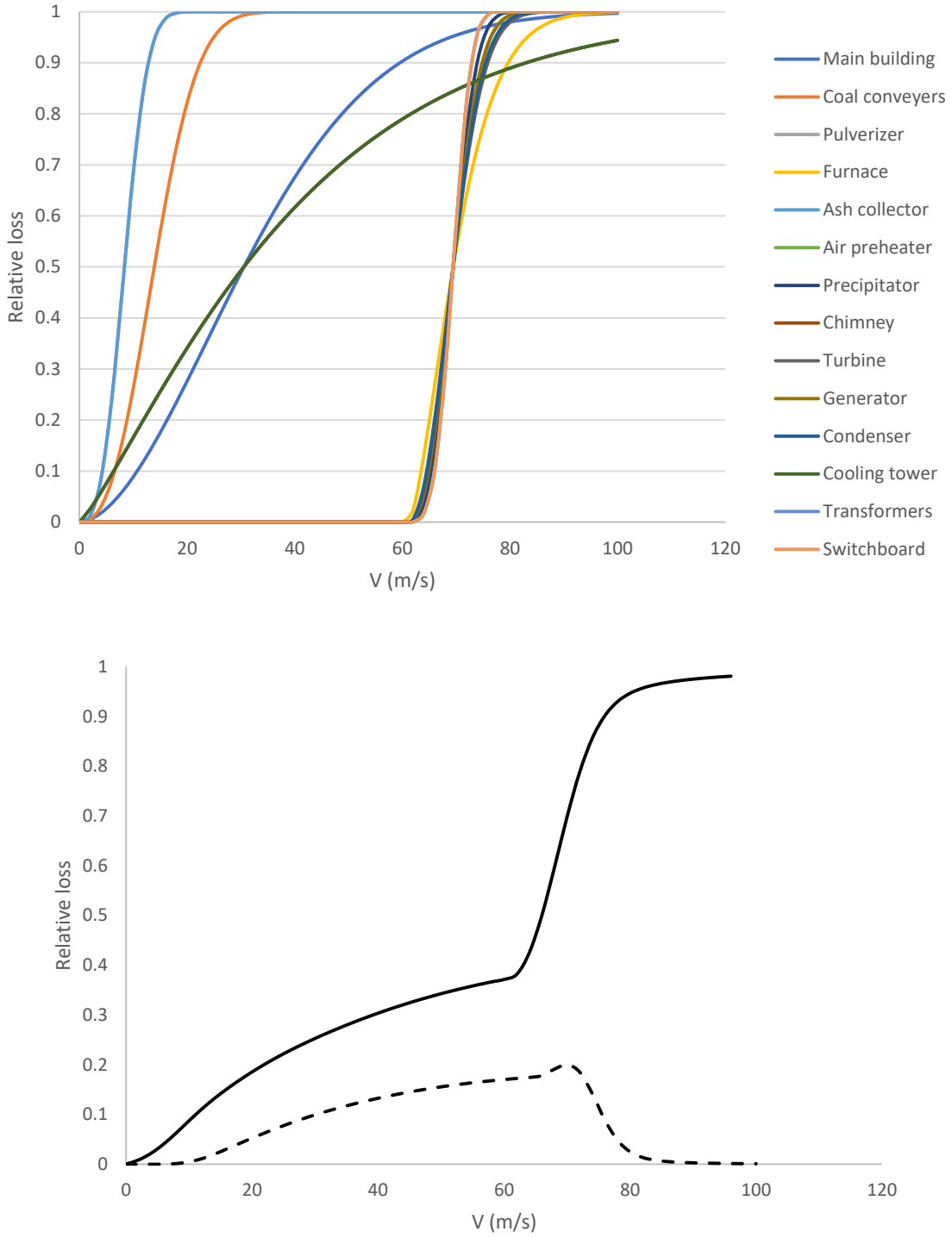

Figure 48. Vulnerability functions for tsunami. Top: by component. Bottom: total.

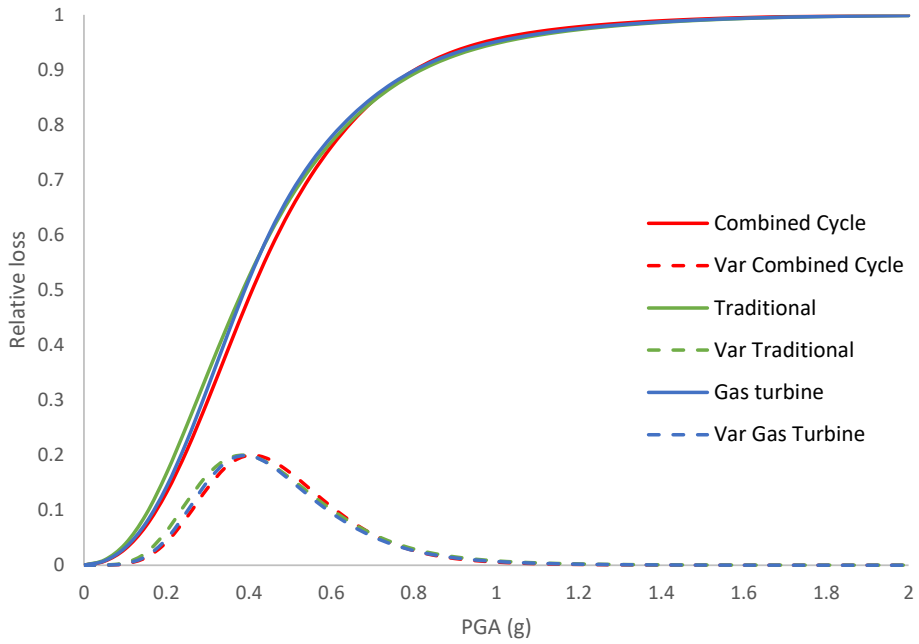

Figure 49. Earthquakes vulnerability functions for the thermal power plant archetypes

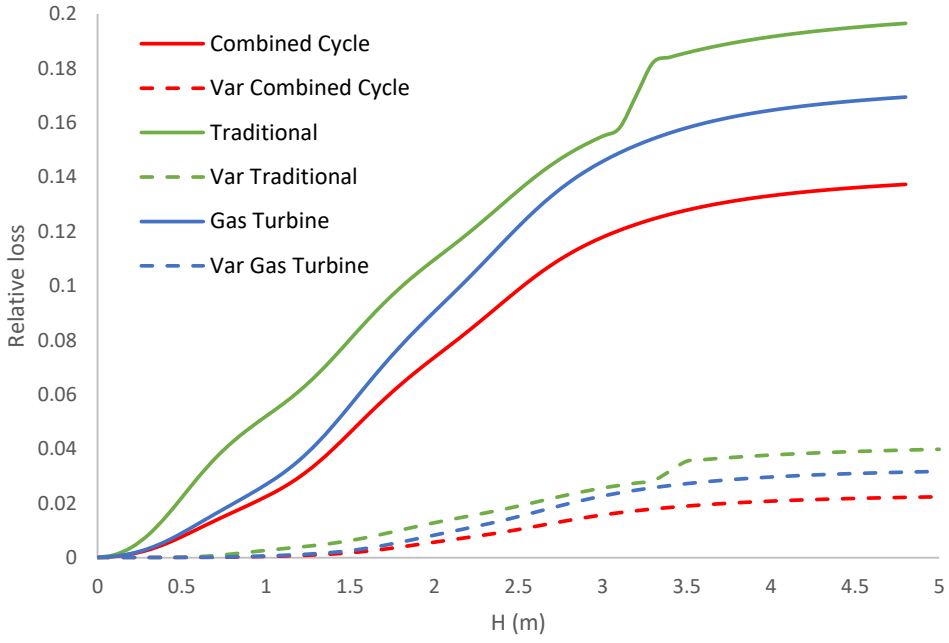

Figure 50. Flood vulnerability functions for the thermal power plant archetypes

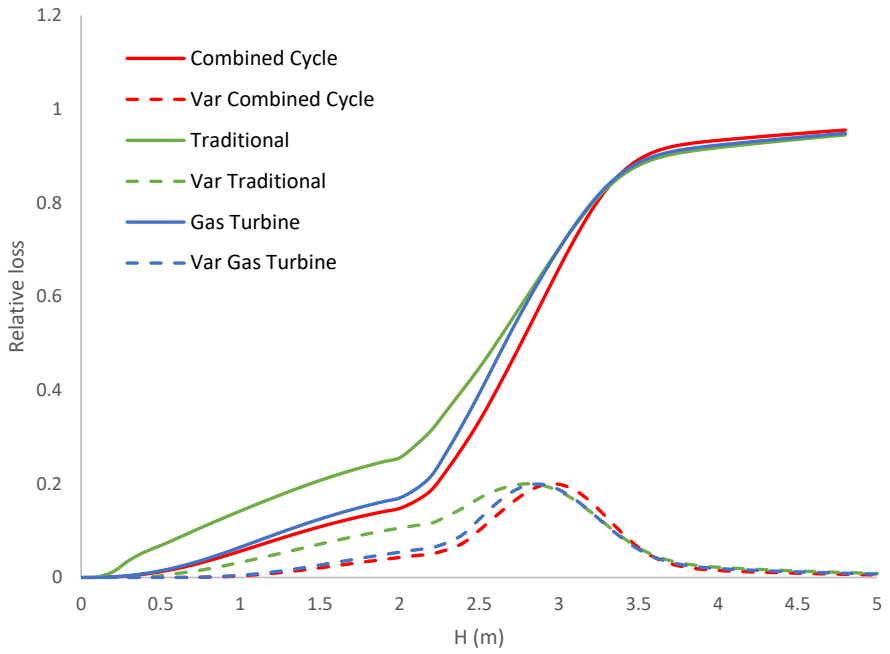

Figure 51. Tsunami vulnerability functions for the thermal power plant archetypes

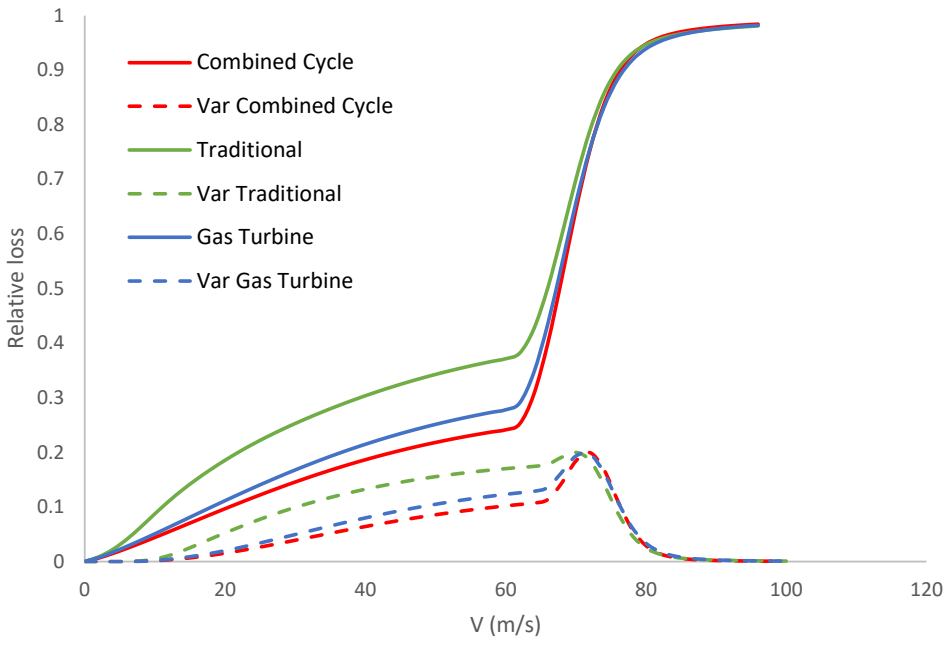

Figure 52. Cyclones vulnerability functions for the thermal power plant archetypes

8 Risk Results

Using the methodology described above, risk metrics for 245 countries and territories across five distinct natural hazards were calculated. In the subsequent sections, global maps illustrating the Average Annual Loss (AAL) for each of these hazards are presented.

For a better visualization and a better reading experience the AAL and the Probable Maximum Loss (PML) results for 10, 25, 50, 100, 250, 500, 1000, 2500 and 5000-years return period for the different hazards for both buildings and infrastructure are available in the following links:

https://ingeniar-risk.com/sites/default/files/documentos/AAL_Infrastructure_per_country.pdf

https://ingeniar-risk.com/sites/default/files/documentos/PML_Infrastructure_per_country.pdf

https://ingeniar-risk.com/sites/default/files/documentos/AAL_Buildings_per_country.pdf

https://ingeniar-risk.com/sites/default/files/documentos/PML_Buildings_per_country.pdf

As previously noted, our risk assessments encompass climate change-induced modifications for floods and tropical cyclones. The outcomes are consolidated in climate hazards risk maps, covering both the baseline climate and two alternative climate change scenarios. In the case of geological hazards, the results have been combined into a single stationary risk map. Furthermore, we have included AAL maps specific to each of the sectors and the three climate scenarios considered in our evaluation.

8.1 Risk Results by Hazard

The following maps present the relative Average Annual Loss results including both the buildings and infrastructure for each hazard. The AAL is relative to the exposed value of each country and is presented to the thousand (‰).

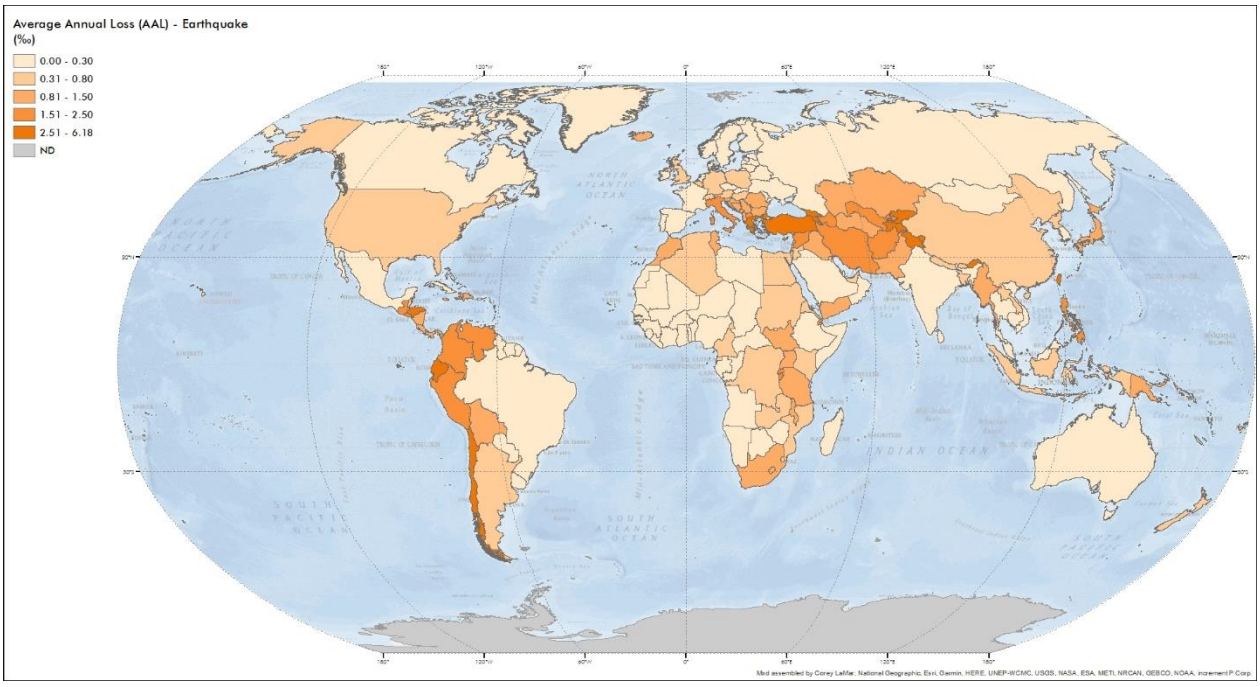

Figure 53. Earthquake relative AAL (‰)

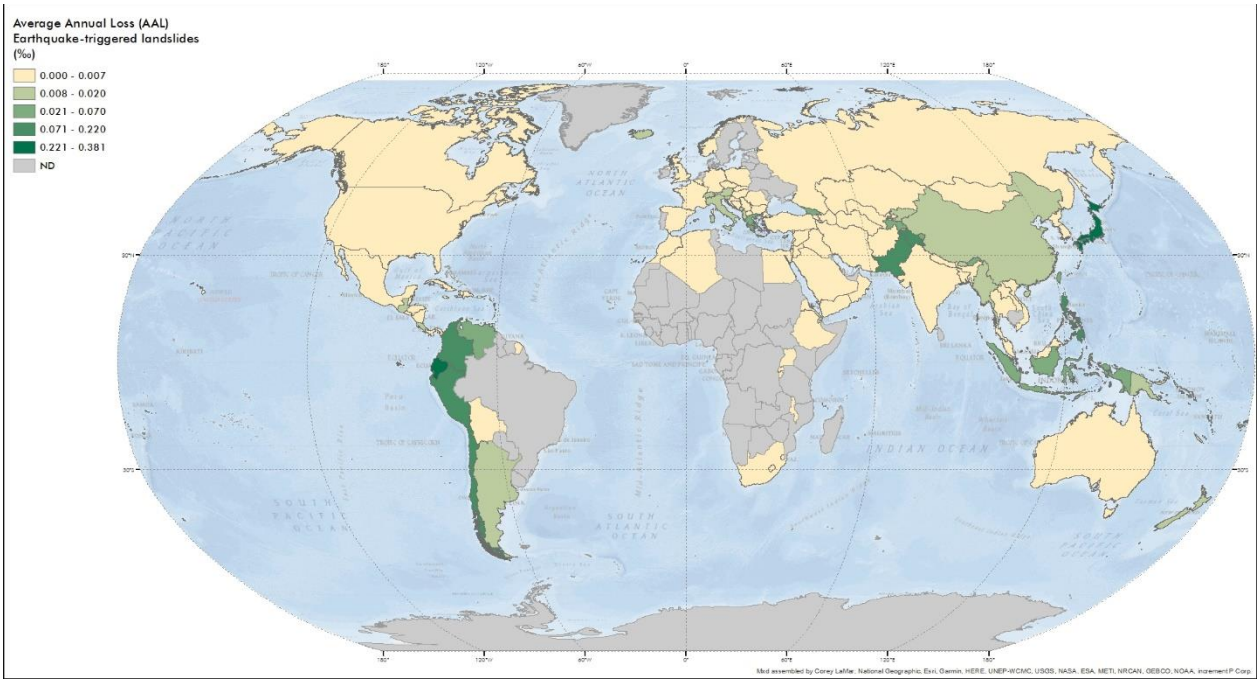

Figure 54. Earthquake triggered landslides relative AAL (‰)

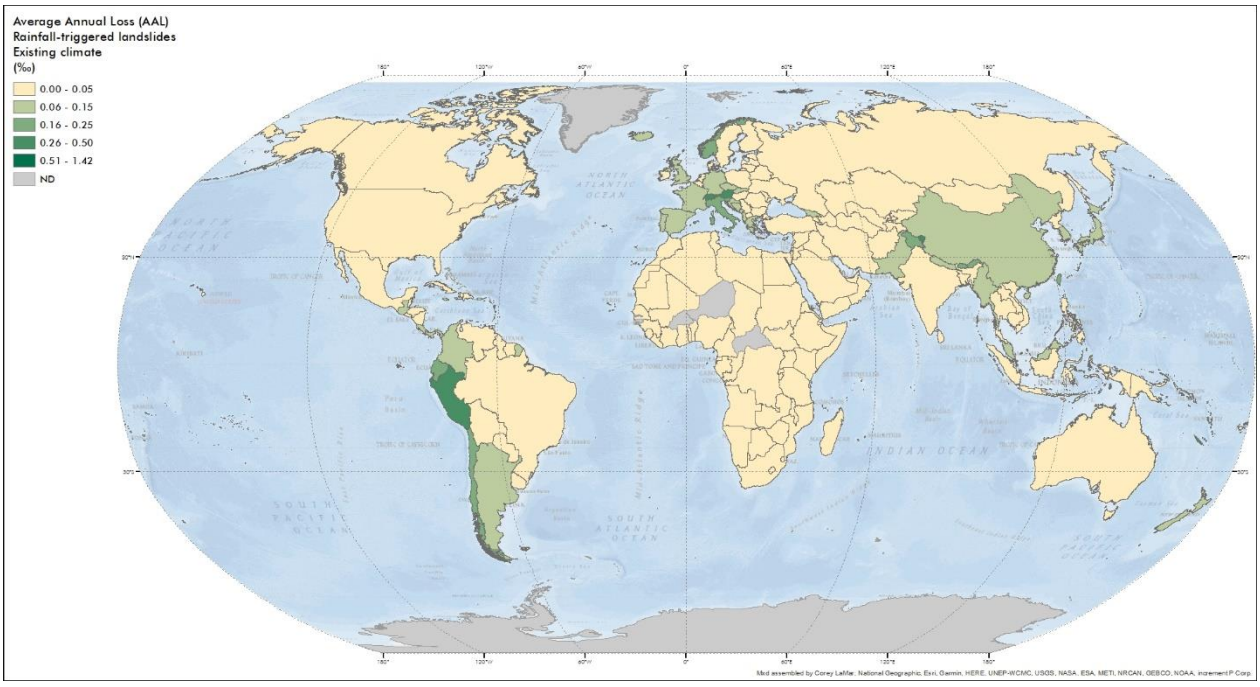

Figure 55. Rainfall triggered landslides relative AAL (‰) for the existing climate scenario.

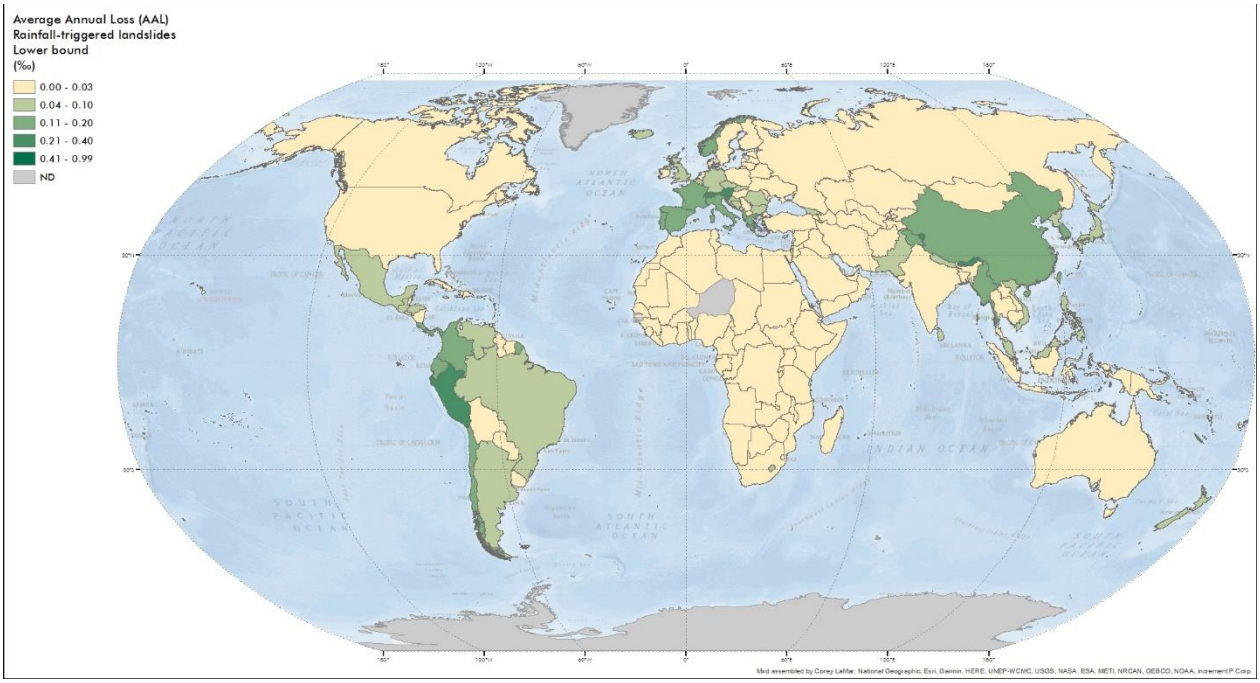

Figure 56. Rainfall triggered landslides relative AAL (‰) for the lower bound climate scenario.

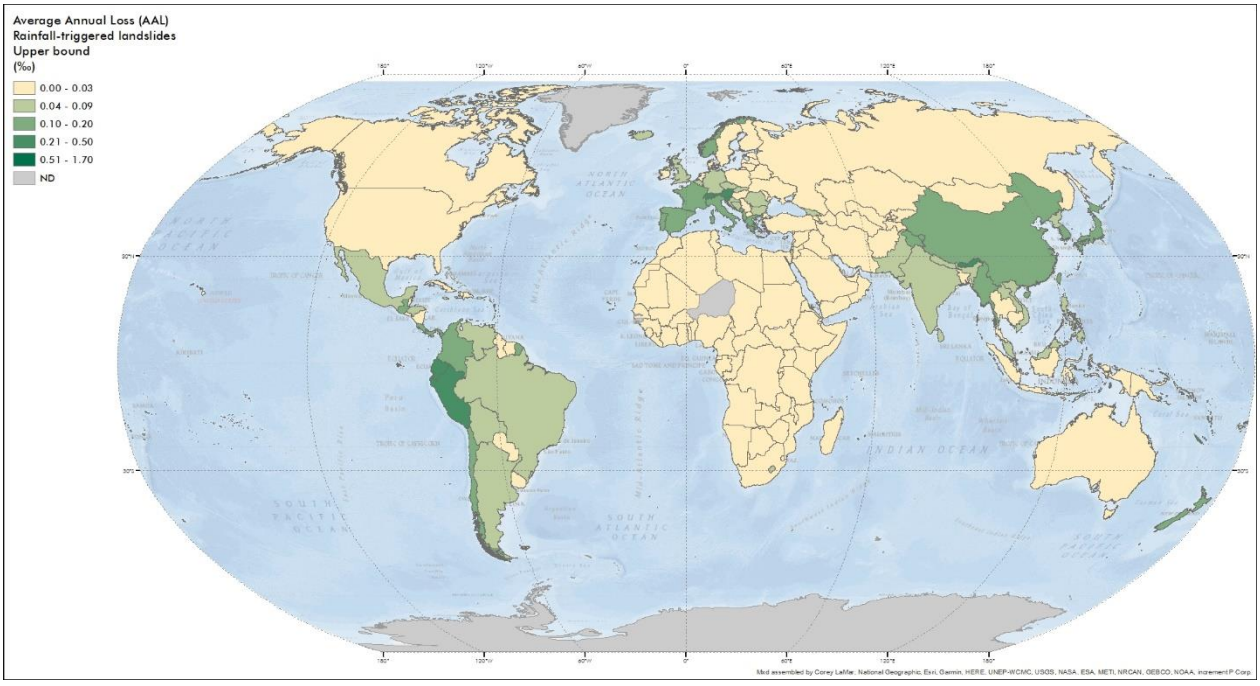

Figure 57. Rainfall triggered landslides relative AAL (‰) for the upper bound climate scenario.

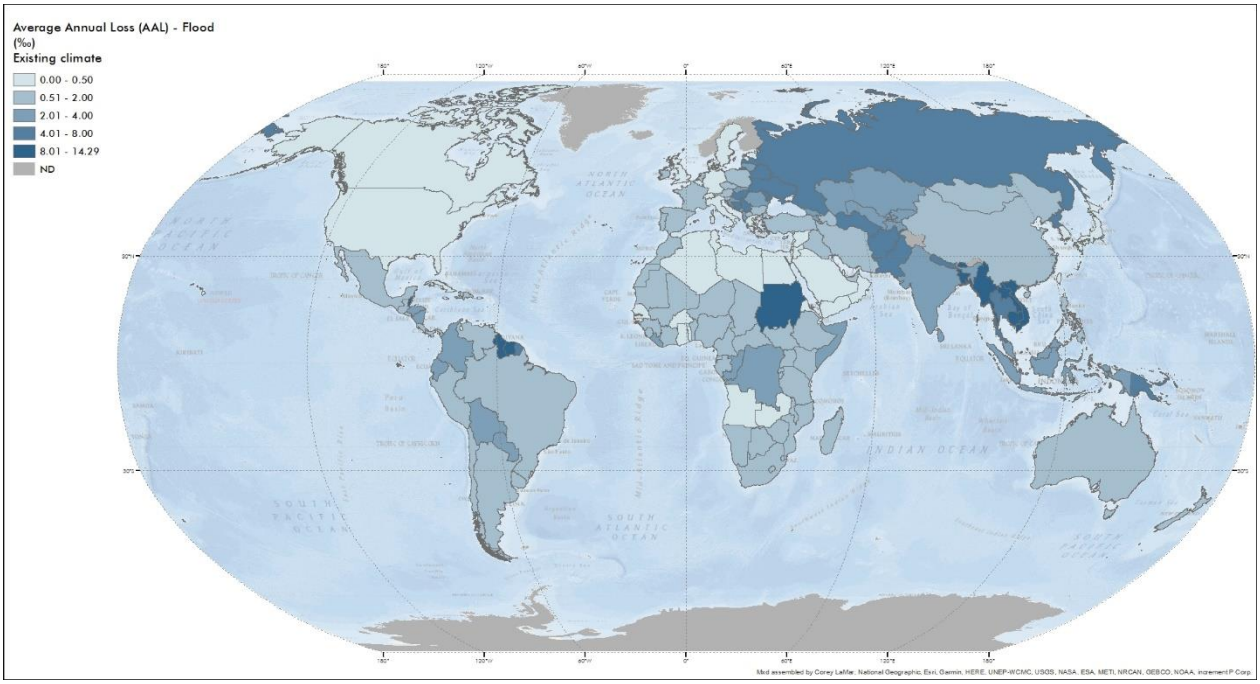

Figure 58. Flood relative AAL (‰) for the existing climate scenario

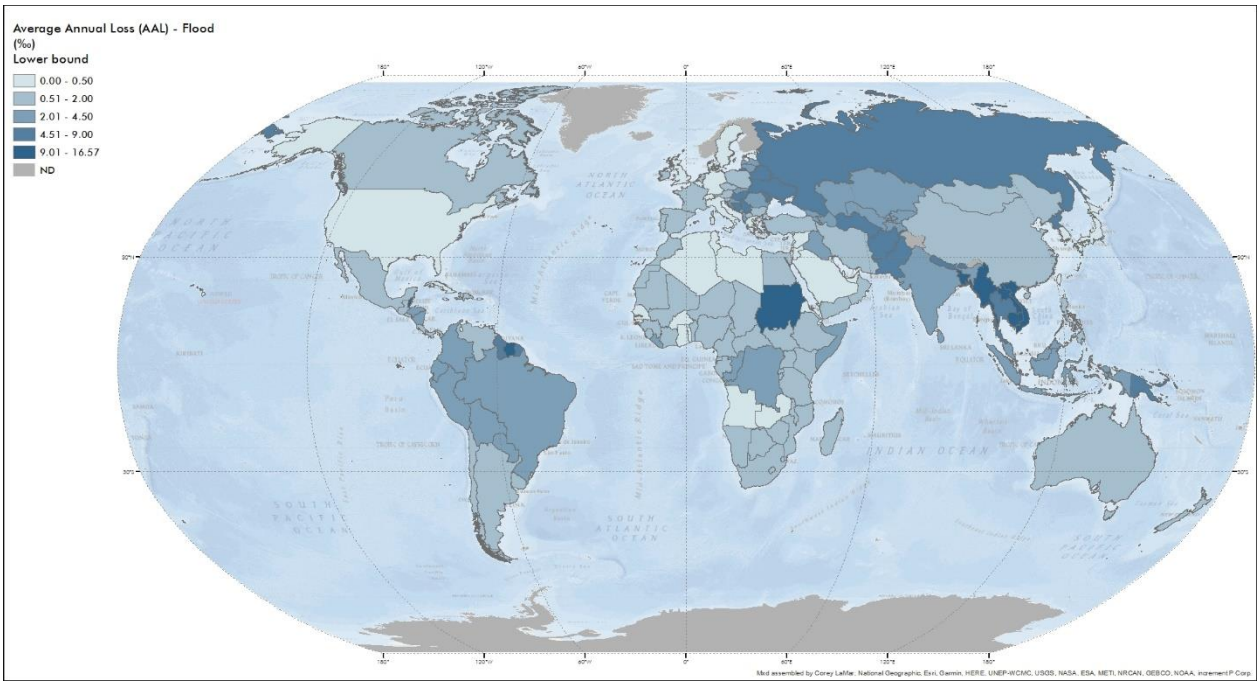

Figure 59. Flood relative AAL (‰) for the lower bound climate scenario

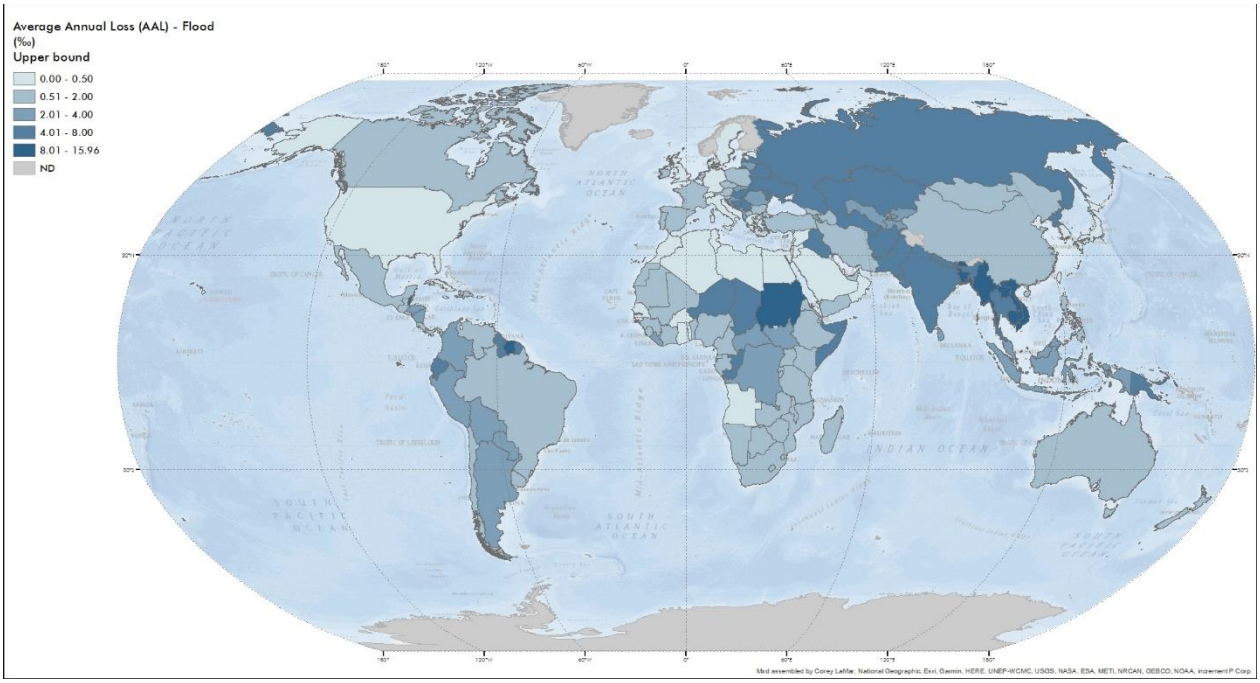

Figure 60. Flood relative AAL (‰) for the upper bound climate scenario

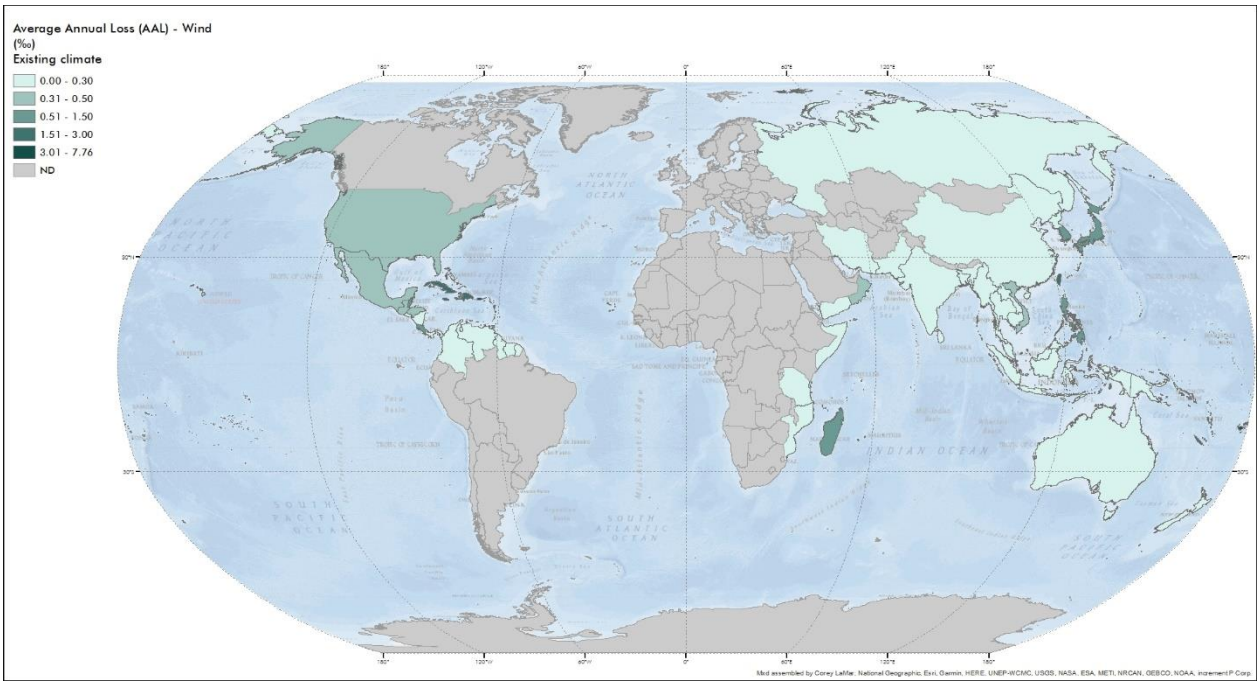

Figure 61. Strong wind (tropical cyclone) relative AAL (‰) for the existing climate scenario

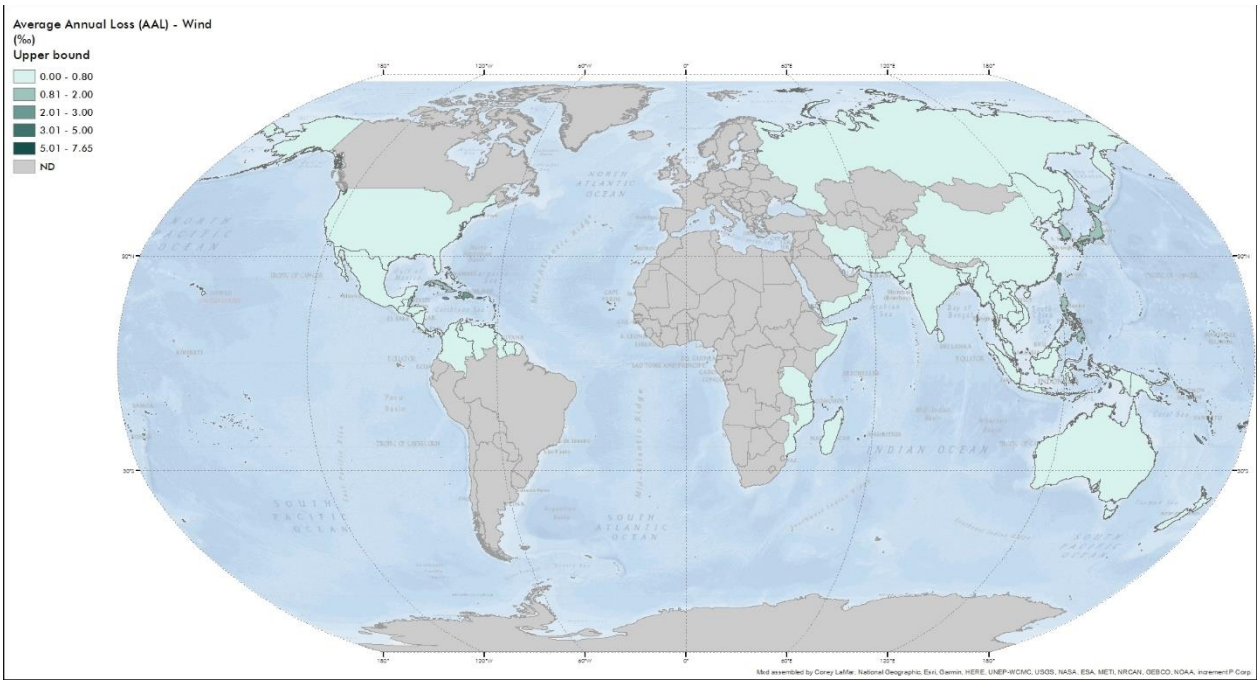

Figure 62. Strong wind (tropical cyclone) relative AAL (‰) for the upper bound climate scenario

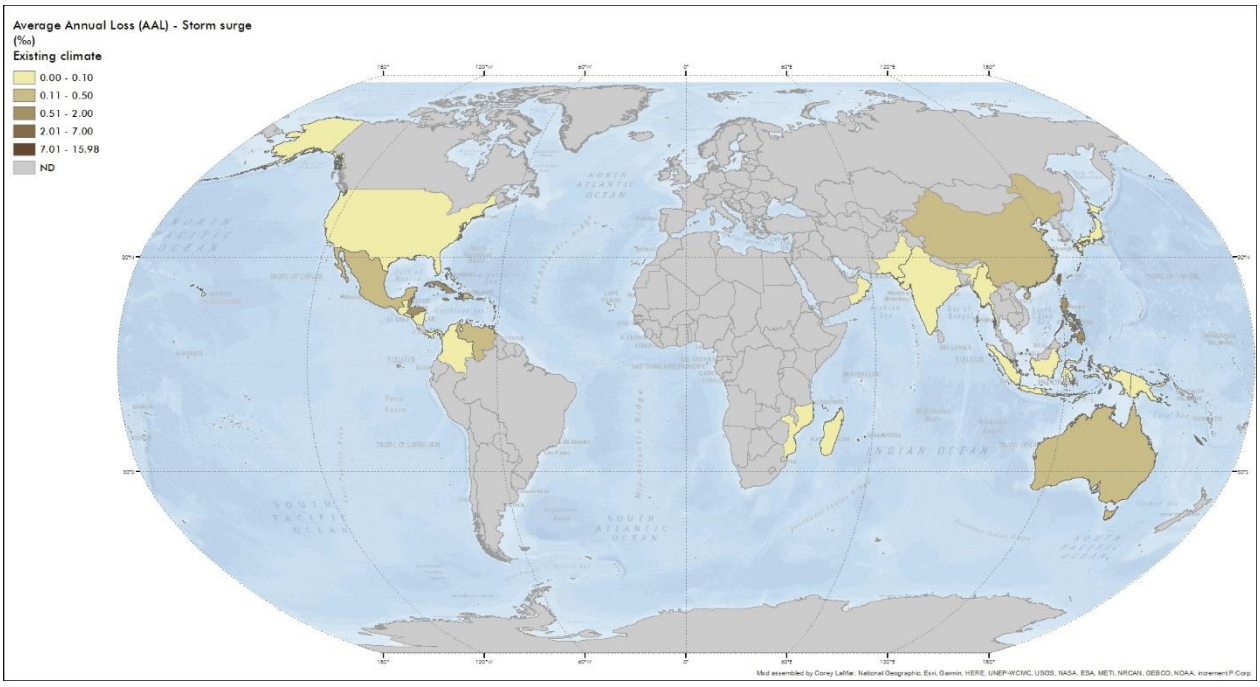

Figure 63. Storm surge (tropical cyclone) relative AAL (‰) for the existing climate scenario

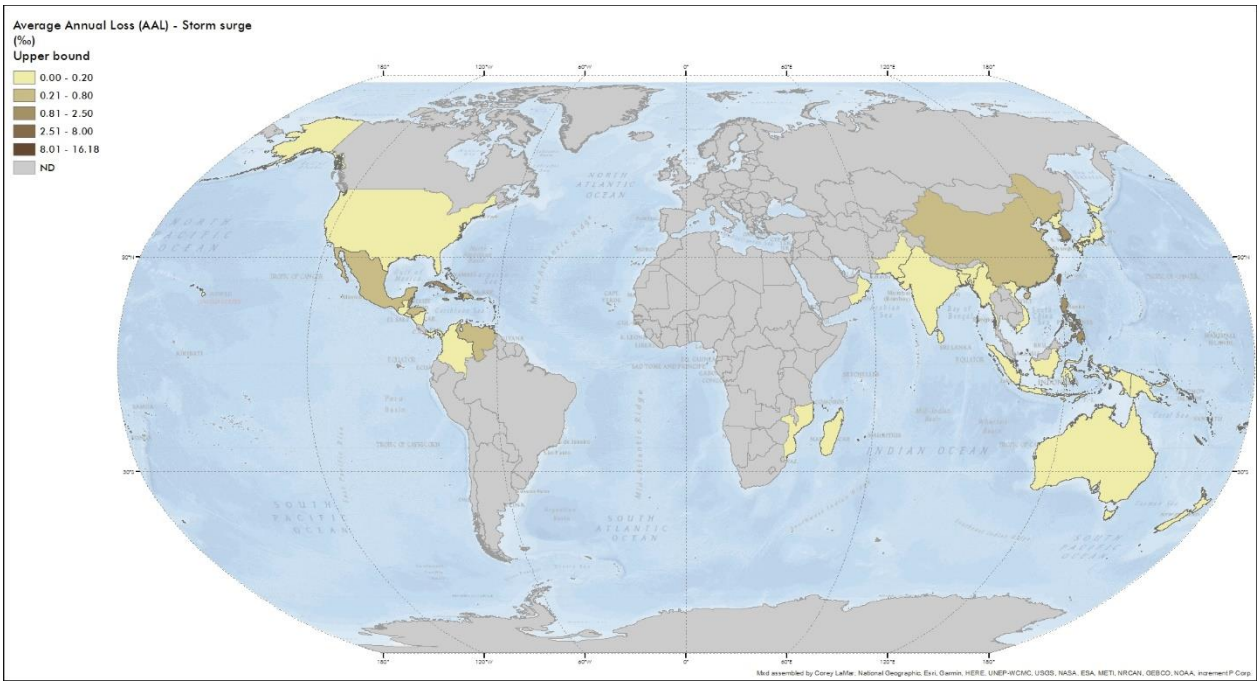

Figure 64. Storm surge (tropical cyclone) relative AAL (‰) for the upper bound climate scenario

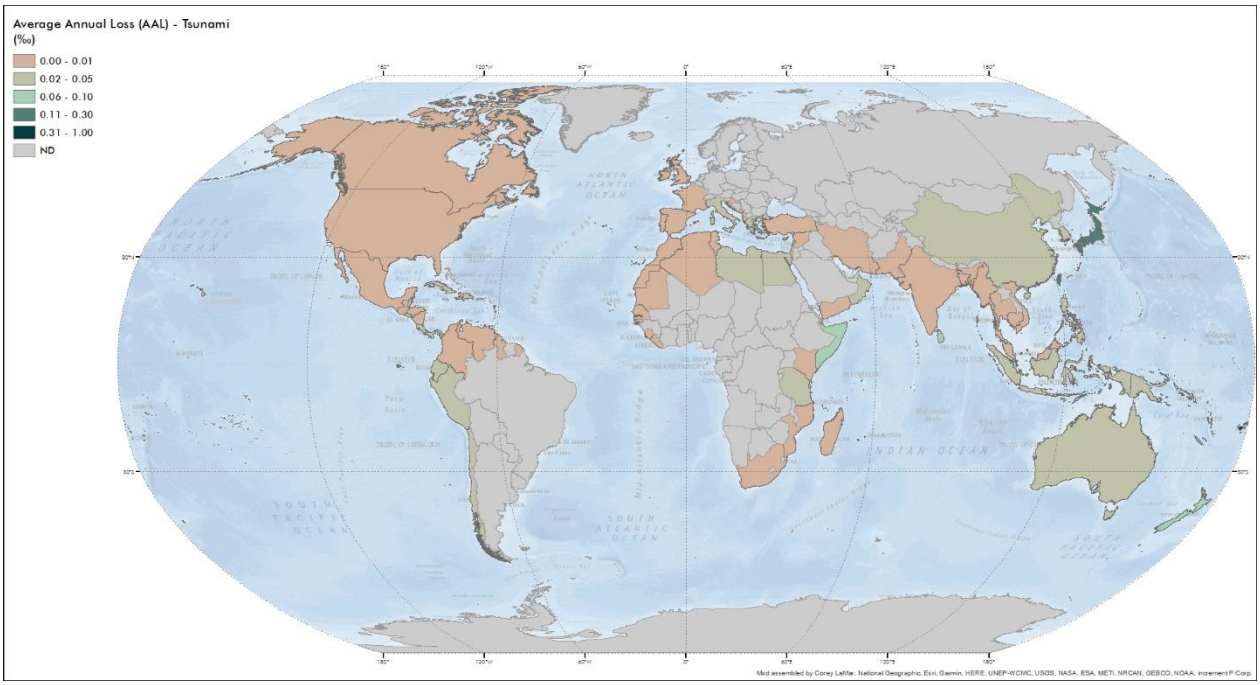

Figure 65. Tsunami relative AAL (‰)

8.2 Risk Results by Sector

The following maps present the multi-hazard Average Annual Loss results for each sector and for each climate scenario. The maps showcase the AAL relative to the exposed value of each country and is presented to the thousand (‰).

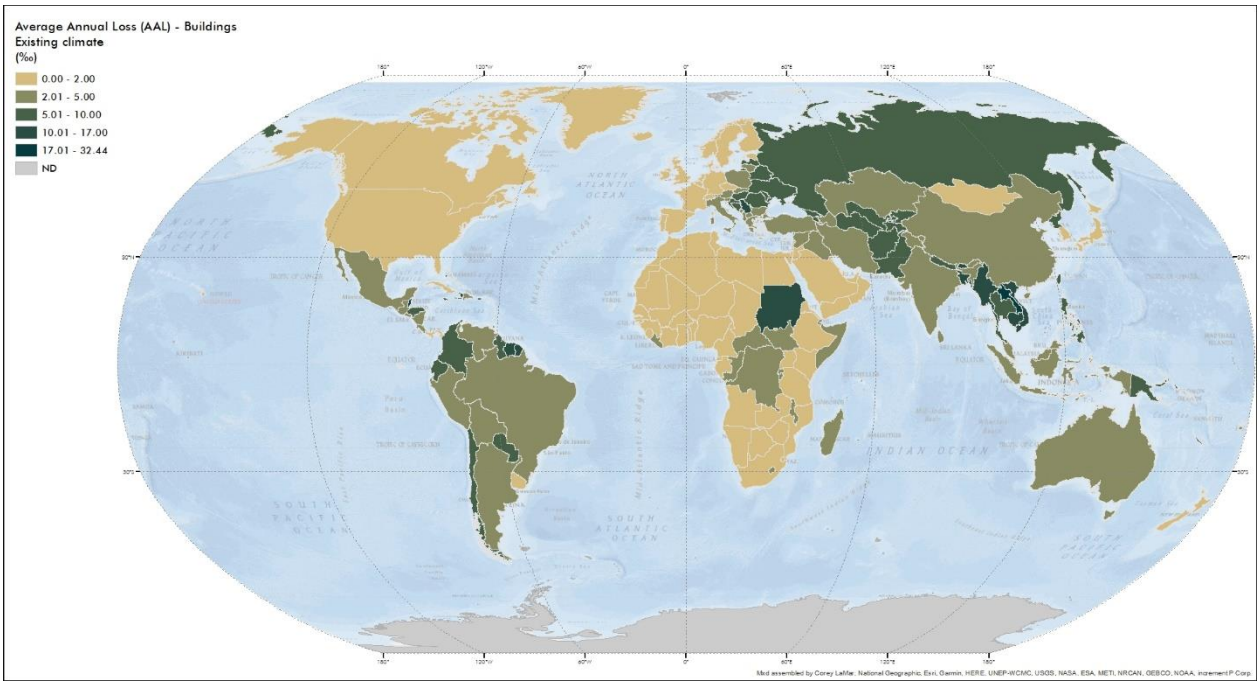

Figure 66. Relative AAL (‰) for buildings. Existing climate

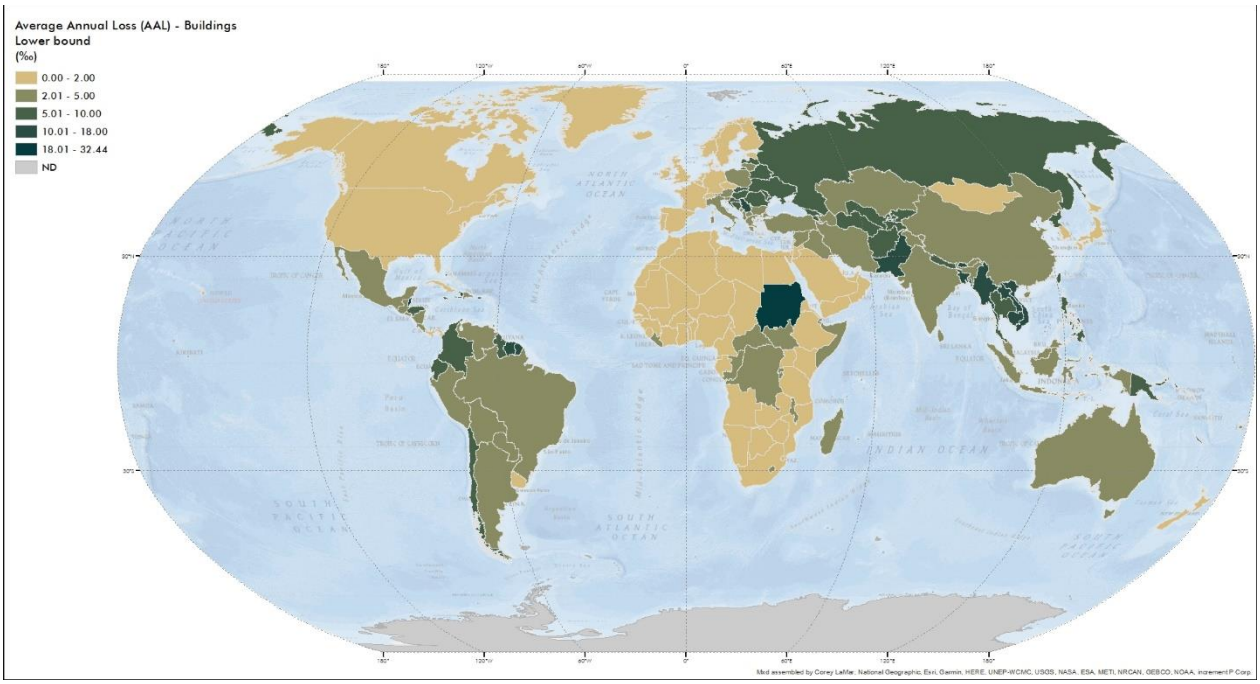

Figure 67. Relative AAL (‰) for buildings. Lower bound climate scenario

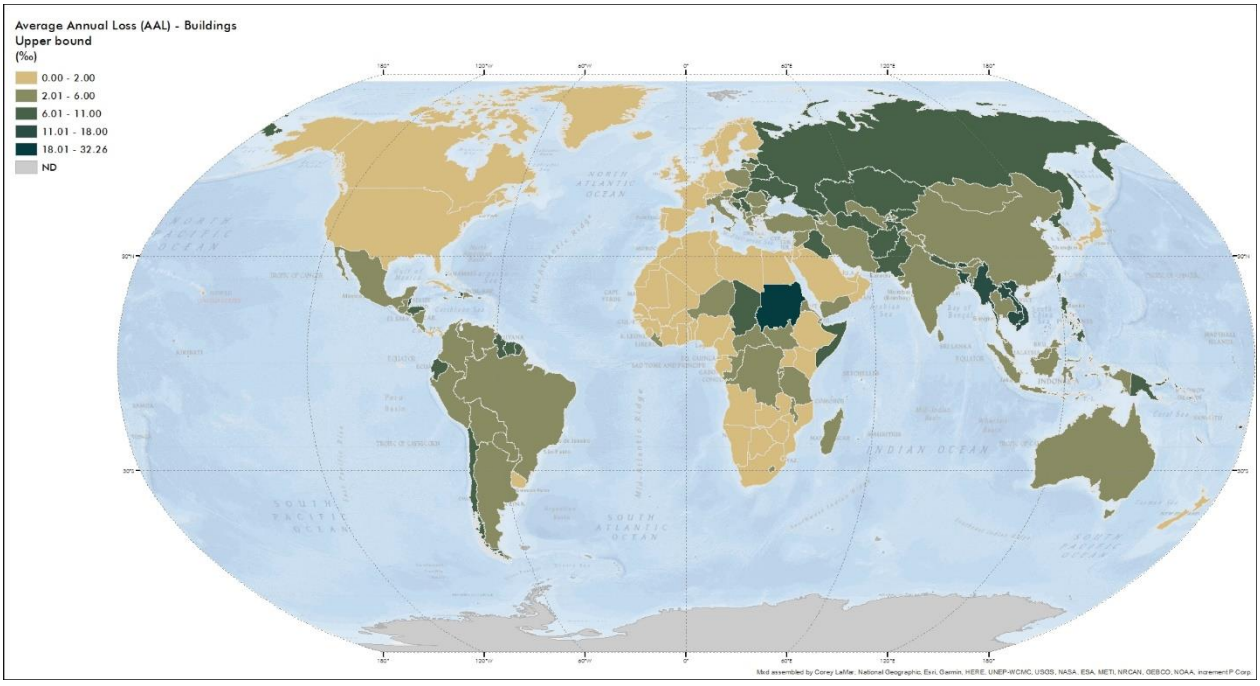

Figure 68. Relative AAL (‰) for buildings. Upper bound climate scenario

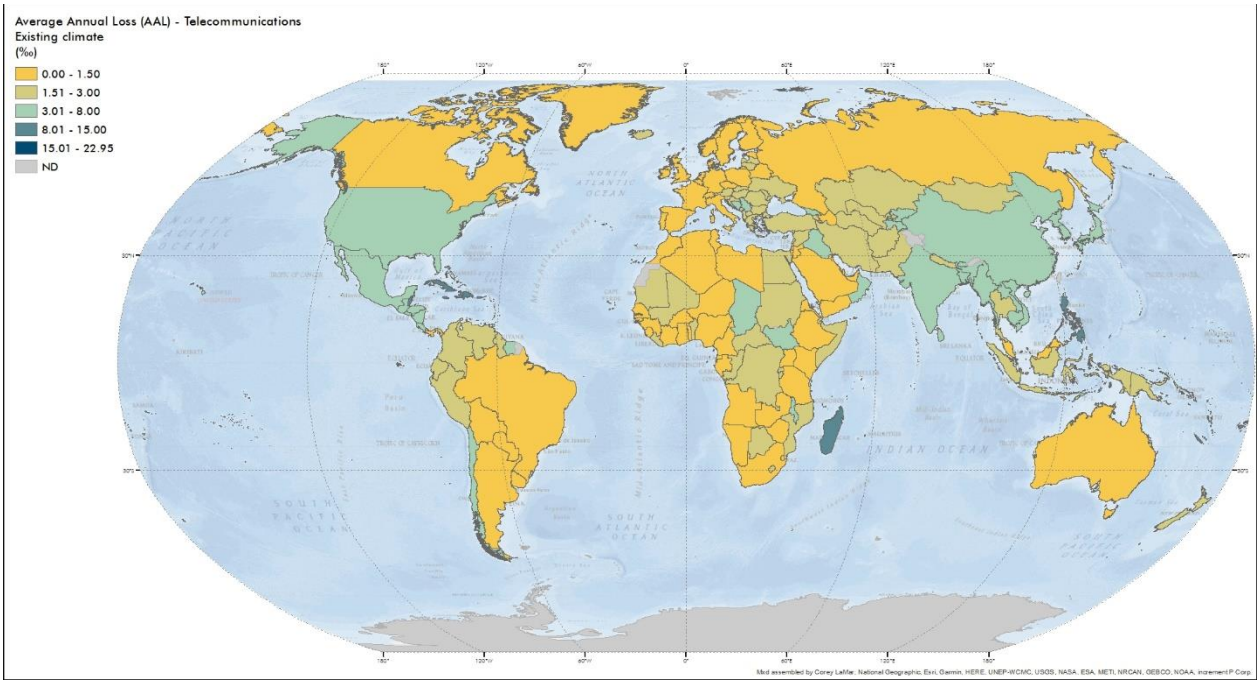

Figure 69. Relative AAL (‰) for the telecommunications sector. Existing climate

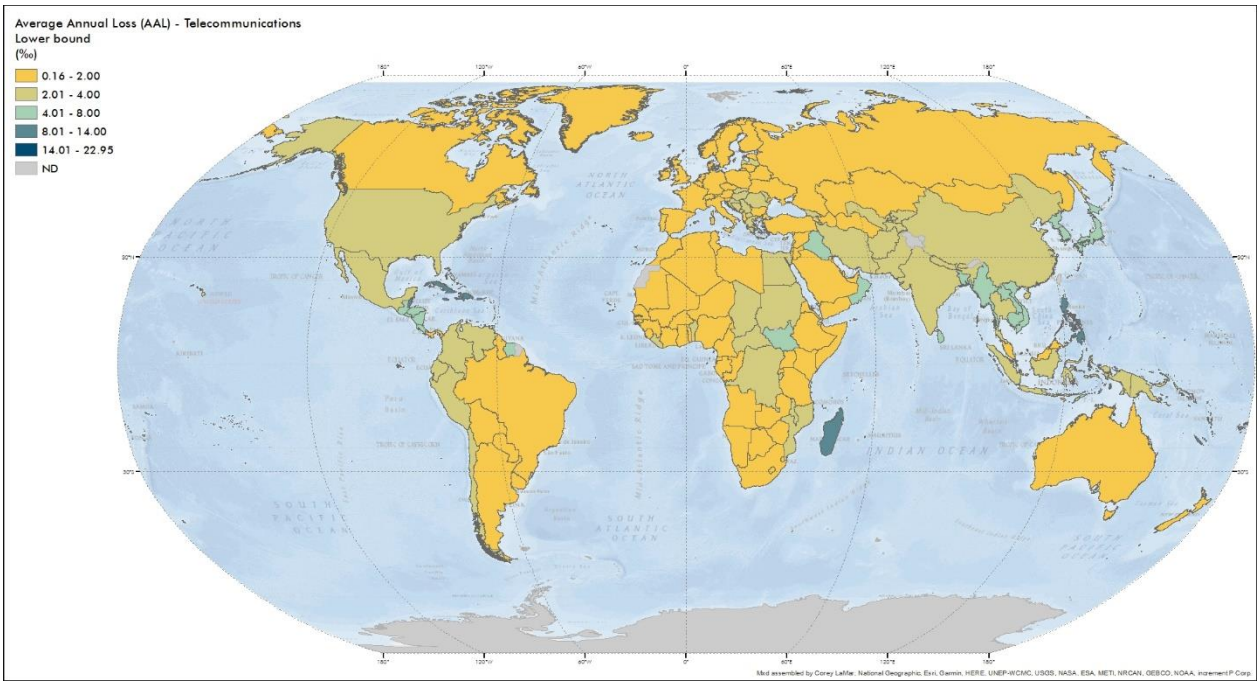

Figure 70. Relative AAL (‰) for the telecommunications sector. Lower bound climate scenario

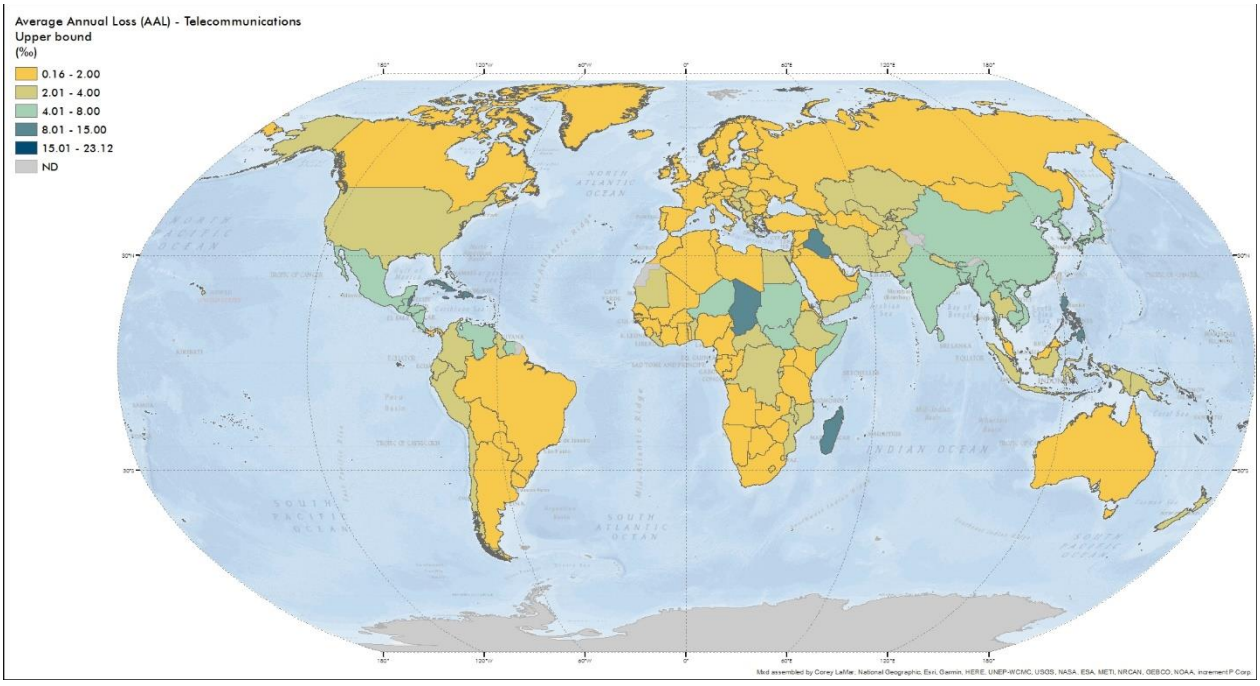

Figure 71. Relative AAL (‰) for the telecommunications sector. Upper bound climate scenario

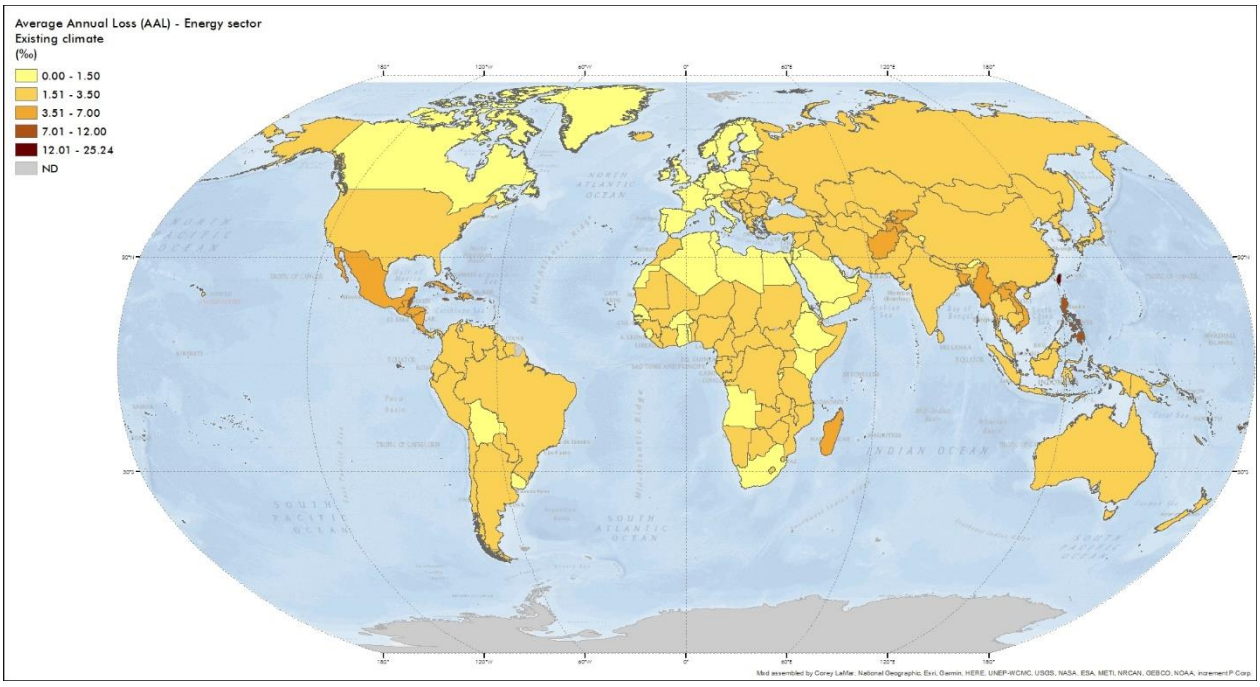

Figure 72. Relative AAL (‰) for the energy sector. Existing climate

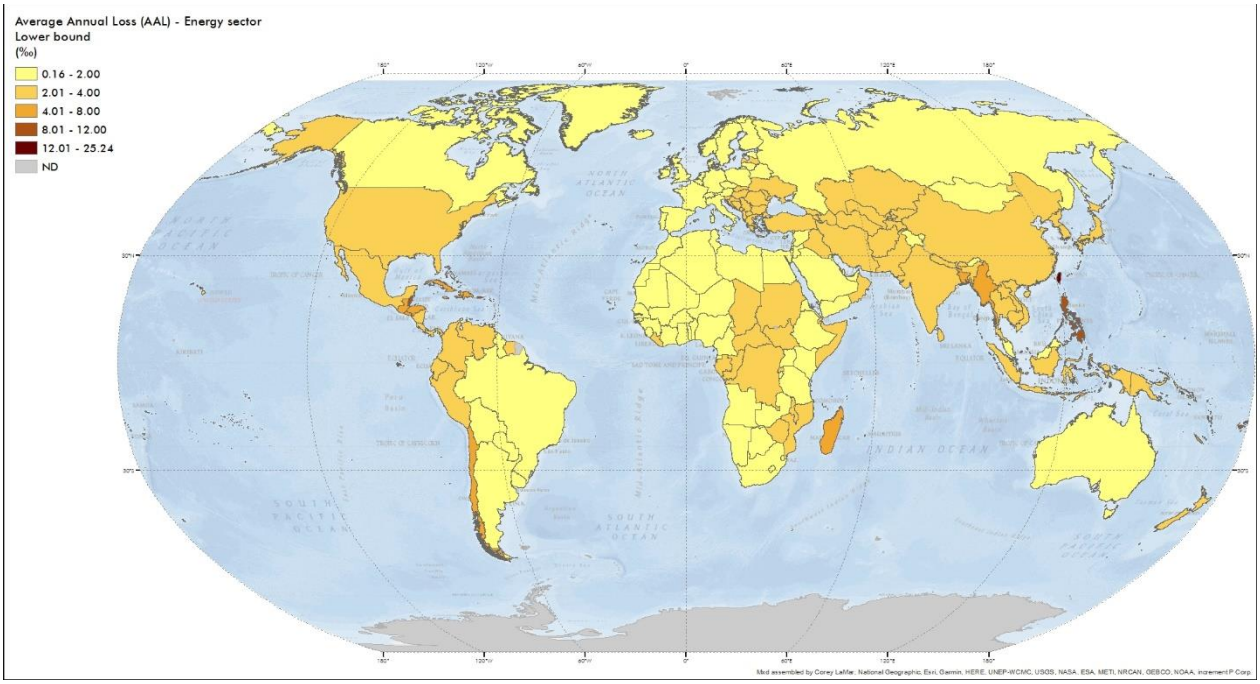

Figure 73. Relative AAL (‰) for the energy sector. Lower bound climate

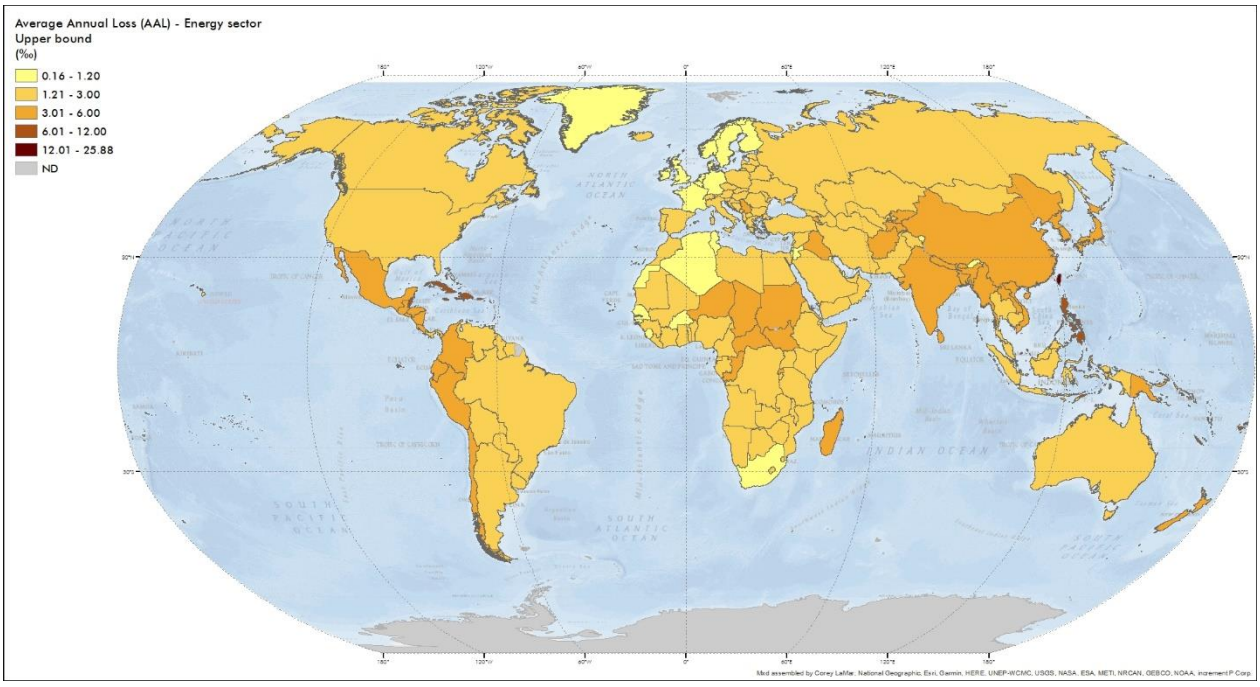

Figure 74. Relative AAL (‰) for the energy sector. Upper bound climate

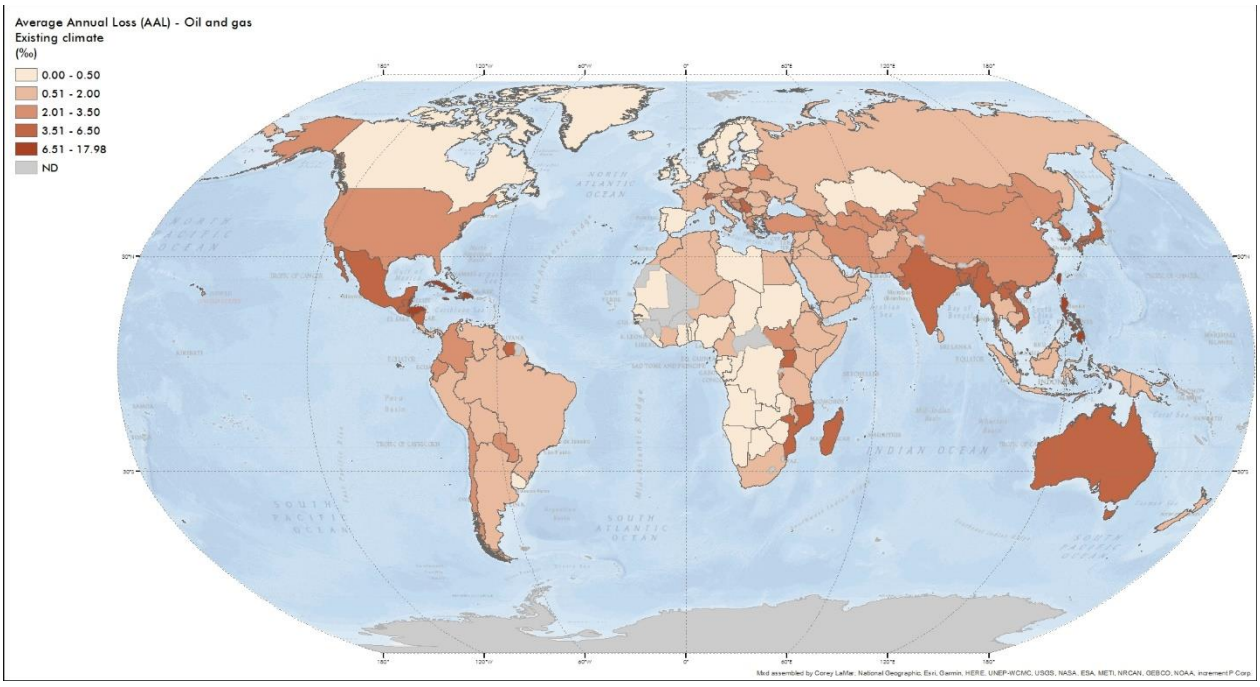

Figure 75. Relative AAL (‰) for the oil and gas sector. Existing climate

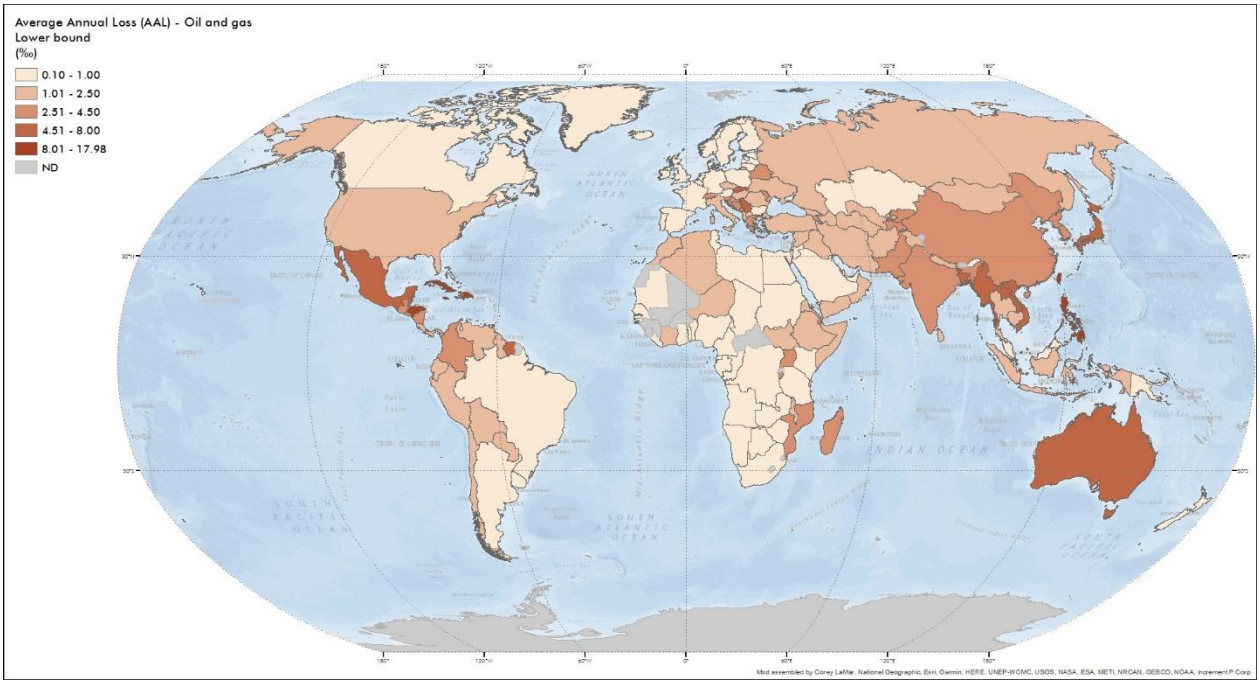

Figure 76. Relative AAL (‰) for the oil and gas sector. Lower bound climate scenario

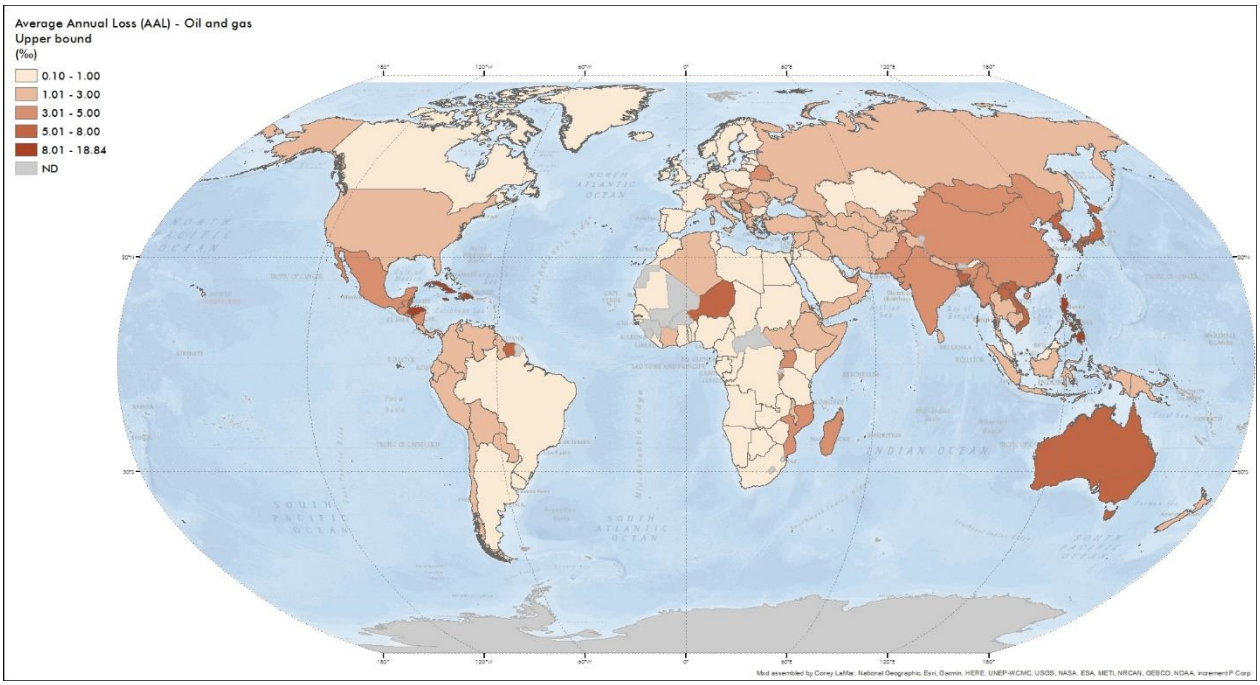

Figure 77. Relative AAL (‰) for the oil and gas sector. Upper bound climate scenario

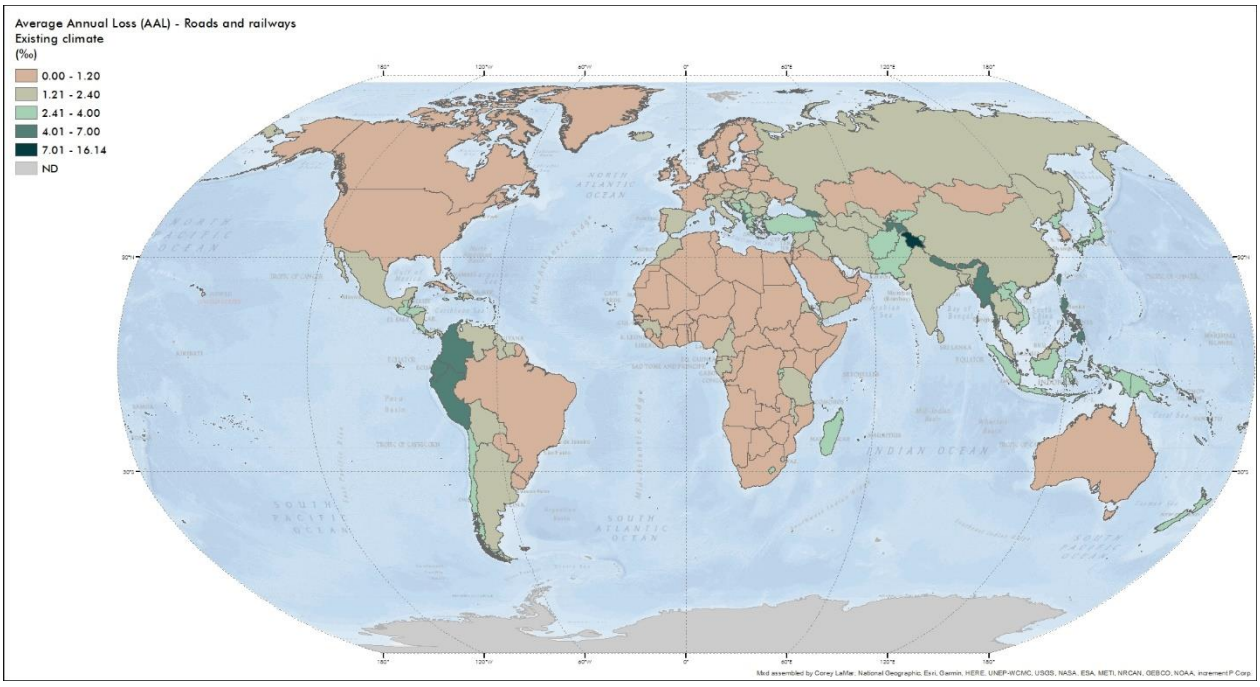

Figure 78. Relative AAL (‰) for the roads and railways sector. Existing climate

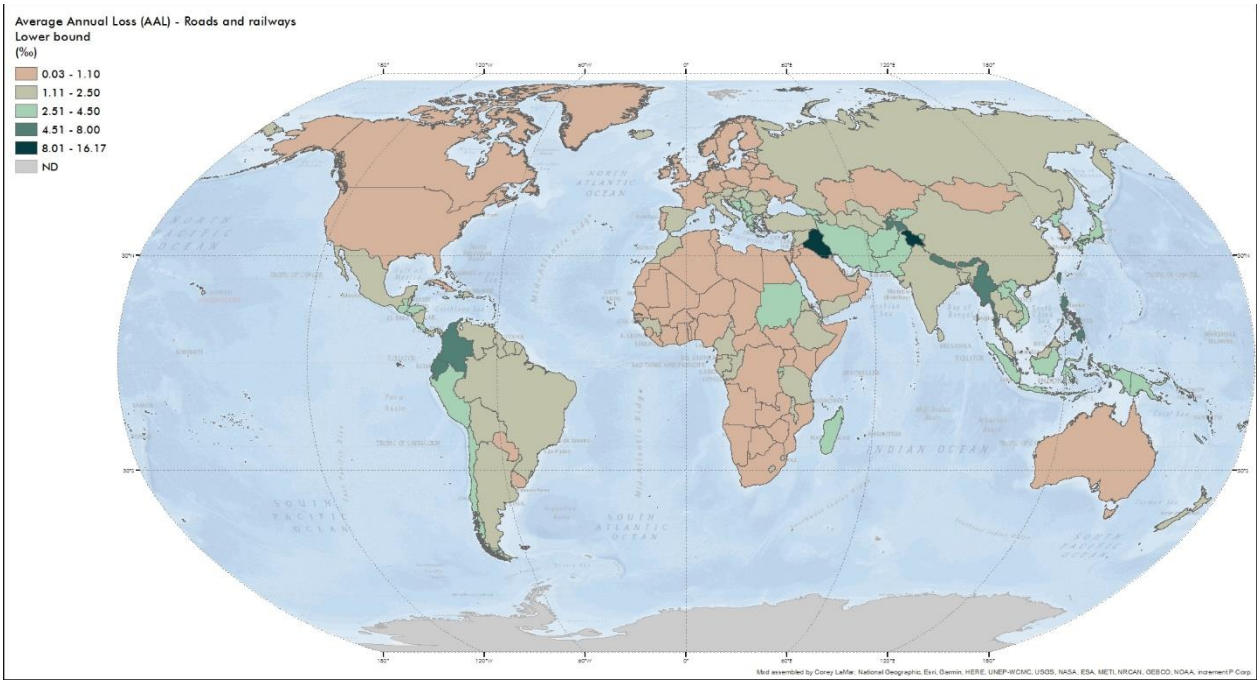

Figure 79. Relative AAL (‰) for the roads and railways sector. Lower bound climate scenario

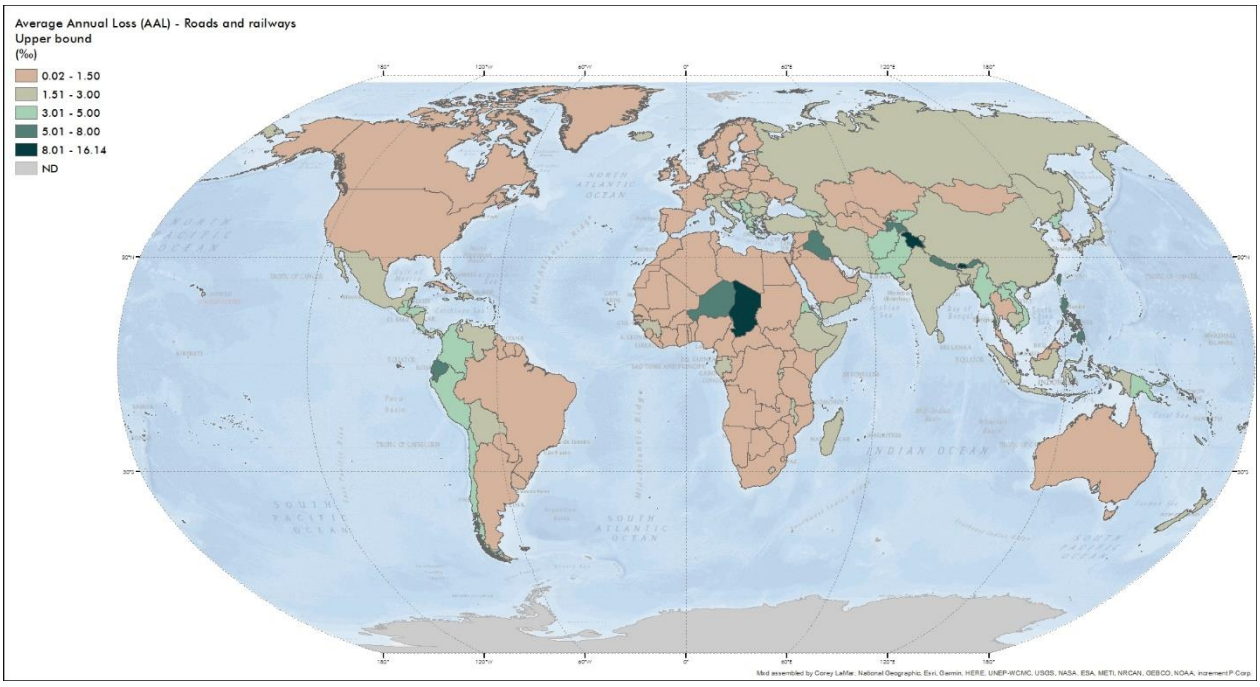

Figure 80. Relative AAL (‰) for the roads and railways sector. Upper bound climate scenario

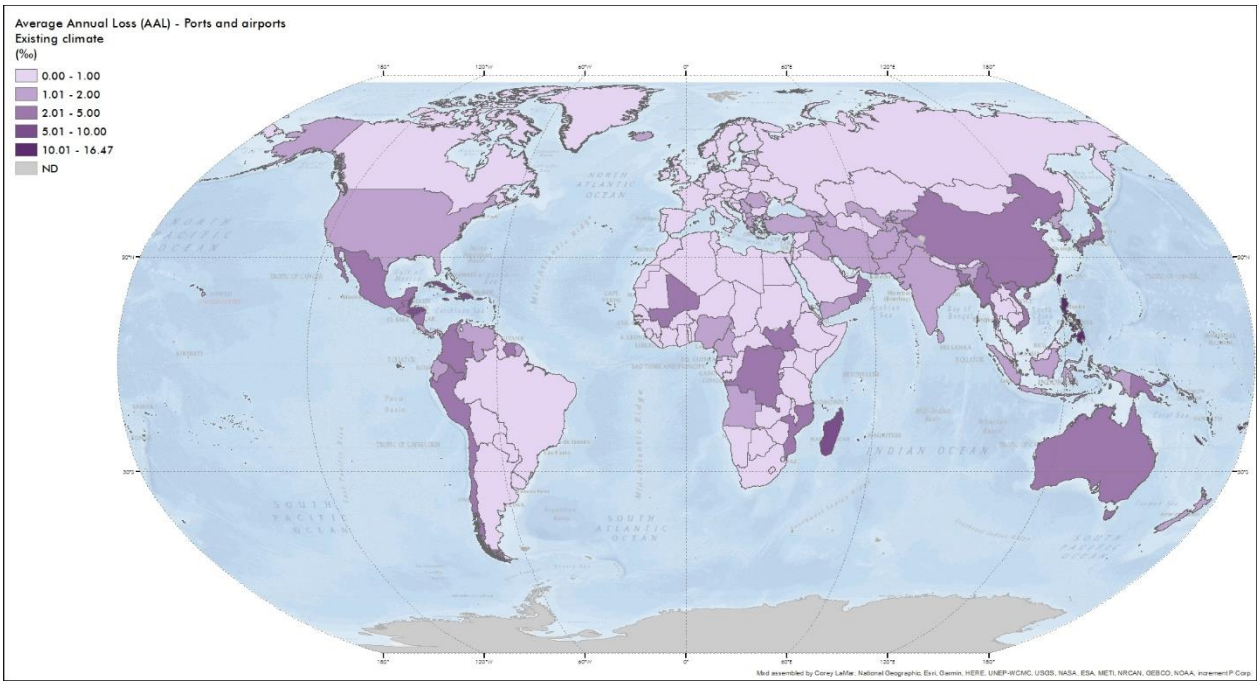

Figure 81. Relative AAL (‰) for the ports and airports sector. Existing climate

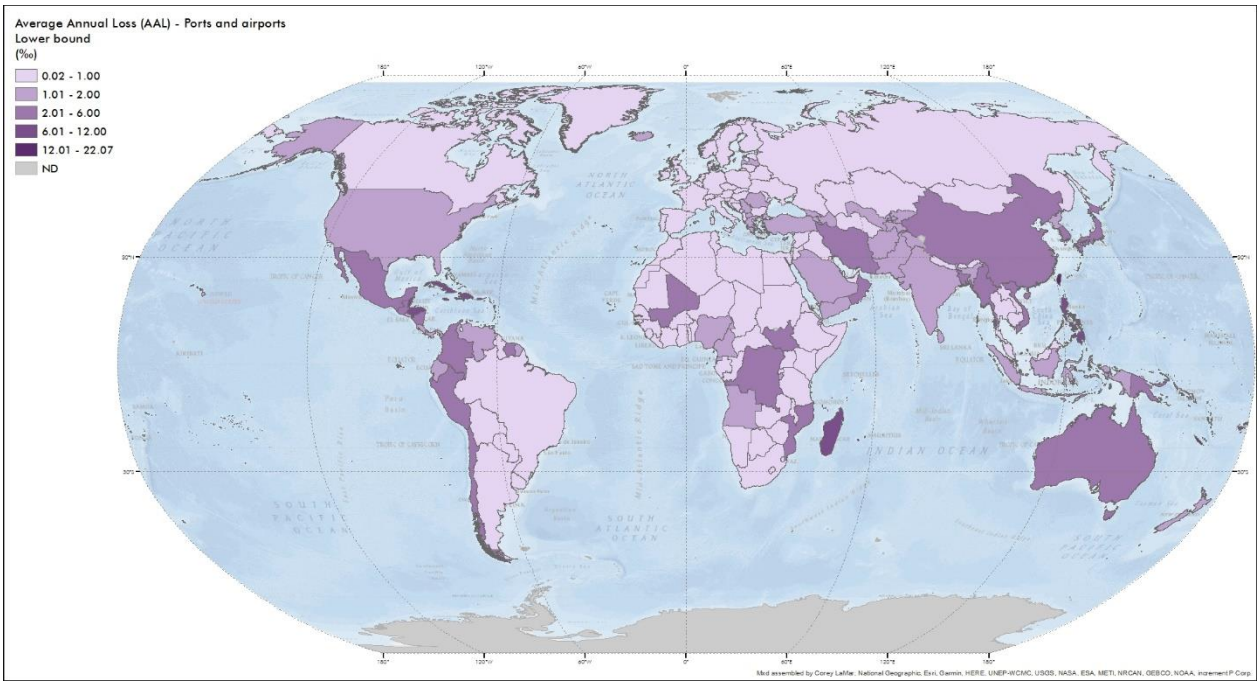

Figure 82. Relative AAL (‰) for the ports and airports sector. Lower bound climate scenario

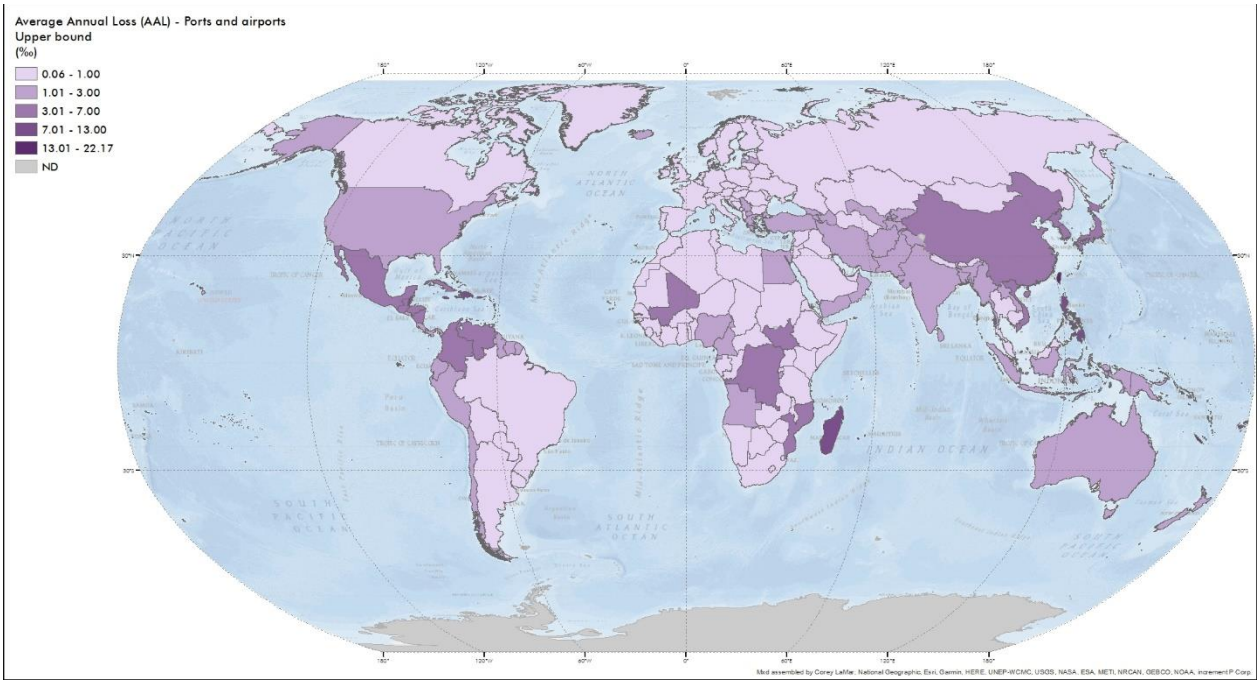

Figure 83. Relative AAL (‰) for the ports and airports sector. Upper bound climate scenario

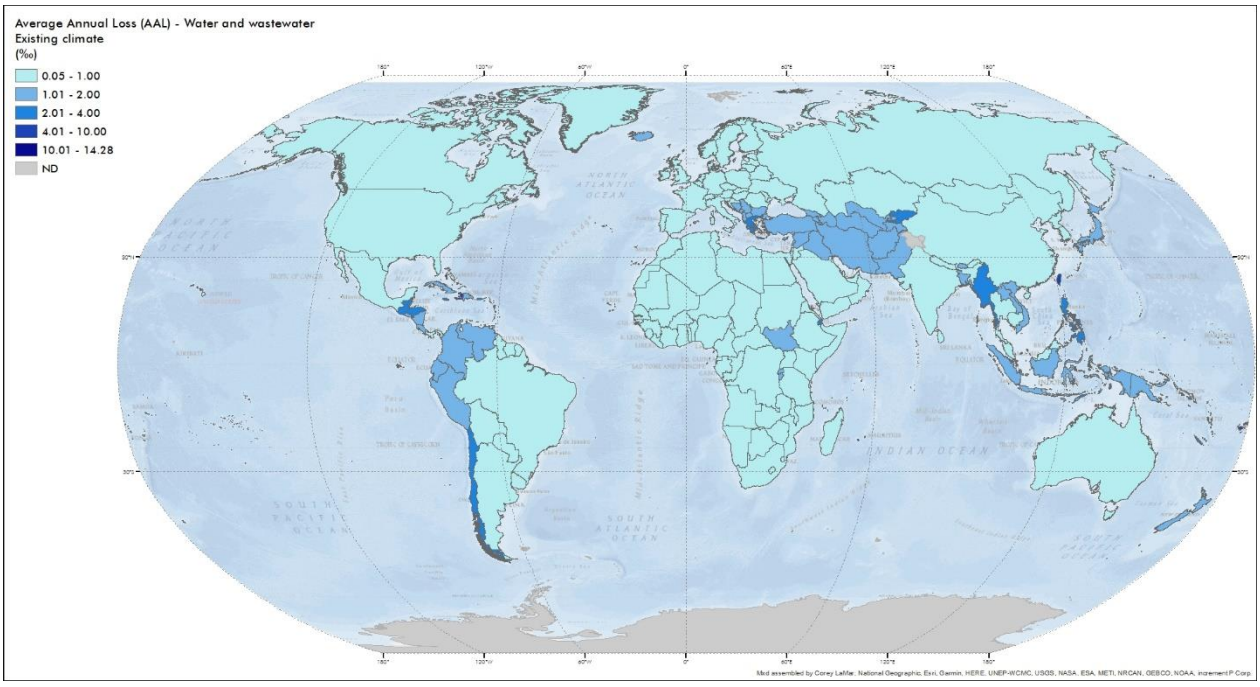

Figure 84. Relative AAL (‰) for the water and wastewater sector. Existing climate

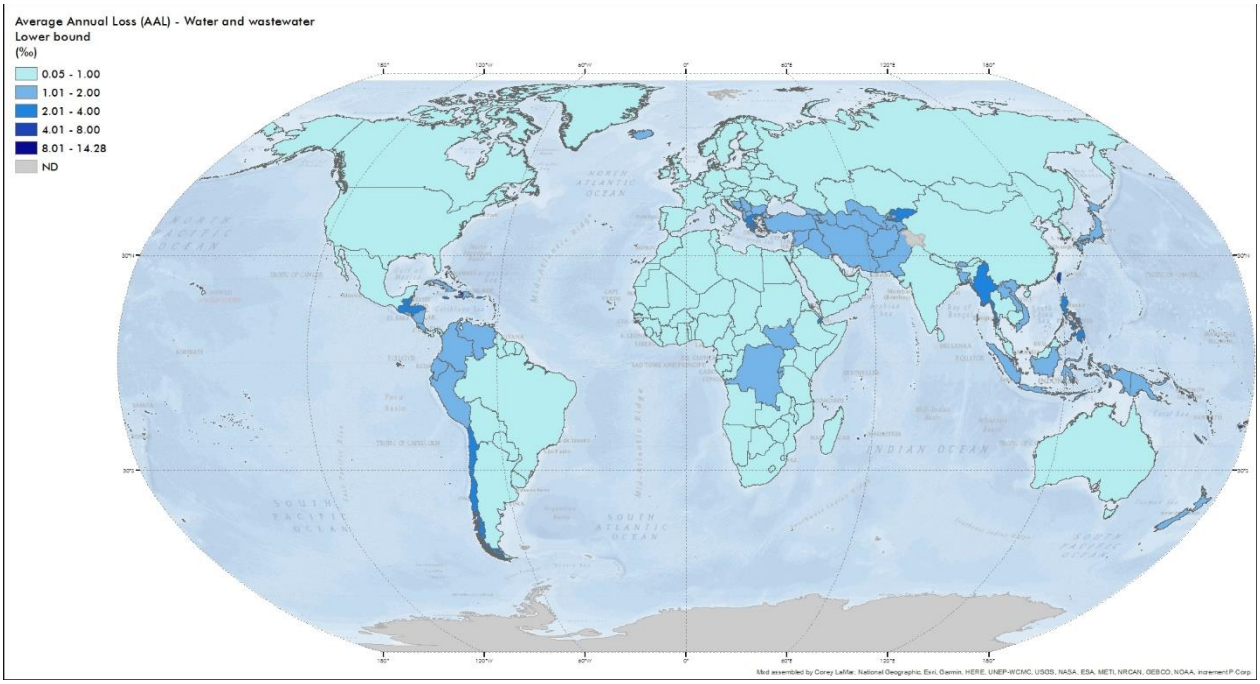

Figure 85. Relative AAL (‰) for the water and wastewater sector. Lower bound climate scenario

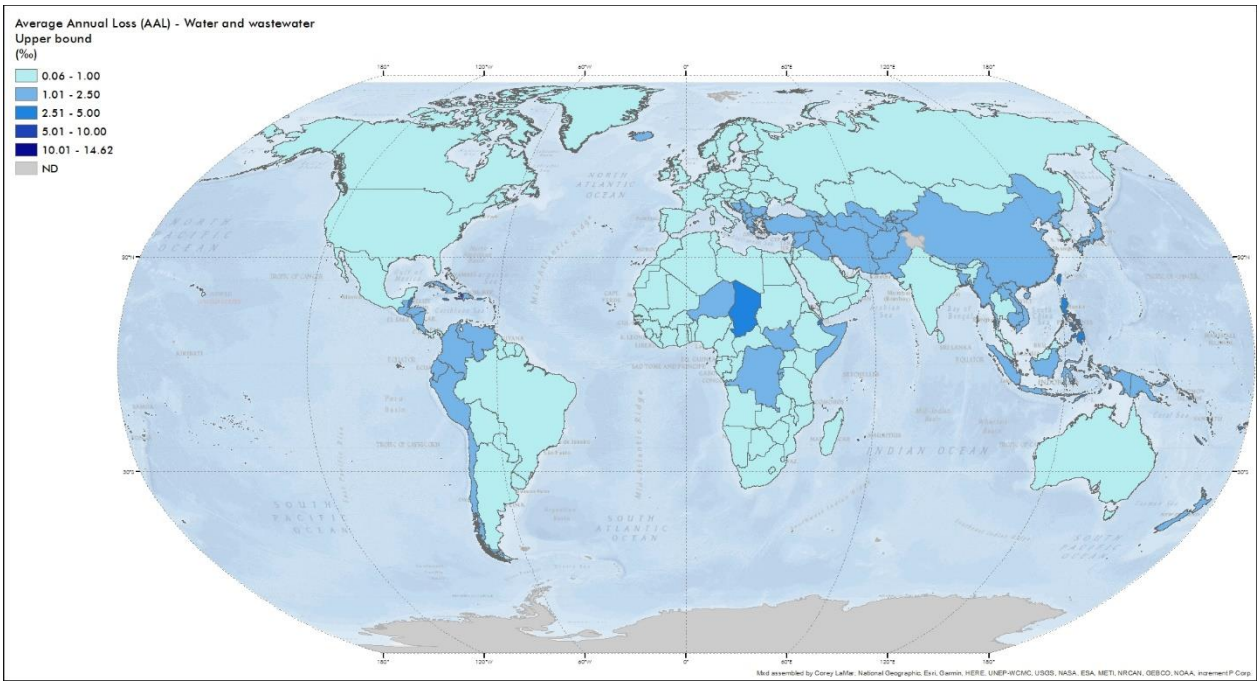

Figure 86. Relative AAL (‰) for the water sector. Upper bound climate scenario

9 Risk Profiles

The Risk Profiles are intended to provide a glimpse into the disaster risk situation of any country. The profiles are built so that the reader may find the most relevant information related to the disaster risk assessment of each country, including the main risk metrics and risk indicators. The profile provides information about which hazards affect the most each country, and which infrastructure sectors are more affected. In addition, the GIRI index is presented along with the position that the country occupies in the global rankings.

The Risk Profiles come to be a fundamental reference for the Governments to know the order of magnitude of their contingent liabilities due to potential disasters. The countries can know their relative situation to other countries, and to bear in mind the implications that disaster risk has on their development from the social, economic and financial growth perspectives.

A preview of the risk profiles for all assessed countries and territories can be found in https://youtu.be/VN-GHLH1yas.

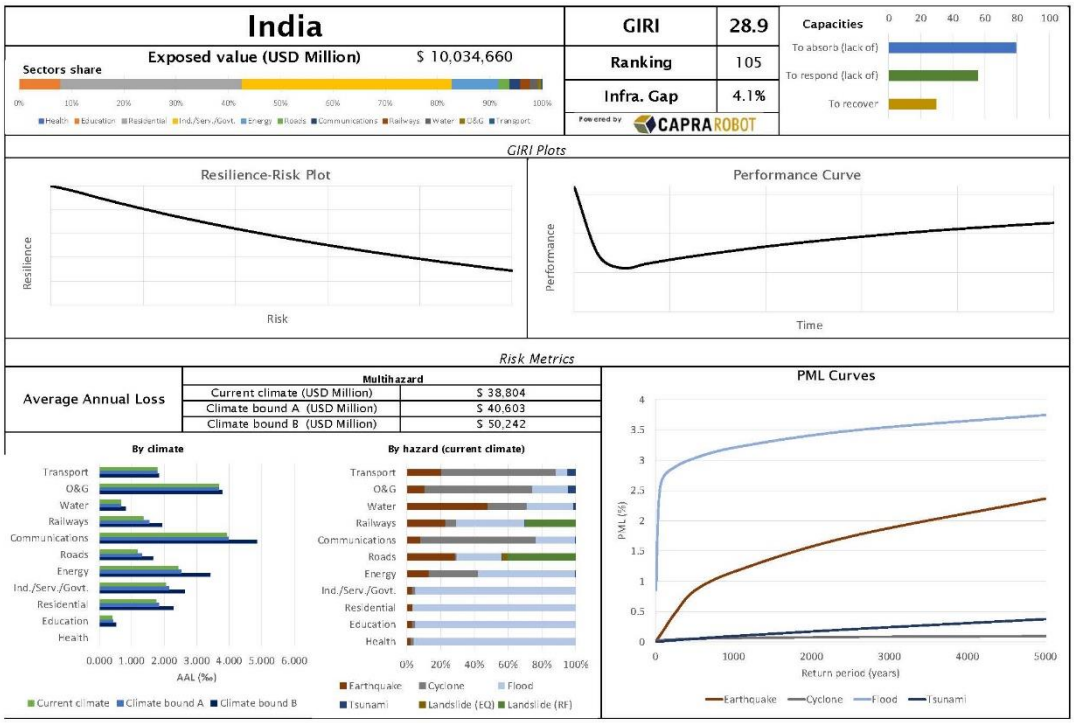

Figure 87. Risk Profile example

10 References

Alfieri, L., Campo, L., Gabellani, S., Ghizzoni, T., Herold, C., Libertino, A., Trasforini, E., & Rudari, R. (2023a). Supplement material to the GIRI global flood hazard model (Global Infrastructure Resilience 2023 Position Paper 2.2). CIMA Foundation, Italy.

Alfieri, L., Campo, L., Gabellani, S., Ghizzoni, T., Herold, C., Libertino, A., Trasforini, E., & Rudari, R. (2023b). The GIRI global flood hazard model (Global Infrastructure Resilience 2023 Position Paper 2.1). CIMA Foundation, Italy.

Alvarez, D.A. 2008. Infinite random sets and applications in uncertainty analysis. Doctoral Thesis. Leopold-Franzens Universität Innsbruck. Austria.

Andersen, E. Sparre. 1957. On the collective theory of risk in case of contagion between claims. Trans. XVth Int. Congress Actuaries. Vol. 2. No. 6. 1957.

Applied Technology Council. 1985. ATC-13. Earthquake Damage Evaluation Data for California.

Ben-Haim, Y. 2001. Information-gap decision theory: Decisions under severe uncertainty. London: Academic Press.

Bernal, G., Cardona, O.D., Marulanda, M., Carreño, M.L. 2019. Dealing with Uncertainty using Fully Probabilistic Risk Assessment for Decision Making. Ch. 14 in: S. Eslamian, F. Eslamian (eds.), Handbook of Disaster Risk Reduction for Resilience. https://doi.org/10.1007/978-3-030-61278-8_14

Bernal, G. A., Escovar, M. A., Zuloaga, D., & Cardona, O. D. 2017a. Agricultural Drought Risk Assessment in Northern Brazil: An Innovative Fully Probabilistic Approach. In V. Marchezini, B. Wiesner, S. Saito, & L. Londe (Eds.), Reduction of Vulnerability to Disasters: from Knowledge to Action. RiMa Ed., pp. 331–356

Bernal G., Salgado-Gálvez, M., Zuloaga, D., Tristancho, J., González, D., Cardona, O. D. 2017b. Integration of Probabilistic and Multi-Hazard Risk Assessment Within Urban Development Planning and Emergency Preparedness and Response: Application to Manizales, Colombia. Int J Disaster Risk Sci. DOI 10.1007/s13753-017-0135-8

Bloemendaal, N., Haigh, I. D., de Moel, H., Muis, S., Haarsma, R., & Aerts, J. C. J. H. (2020). Generation of a global synthetic tropical cyclone hazard dataset using STORM. Scientific Data, 7(1), 1-12. [40]. https://doi.org/10.1038/s41597-020-0381-2, https://doi.org/10.1038/s41597-020-0381-2

Cardona, O.D, Bernal, G., Zuloaga, D., Escovar, M. A., Villegas, C., Gonzáles, D., Molina, J. F. 2016. Sistema de Modelación de Amenazas y Riesgos de Bogotá. DOI: 10.13140/RG.2.2.31828.60800

Cardona O.D., Ordaz M.G., Mora M., Salgado-Gálvez M.A., Bernal G.A., Zuloaga-Romero D., Marulanda M.C., Yamín L. and González D. 2014. Global risk assessment: a fully probabilistic seismic and tropical cyclone wind risk assessment. International Journal of Disaster Risk Reduction. 10:461-476.

Cardona, O.D. 1986. Estudios de vulnerabilidad y evaluación del riesgo sísmico: Planificación física y urbana en áreas propensas. Asociación Colombiana de Ingeniería Sísmica. Reporte AIS-33. Diciembre, 1986

Cardona, O.D., Bernal, G., Olaya, J., Mora, G., Yamín, L. 2013. Estimación de la amenaza y el riesgo probabilista por huracán en Guatemala, incorporando el impacto asociado al cambio climático. Reporte técnico preparado al BID. CIMNE, España.

CIMNE, ITEC S.A.S., INGENIAR LTDA., EAI S.A. (2012) Probabilistic modelling of natural risks at the global level: Global Risk Model. Background paper for the GAR13.

Cramér, H. (1930) On the Mathematical Theory of Risk, Skandia Jubilee Volume, Stockholm.

Dempster, A. P. 1967. Upper and lower probabilities induced by a multivalued mapping. Annals of Mathematical Statistics, 38:325-339.

Grossi, P. & Kunreuther, H. 2005. Catastrophe Modeling: A new approach to managing risk. Huebner International Series on Risk, Insurance and Economic Security. Volume 25. Springer

Jenkins, S. F., Magill C. R., McAneney J., and Blong R. James. 2012. Regional ash fall hazard I: A probabilistic assessment methodology. Bulletin of Volcanology. 74(7), 1699-1712.

Kendall, D. G. 1974. Foundations of a theory of random sets. In Harding, E. F. and Kendall, D. G., editors, Stochastic geometry, pp 322-376, London.Wiley.

Kirgman, J., 1992. Poisson Processes. Clarendon Press. Ofxord.

Knapp, K. R., H. J. Diamond, J. P. Kossin, M. C. Kruk, C. J. Schreck, 2018: International Best Track Archive for Climate Stewardship (IBTrACS) Project, Version 4. [indicate subset used]. NOAA National Centers for Environmental Information. doi:10.25921/82ty-9e16

Knapp, K. R., M. C. Kruk, D. H. Levinson, H. J. Diamond, and C. J. Neumann, 2010: The International Best Track Archive for Climate Stewardship (IBTrACS): Unifying tropical cyclone best track data. Bulletin of the American Meteorological Society, 91, 363-376. doi:10.1175/2009BAMS2755.1

Kohlas, J., Monney, P. 1995. A Mathematical Theory of Hints. Lecture Notes in Economics and Mathematical Systems. Volume 425. Springer

Løvholt F., Glimsdal, S., Harbitz, C., Horspool, N., Smebye, H., Del bono, A., Nadim, F. (2014). Global tsunami hazard and exposure due to large co-seismic slip. International Journal of Disaster Risk Reduction, Volume 10, Part B, December 2014, Pages 406–418. doi:10.1016/j.ijdrr.2014.04.003.

Lundberg, F. (1903) Approximerad Framställning av Sannolikehets-funktionen. Återförsäkering av Kollektivrisker, Almqvist & Wiksell, Uppsala.

Marchau, V., Walker, W., Bloemen, P., Popper, S. 2019. Decision making under deep uncertainty. Springer. Open Acces. DOI: 10.1007/978-3-030-05252-2

Marulanda, M.C., Carreño, M.L., Cardona, O.D., Ordaz, M.G., Barbat, A.H. 2013. Probabilistic earthquake risk assessment using CAPRA: Application to the city of Barcelona, Spain. Natural Hazards 69(1): 59–84.

Maskrey, A., Cardona, O.D., Bernal, G., Escovar, M. A., Villegas, C., Grajales, S., Rincón, D. 2019. Agricultural Drought Risk: The case of Kazakhstan. Report for the UN Economic and Social Commission for Asia and the Pacific – ESCAP. 2019

Matheron, G. 1975. Random sets and integral geometry. Wiley, New York.

Molchanov, I. 2005. Theory of random sets. Springer Verlag. London.

Möller, B. and Beer, M. 2004. Fuzzy Randomness - Uncertainty in Civil Engineering and Computational Mechanics. Springer, Berlin.

Mora, S. y Vahrson, W. (1994). Macrozonation methodology for landslide hazard determination. Bulleting of the Association of Engineering and Geologist, 31(1), 49-58.

Nadim, F., Palau, R. M., Paulsen, E. M., & Storrøsten, E. B. (2023). A new model for global landslide susceptibility assessment and scenario-based hazard assessment (Global Infrastructure Resilience 2023 Position Paper 2.6). Norwegian Geotechnical Institute (NGI), Norway.

Nelsen, R. B. 1999. An Introduction to Copulas, volume 139 of Lectures Notes in Statistics. Springer Verlag, New York.

Niño, M., Jaimes, M., Reinoso, E. 2015. Seismic-event-based methodology to obtain earthquake induced translational landslide regional hazard maps. Natural Hazards, Springer Ed. DOI: 10.1007/s11069-014-1163-y

Ordaz, M. 2000. Metodología para la evaluación del riesgo sísmico enfocada a la gerencia de seguros por terremoto. Universidad Nacional Autónoma de México. México D.F., México.

Piller, T., Benvenuti, A. & De Bono, A. (2023). The GIRI global building exposure model (BEM) (Global Infrastructure Resilience 2023 Position Paper 2.7). GRID, University of Geneva, Switzerland.

Quijano, J. A., Jaimes, M. A., Torres, M. A., Reinoso, E., Castellanos, L., Escamilla, J., and Ordaz, M. 2014. Event-based approach for probabilistic agricultural drought risk assessment under rainfed conditions, J. Int. Soc. Prev. Mitig. Nat. Hazards, 76, 1297–1318, doi:10.1007/s11069-014-1550-4.

Salgado-Gálvez M.A., Cardona O.D., Carreño M.L. and Barbat A.H. 2015. Probabilistic seismic hazard and risk assessment in Spain. Monographs on earthquake engineering. International Center for Numerical Methods in Engineering – CIMNE. ISBN: 978-84-993307-7-3.

Salgado-Gálvez M.A., Zuloaga D., Bernal G., Mora M.G. and Cardona O.D. 2014. Fully probabilistic seismic risk assessment considering local site effects for the portfolio of buildings in Medellín, Colombia. Bulletin of Earthquake Engineering. 12:671-695.

Salgado-Gálvez, M., Bernal G., Zuloaga, D., Marulanda, M., Cardona, O. D., Henao, S. 2017. Probabilistic Seismic Risk Assessment in Manizales, Colombia: Quantifying Losses for Insurance Purposes. Int J Disaster Risk Sci. DOI 10.1007/s13753-017-0137-6

Shafer, G. 1976. A mathematical theory of evidence. Princeton University Press, Princeton, NJ.

Torres, M. A., Jaimes, M. A., Reinoso, E., Ordaz, M. 2013. Event-based approach for probabilistic flood risk assessment. Intl. J. River Basin Management. 2013. pp. 1–13.

Wong, I. G. 2014. How big, how bad, how often: Are extreme events accounted for in modern seismic hazard analysis? Nat. Hazards 72, no. 3, 1299–1309, DOI: 10.1007/s11069-013-0598-x